



This is to certify that the
dissertation entitled

Laser Direct Fabrication of 3-D Components

presented by

Yiping Hu

has been accepted towards fulfillment
of the requirements for

Ph.D. degree in Materials Science
and Engineering


Major professor

Date May 4, 2000

PLACE IN RETURN BOX to remove this checkout from your record.
TO AVOID FINES return on or before date due.
MAY BE RECALLED with earlier due date if requested.

DATE DUE	DATE DUE	DATE DUE

LASER DIRECT FABRICATION OF 3-D COMPONENTS

By

Yiping Hu

A DISSERTATION

**Submitted to
Michigan State University
in partial fulfillment of the requirements
for the degree of**

DOCTOR OF PHILOSOPHY

Department of Materials Science and Mechanics

2000

ABSTRACT

LASER DIRECT FABRICATION OF 3-D COMPONENTS

By

Yiping Hu

A novel laser direct deposition of composite materials has been investigated to manufacture 3-D components. This process allows for either the direct production of an industrial component or rapid, and low-cost fabrication of tooling dies and injection molds.

In present research, an integrated powder feeding system is designed for laser cladding. It can provide a stable, continuous, and accurate powder feeding rate, and deliver the powder stream coaxially into the molten pool under the laser beam. The experimental results showed that this powder feeding system is suited for depositing high quality cladding tracks, along complicated geometric paths, on flat or curved surfaces. Due to the change of powder feeding mechanism, the characteristic of cone-shaped powder stream and interaction between the laser beam and the powder stream have also been investigated.

Although laser cladding is a complicated process, based on reasonable approximations, a simple but realistic process model, relating the clad thickness and processing parameters, is successfully developed. The calculated results of this model are in good agreement with the experimental ones.

A novel process for manufacturing tooling dies, with required geometric patterned cutting blades, has been successfully developed directly by laser cladding process. Fully functional prototype of an industrial rotary cutting die, for pilot testing, has been produced. This new process has been implemented in tooling-die manufacturing industry. In addition, various geometric laminated 3-D components have been directly produced by the same process. The laminated composites have relatively smooth surface and good planner interfaces, are free of pores and cracks, and good metallurgical bonding with the substrate.

Finally, the measurement of the thermal cycle, and the temperature distributions for laser cladding process has been made. Within optimized operation window, a wide range of processing parameters, and various clad materials have been used in laser cladding experiments. The clad-zone temperatures, under various processing conditions, lies between 1650 °C and 1800 °C. These results are in good agreement with those obtained by optical pyrometer and CCD techniques. In addition, in both cases of laser remelting and cladding processes, the temperature gradients along y-direction have Gaussian distribution.

**Copyright by
Yiping Hu
2000**

To my lovely wife Zanping and daughter Dianna.

ACKNOWLEDGMENTS

I wish to thank my dissertation advisor, University Distinguished Professor K. Mukherjee, for his academic guidance, advice, and financial support throughout the duration of this research work. I would also like to extend my sincere appreciation to my dissertation committee members: Professor J. Lucas and Professor K.N. Subramanian of Department of Materials Science and Mechanics, and Professor S.D. Mahanti of Physics and Astronomy Department, Michigan State University, for their invaluable advice and suggestions in conducting this research work.

My sincere gratitude is extended to my parents for their encouragement, and spiritual support. Special thanks are due to my uncle, Dr. Kuang Y. Chen, who generously supports me. I would also like to thank Dr. C.W. Chen for his kind assistance and valuable technical advice. I want to thank Drs. S. Kudapa and J.K. Park for their friendship and help.

TABLE OF CONTENTS

LIST OF TABLES.....	x
LIST OF FIGURES.....	xi
INTRODUCTION.....	1
1. Background and Motivation.....	1
2. Scope.....	4
CHAPTER 1	
REVIEW OF LASER SURFACE TREATMENT PRINCIPLE.....	6
1.1 Basic Principle of Laser Operation.....	6
1.1.1 Radiation Transitions.....	7
1.1.2 Spontaneous and Stimulated Emission.....	8
1.2 Laser-Beam Mode.....	10
1.3 Laser Parameters.....	14
1.3.1 Laser-Beam Diameter.....	14
1.3.2 Laser-Beam Power.....	15
1.3.3 Power Density.....	16
1.4 Industrial Lasers.....	17
1.4.1 The Nd:YAG Laser.....	18
1.4.2 The CO ₂ Laser.....	20
1.5 Laser Beam-Material Interaction.....	23
CHAPTER 2	
LASER SURFACE TREATMENT.....	25
2.1 Laser Solid-Transformation Hardening.....	25
2.2 Laser Remelting.....	27
2.3 Laser Surface Alloying.....	27
2.4 Laser Dispersing.....	28
2.5 Laser Surface Cladding.....	29
2.5.1 General Description.....	29
2.5.2 Scope of Laser Cladding	29
2.5.3 Processing Parameters	30
2.5.3.1 Absorptivity.....	30
2.5.3.2 Traverse Speed.....	32
2.5.3.3 Power Feeding Techniques.....	32
2.5.3.4 Shielding Gas.....	33
2.5.4 Advantages of Laser Cladding Process.....	34
2.5.5 Limitations of Laser Cladding Process.....	34

2.5.6	Applications of Laser Cladding Process.....	35
-------	---	----

CHAPTER 3

EXPERIMENTAL PROCEDURES.....	37
3.1 General Description.....	37
3.2 Choice of Materials.....	37
3.2.1 Substrate Materials.....	38
3.2.2 Clad Materials.....	39
3.3 Laser Cladding System.....	44
3.3.1 CO ₂ Laser.....	45
3.3.2 Beam Delivery System	45
3.3.3 Powder Feeding System.....	45
3.3.3.1 Powder Feeder.....	48
3.3.3.2 Powder-Flow Splitter.....	48
3.3.3.3 Coaxial Nozzle.....	48
3.3.4 CAM System.....	51
3.4 Laser Cladding.....	51
3.5 Temperature Measurement.....	52
3.6 Post-Clad Treatment.....	55
3.7 Microstructures and Hardness Measurements.....	55
3.8 Hardness Movement.....	56

CHAPTER 4

RESULTS AND DISCUSSION.....	44
4.1 Characteristics of Cone-Shaped Powder Stream.....	44
4.2 Desirable Powder Morphology and Particle-Size Distribution.....	60
4.3 Effect of Powder Feeding Systems on Clad Quality.....	61
4.4 Measurement of Powder Utilization Coefficient.....	62
4.5 Relationships between Clad Width and Process Parameters.....	66
4.6 Process Modeling.....	69
4.6.1 Assumptions.....	69
4.6.2 Basic Equations.....	70
4.6.3 Energy Density Equation.....	71
4.6.4 Clad Thickness-Energy Density Equation.....	72
4.7 Relationships Derived from Basic Equation.....	73
4.7.1 Relationship Between Clad Thickness and Traverse Speed.....	73
4.7.2 Relationship Between Clad Thickness and Powder Feed Rate.....	74
4.8 Correlation Derived from the Energy Density Equation.....	75
4.8.1 Relationship between Energy Density and Spot Size.....	75
4.8.2 Relationship between Energy Density and Traverse Speed.....	76
4.8.3 Relationship between Energy density and Laser Power.....	77
4.9 Correlation between Clad Thickness and Energy Density.....	79
4.10 Relationship Between Penetration Depth and Energy Density.....	79

4.8.3	Relationship between Energy density and Laser Power.....	77
4.9	Correlation between Clad Thickness and Energy Density.....	79
4.10	Relationship Between Penetration Depth and Energy Density.....	79
4.11	Evaluation Standards of Laser Cladding Quality.....	81
4.12	Overlapping Rate.....	85
4.13	Dilution.....	86
4.14	Calculation of Deposition Rate.....	88
4.15	Geometric Characteristics of Single Cladding Tracks.....	89
4.16	Laser Direct Fabrication of 3-D Components.....	92
4.16.1	Tooling Dies.....	92
4.16.1.1	Fabrication of Tooling Dies.....	92
4.16.1.2	Microstructure of Clad Bead.....	94
4.16.1.3	Microhardness of Clad Bead.....	94
4.16.2	Laminated Metal Matrix Composites (LMMCs).....	99
4.16.2.1	Direct Fabrication of LMMCs.....	99
4.16.2.2	Microstructure of the Cross Section of LMMCs.....	104
4.16.2.3	X-Ray Dot Mapping.....	107
4.16.2.4	Microhardness Measurement of LMMCs.....	110
4.17	Temperature	
Measurement.....		111
4.17.1	Temperature Distributions without Powder Feeding.....	111
4.17.2	Temperature Distributions for Laser Cladding Process.....	114
CHAPTER 5		
CONCLUSIONS.....		121
BIBLIOGRAPHY.....		126

LIST OF TABLES

3.1	Chemical compositions of substrates and clad materials.....	39
3.2	Characteristics of the RF excited CO ₂ laser.....	45
3.3	CNC machine specifications.....	51
4.1	Processing parameters for producing rotary cutting dies.....	93
4.2	Processing parameters used for the laser cladding operations.....	100

LIST OF FIGURES

1.1	Types of emission processes between two energy levels [13].....	9
1.2	Transverse mode patterns in cylindrical and rectangular coordinates [15].....	11
1.3	Variation of relative intensity and percentage total power with radius for a Gaussian TEM ₀₀ beam [18]. Note that for the vertical line representing e^{-1} , the value should read 0.71 instead of 0.59.....	13
1.4	Laser materials interaction energy diagram [21].....	17
1.5	Energy level of Nd: YAG laser [24].....	19
1.6	Three vibrational modes and various energy levels for CO ₂ laser [25].....	21
3.1	An overview of powder morphology. (a) CPM10V tool steel. (b) 304L stainless steel.....	40
3.2	Wear resistance of CPM 10V and conventional tool steels at indicated hardness [80]. CPM 10V* (hardened) is subjected to quenching, which increases its hardness, and thus the extra wear resistance.....	42
3.3	Charpy C-notch impact properties of CPM 10V and conventional tool steels at indicated hardness [80].....	42
3.4	A schematic drawing of the laser cladding system [4].....	44
3.5	An overview of powder feeding systems. (a) Lateral powder feeding system. (b) Integrated coaxial powder feeding system.....	47
3.6	A schematic drawing of the transverse section of a coaxial nozzle [10].....	49
3.7	A view of cone-shaped powder stream irradiated by laser beam.....	50

3.8	An overview of specimen dimension, thermocouple layout and location [102].....	54
4.1	A view of cone-shaped powder stream. (a) Without laser beam. (b) With laser beam. Process parameters are as follows: laser power is 2.1 kw, laser spot size 2.9 mm, powder feed rate 0.25 g/sec, and cover gas flow rate 0.85 m ³ /hr.....	58
4.2	Effect of cover gas flow rate on cone-shaped powder stream. (a) Without laser beam irradiation. (b) With laser beam irradiation. Cover gas flow rate 3.4 m ³ /hr. Other processing parameters are the same as those of Figure 4.1.....	59
4.3	A view of circular cladding tracks on a solid cylinder. Cladding track 2 is an example of poor quality clads due to higher cover gas flow rate.....	60
4.4	A view of desirable powder morphology for laser cladding process.....	61
4.5	Effect of powder feeding systems on cladding quality. (a) Rectangular cladding tracks with smooth surface. (b) Perpendicular cladding tracks with rough surface via lateral powder feeding system.....	62
4.6	Plot of powder utilization coefficient vs. traverse speed.....	64
4.7	Plot of powder utilization coefficient vs. powder feed rate.....	65
4.8	Plot of powder utilization coefficient vs. laser spot size.....	65
4.9	Clad width as a function of traverse speed.....	67
4.10	Clad width as a function of energy density.....	68
4.11	Clad width as a function of powder feed rate.....	68
4.12	Parabolic shape of the cross-section of a single cladding track.....	70
4.13	Clad thickness as a function of traverse speed.....	74

4.14 Clad thickness as a function of powder feed rate.....	75
4.15 Energy density as a function of reciprocal of spot size.....	76
4.16 Energy density as a function of reciprocal of traverse speed.....	77
4.17 Energy density as a function of laser power.....	78
4.18 Clad thickness as a function of energy density.....	80
4.19 Penetration depth as a function of energy density.....	80
4.20 Overview of the transverse section of cladding tracks or layers. (a) High dilution. (b) Optimized condition. (c) Porosity. (d) Lack of fusion. (e) Inclusion. (f) Cracking A: Clad. B: Base metal.....	82
4.21 Schematic drawing of the transverse section of multi-track overlapping.....	86
4.22 Schematic drawing of cladding and intermixing zones for calculating dilution ratio.....	87
4.23 Optical microstructure of the transverse section of a cladding track, showing a low intermixing zone.....	88
4.24 Schematic drawing of multi-track overlapping to produce a platform layer by laser cladding process.....	89
4.25 Schematic drawing of transverse geometric shapes of single cladding tracks. (a) Small aspect ratio. (b) Desirable aspect ratio.....	91
4.26 An overview of lack of fusion forming under the following condition: two adjacent tracks with a small aspect ratio overlap. Unetched.....	91
4.27 An overview of near-net-shaped cutting blades deposited on a steel roller by laser cladding process. (a) As-cladded condition. (b) After machining [4].....	93

4.28 Overview of carbides in CPM 10V and D2 alloys. (a) Fine vanadium carbide uniformly dispersed in the matrix in CPM 10V tool steel. (b) Segregation and flake morphology of coarse chromium carbides in D2 alloy.....	95
4.29 SEM micrograph of clad bead, showing morphology of vanadium carbides.....	96
4.30 Microhardness profiles of the cladding track. (a) As-clad. (b) As-clad + tempering. (c) As -clad + tempering + liquid nitrogen treatment.....	97
4.31 Photos of LMMC samples. (a) Buildup coupon (sample 2). (b) Square (sample 3).(c) Saddle prototype (sample 4) with smooth surface via laser cladding.....	101
4.32 A view of LMMC cylinder prototype produced by laser cladding (sample 5). (a) is a good sample, and (b) and (c) show some forming defects as discussed in this section.....	103
4.33 An overview of the cross section of LMMC samples 6 and 7. A and C are tool steel CPM10V layers, while B and D are stainless steel layers. E is heat-affected zone [87].....	105
4.34 Higher magnified optical micrographs of laser clad stainless steel 304L layer. (a) Cellular dendrite structure. (b) The same sample, but higher magnified micrograph shows the precipitated carbides dispersed in the austenite matrix.....	106
4.35 Overview of X-ray dot mapping of sample 6. (a) SEM micrograph of 304 stainless steel-1045 steel interface zone. (b) Chromium distribution in the inter-diffusion zone. (c) Nickel distribution in the inter-diffusion zone.....	108
4.36 X-ray dot mapping of sample 6. (a) SEM micrograph of CPM10V tool steel and SS304L stainless steel interface zone. (b) Chromium distribution in the inter-diffusion zone. (c) Nickel distribution. (d) Vanadium distribution.....	109
4.37 Vickers hardness profile of LMMC sample 6.....	110

4.38	A temperature distribution of a laser beam and substrate interaction without powder feed.....	113
4.39	Temperature distributions on the surface of the substrate as a function of the distance from laser beam center along y-direction [102].....	113
4.40	Surface temperature at laser beam center as a function of laser power input [102].	114
4.41	Temperature distributions of laser cladding process under given process conditions [102].....	116
4.42	Temperature gradients along y direction [102].....	116
4.43	Temperature distribution of laser cladding process under laser beam center. (a) CPM10V tool steel. (b) SS304L stainless steel. (c) IN-738LC nickel-base superalloy. (d) Carbide blend.....	117
4.44	Optical macrograph of the cross section of a single cladding track, and its processing conditions are given in Figure 5.43(a) [102].....	120

INTRODUCTION

1. Background and Motivation

I have been investigating a novel laser direct deposition of composite materials for manufacturing 3-D components in the past six (6) years. This process allows for either the direct production of an industrial component or rapid, and low-cost fabrication of tooling dies and injection molds. If this brand-new process can be successfully developed, it will significantly reduce production costs and time in getting a functional prototype or product ready for use.

Cutting, stamping, and corrugating dies have been widely used in packaging, automobile, and printing industries, and the like. For example, rotary cutting and scoring dies are extensively applied in packaging industry to cut and fold cereal and soft beverage containers, and cut facial tissues, paper money, credit cards, high way tickets, and disk floppies, and so on. The cutting speed is fast, and impact loads or shear stresses are large, and thus the service life of rotary cutting dies is usually very short. Typically, such rotary cutting dies can work for a few months depending on the chemical composition, hardness, and other physical or chemical properties of the materials to be cut.

In conventional cutting-die manufacturing process, both die body and cutting blades are made of an expensive tool steel, such as D2 and M2. In order to prevent the distortion of cutting blades, the entire die body is first quenched to obtain the hardness of approximately HRC 60, then the hardened body is machined by electrical discharge machining (EDM), or photochemical etching to produce the cutting blades. Thus, for the conventional process, the cost of materials is high, the process is time-consuming and

complicated, the production efficiency is very low, and the overall production costs are extremely high. Moreover, conventional tool steel ingots often inherit the pronounced segregation and flake morphology of carbides, and give rise to a coarse non-uniform microstructure. This causes poor mechanical properties along the transverse direction. The larger the tool steel ingots, the poorer is their mechanical properties. For this reason, the service life of cutting dies, made of conventional tool steel D2, is relatively short.

In order to greatly improve the durable life of cutting and stamping dies, a new wear-resistant tool material with hard surface and tough core, and/or an innovative process has to be sought to form patterned cutting blades, which can withstand imposed service loads without deformation, fracture, and excessive wear. Based on the practical application of cutting dies, only the cutting blades are used for cutting functions. Therefore, the die body made entirely of an expensive tool steel D2 is completely wasteful. It is highly desirable to develop a novel processing technique to produce such cutting and stamping dies at a significantly reduced production cost.

Laser surface cladding offers the potential to deposit new materials with required mechanical and physical properties onto various metallic substrates. In this process, an alloy powder or metal/carbide mixtures are allowed to interact with the laser beam on a substrate surface to form a rapidly solidified cladding layer, without affecting the performance of bulk material. The chemical compositions of the clad layer is usually very close or equal to those of the alloy powder used because the dilution of the cladding layer can be controlled by choosing optimized process variables. By laser cladding, high hardness and high wear-resistant, high corrosion-resistant, and high oxidation-resistant coatings, in the geometric contours and dimensions of cutting blades or a component, can

be deposited on selected areas and/or in a precisely defined pattern on a variety of metallic substrates [1-7]. In addition, laser surface cladding has many advantages over other competing techniques, such as plasma spraying, flame spraying, and tungsten inert gas (TIG) welding. Compared to plasma spraying, the laser process offers a good bonding between the coatings and the substrate, and a lower level of porosity. Compared to TIG welding, the laser surface cladding has the advantage of smoother coating surface, lower dilution, more economic use of expensive alloys, lower thermal distortion, less machining, higher process flexibility, and better suitability for on-line process control and automatic production [8, 9]. It is the advantages and the process flexibility of laser cladding technique that we have employed to directly fabricate functional tooling dies or 3-D components at a sharply reduced production cost, compared with the conventional process [10]. I have already done pioneer work in this field, and opened a novel application field of laser cladding process in tooling-die manufacturing industry.

Compared with the conventional cutting-die manufacturing processes, this new technology, in which cutting blades with required geometric patterns and dimension, are directly deposited by laser cladding onto a substrate, has many advantages:

1. Material cost can be greatly reduced because an expensive tool steel die body can be replaced by a cost-effective structural steel, such as AISI 1045 or 4140 steels.
2. Production costs can also be significantly reduced due to the elimination of costly heat treatment, and no or greatly reduced demand for electric discharge machining (EDM).

3. Durability of cutting and stamping dies is expected to be significantly improved because the wear resistant property of clad materials is much better than that of the tool steel D2, currently used in industry.
4. Production efficiency can be much higher than that for the conventional process due to the eliminated or greatly reduced demand on the EDM, and the elimination of the costly tool steel heat treatment.
5. Such a processing technique can also be used for repairing worn or damage cutting blades.
6. The new processing technology is more flexible because different substrates and clad materials, with desired mechanical and physical properties, can be chosen for various applications.

2. Scope

The aim of this research is to investigate the possibility and the feasibility of developing a novel technique for directly manufacturing cutting dies, and rapidly prototyping industrial components by laser cladding process. The detailed research scopes are described as follows:

1. Design a new powder feeding system to provide a stable, continuous, and accurate powder feeding rate, and deliver the powder stream coaxially into the molten pool on the surface of a substrate under the laser beam.
2. Investigate the effect of powder feeding systems (lateral and coaxial powder feeding mechanisms) on the laser cladding quality and geometry.
3. Perform preliminary experiments to obtain initial processing parameters, such as laser power, laser spot size, traverse speed, powder feed rate, and shielding gas flow rate.

4. **Develop a simple but realistic process model, governing various relationships between the clad thickness and different processing variables, and determine the minimum energy density for clad formation under the experimental condition.**
5. **Establish an embodied standard for evaluating laser cladding quality, and discuss the mechanisms of forming cladding defects.**
6. **Characterize the microstructures of cladding layer, interface, and heat-affected zone by using optical microscopy (OM) and scanning electron microscopy (SEM).**
7. **Eliminate any unacceptable defects in the clads, such as porosity, microcracks, and poor metallurgical bonding between the clad and the substrate by modifying the process parameters and other related factors.**
8. **Based on the fundamental study, investigate the feasibility of directly depositing 3-D components with required geometric patterns and dimension by laser cladding process.**
9. **Measure the microhardness of the samples produced by laser cladding, and compare these experimental values with those of tool steel D2 in order to support this brand-new process.**
10. **A successful laser cladding process is a rapidly solidifying process. Due to high cooling rate, fine microstructure is expected to be obtained. For above-mentioned special application purpose, the temperature distributions of clad zone, heat-affected zone, and substrate during laser cladding, will be investigated by using high temperature thermocouples.**

Chapter 1

REVIEW OF LASER SURFACE TREATMENT PRINCIPLE

1.1 Basic Principle of Laser Operation

The laser, which is an acronym for light amplification by stimulated emission of radiation, is a source of optical frequency radiation which is monochromatic, coherent, controllable, and intense. It is these properties that make such lasers as Nd:YAG (Neodymium-doped yttrium aluminum garnet) and CO₂ competing heat sources, which are being widely used for materials processing.

Laser requires the combination of population inversion, stimulated emission, and amplification. An amplifying medium or active medium, a means of excitation, and an optical resonator are the essential components for lasing to take place [11, 12]. The amplifying medium determines the laser wavelength and the type of excitation required. A medium can be potentially used as an optical frequency amplifier if the population of its energy levels can be changed so that there are more emissions than absorptions per unit time. This phenomenon is so called the population inversion, which is absolutely necessary for amplification of light to occur. Otherwise, a beam of light directing through the active medium with photon energy will be absorbed.

In terms of different energy state schemes, population inversion requires excitation of atoms or molecules to the higher laser level by pumping methods or means of excitation. Pumping methods includes optical pumping, gas discharge pumping, and chemical reaction pumping. The use of pumping methods really depends on the active medium. For Nd:YAG and CO₂ lasers, optical pumping and gas discharge pumping are

employed, respectively, to create excited atoms or the passages of an electrical discharge through gaseous media to produce collisionally excited atoms or molecules. The former is used to excite an Nd:YAG crystal to lase at 1.06 μm , and the latter is employed to excite a CO_2 gas laser at 10.6 μm .

The optical resonator consists of a system of mirrors. Such a device causes the light emitted parallel to its axis to reflect back and forth through the amplifier. When the amplifier gain is equal to the round trip losses in the resonator, then the combination of the amplifier and the resonator is at the threshold for lasing. Upon reaching or exceeding the threshold the light in the resonator traveling parallel to its axis is amplified many times. The fraction removed on each pass by transmission through the output coupler results in a laser beam. Such multiple use of the amplifier leads to highly energetic laser outputs.

1.1.1 Radiation Transitions

When an electron orbiting around the nucleus undergoes transition in energy levels, it either spontaneously emits or absorbs energy. These emission and absorption processes are known as radiation transitions. Associated with each transition is a specific quantum of energy and wavelength of the radiation, given by the following relation:

$$E_i - E_j = h\nu = \frac{hc}{\lambda} \quad (1.1)$$

where E_i and E_j are the energies at the excited state and the lower state, respectively, h is the Planck's constant (6.6×10^{-34} j-sec), c is the velocity of light (3×10^8 m/s), λ is the wavelength in meters, and ν is the frequency of the emitted radiation. $h\nu$ is the photon energy.

Two main methods are commonly used to pump or energize electrons in a laser cavity: (1) photon energy transfer (e.g., flash tube) and (2) transfer of energy by colliding with excited electrons or molecules in an electrical field. The result of either type of excitation is to pump an electron in a ground state to a higher energy level by absorbing a quantum of energy as described by Equation (1.1). This process eventually creates an inverted state. It has been found that energy absorption depends on material properties and the intensity of the radiation, while spontaneous emission is governed only by the internal properties of the material. Einstein had postulated that an additional type of radiation with proper intensity is responsible for laser operation. This is known as stimulated emission

1.1.2 Spontaneous and Stimulated Emission

An atom in an upper energy level spontaneously decays to a lower level, emitting a quantum of energy difference as a photon with the appropriate frequency to satisfy Equation (1.1). This release of photon energy is known as fluorescent or spontaneous emission. The emitted photon has arbitrary phase and direction, as shown in Figure 1.1. When an atom in an upper energy level is stimulated by incoming radiation of frequency ν_{ij} satisfying Equation (1.1) to give up its energy and fall to a lower energy level. The result of this process is that one photon interacts with the atomic system and two photons emerge. Both photons have the same frequency and travel in the same direction. Thus, the light intensity has been amplified during the stimulated emission process. It is the stimulated emission process which is responsible for laser operation.

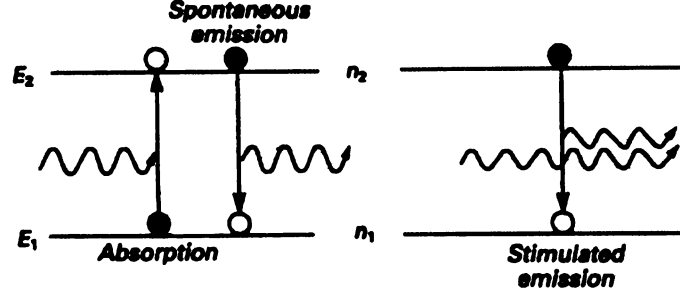


Figure 1.1 Types of emission processes between two energy levels [13].

Absorption of energy of light traveling in the z direction through a material with densities of atoms N_i and N_j in two energy levels is given by [14]

$$I_z = I_0 \exp(-\alpha z) \quad (1.2)$$

where I_z and I_0 are intensities before and after absorption, α is the absorption coefficient and is given (for a Gaussian line shape) by

$$\alpha = \left(\frac{c^2}{4\pi f^2 \tau} \right) \sqrt{\frac{\ln 2}{\pi}} \left(\frac{N_j}{\Delta f} \right) \quad (1.3)$$

where τ is the average fluorescent life time (relaxation time) of the material, c is the velocity of light in the material, f is the frequency, and Δf is the half-width of the Gaussian line.

Similarly, amplification of light energy by stimulated emission is given by

$$I_z = I_0 \exp(+gz) \quad (1.4)$$

where g is the coefficient of gain and is given (for a Gaussian line) by

$$g = \left(\frac{c^2}{4\pi f^2 \tau} \right) \sqrt{\frac{\ln 2}{\pi}} \left(\frac{N_i}{\Delta f} \right) \quad (1.5)$$

The similarity of the forms for α and g indicates that absorption and stimulated emission are inverse processes. The net effect of these two expressions can be written as

$$I_z = I_0 \exp \left[\left(\frac{c^2}{4\pi f^2 \tau} \right) \sqrt{\frac{\ln 2}{\pi}} \left(\frac{1}{\Delta f} \right) (N_i - N_j) z \right] \quad (1.6)$$

If $N_i > N_j$, the light intensity will increase as it travels; otherwise, light intensity will decrease. The condition $N_i > N_j$ should to be satisfied for lasing to occur. This condition is called "population inversion". The population inversion is simply having more electrons in a high-lying energy level than in the lower-lying energy level. Equation (1.6) indicates that, without the population inversion, there will be a net absorption at frequency f . With the population inversion, there will be light amplification by stimulated emission of radiation. The process of stimulated emission can cause photon yield amplification that travels in a particular direction. Thus, a preferential direction is established by placing mirrors at both ends of an optical cavity (resonator).

1.2 Laser-Beam Mode

The output of the laser is often characterized by its spatial and temporal coherence. Spatial coherence describes the phase relation in a plane perpendicular to the direction of beam propagation, temporal coherence indicates the phase relation in the direction of the beam. The spatial distribution of the electromagnetic field inside the optical cavity of a laser is described by resonant electromagnetic modes, which is referred to as the configurations of electromagnetic field inside a laser resonator cavity. By convention, the laser-beam profile is normally characterized by its transverse electromagnetic mode (TEM) and represented in the form TEM_{mn} , where the subscripts m and n (small integers) represent the number of nodes/nulls in the directions orthogonal to

the beam propagation. Thus, intensity distribution, beam diameter, and beam divergence along the plane of the laser beam's cross section are governed by the transverse modes. Figure 1.2 displays the intensity distribution in the plane perpendicular to the plane in which the mode distribution lies.

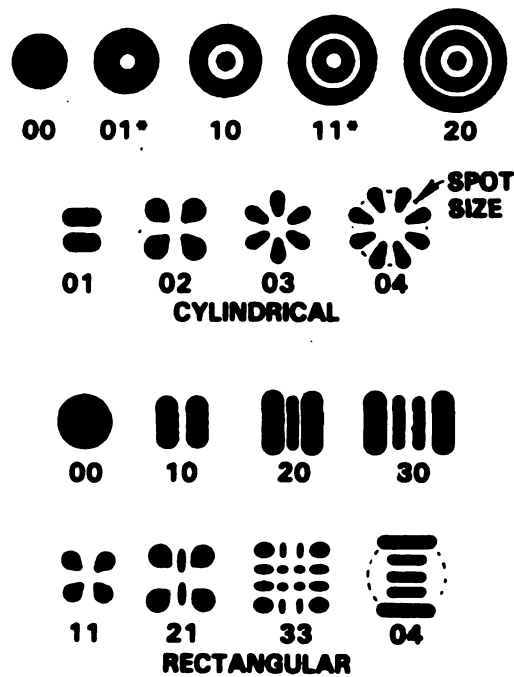


Figure 1.2 Transverse mode patterns of gas lasers in cylindrical and rectangular coordinates [15].

The transverse beam modes can be represented by either Cartesian coordinates or cylindrical coordinates. For rectangular symmetry, the notation TEM_{mn} is interpreted as the number of nulls which occur in the spatial pattern in each of the two orthogonal directions, transverse to the direction of beam propagation [16]. For cylindrical symmetry, the integer m indicates the number of nulls in a radial direction, and n indicates half the number of nulls in an azimuthal direction. The modes marked with an

asterisk are linear superposition of two modes rotated by 90° about the central axis [17]. In Figure 1.2, TEM_{01^*} mode is the linear combination of TEM_{01} and TEM_{10} modes. A laser beam with TEM_{01^*} has a ring of intense energy surrounding a circle with no intensity, and this mode is commonly referred to as the doughnut mode.

The above discussion about the mode patterns is related to gas lasers, such as the He-Ne laser and the CO_2 laser. Solid-state lasers such as the Nd: YAG laser and Nd: glass laser etc., exhibit more complicated spatial patterns, which are not easily describable in simple mathematical terms.

For laser surface treatment processes, low-order laser beams are usually used due to more uniform intensity distribution. Therefore, it is often desirable to obtain laser operation in the lowest order mode known as TEM_{00} mode (Gaussian mode). Compared with other higher order transverse modes, TEM_{00} mode has uniform intensity distribution, and low beam divergence. A plot of Gaussian intensity distribution (power per unit area vs. radial distance) is illustrated in Figure 1.3. The plot shows that TEM_{00} mode has maximum intensity at its center with exponential fall-off (decay) of the square of radius of the beam.

The intensity of the Gaussian mode as a function of radius r from the center of the beam is expressed by

$$I(r) = I_0 \exp\left(\frac{-2r^2}{r_0^2}\right) \quad (1.7)$$

where I_0 is the intensity of the beam at the center, and r_0 is the so-called Gaussian beam radius, where the intensity is reduced from its central value by a factor e^2 or e . It is more common to use the standard of $\frac{1}{2}$ of the peak intensity as the Gaussian beam radius. In

this case, the spot radius r_0 implies that at $r = r_0$, $I = \frac{I_0}{e^2} = 0.135 I_0$, i.e., approximately 86% of the total power is included. In the case of $\frac{1}{e}$, $I = 0.368 I_0$, which indicates that about 63% of the total power is accounted.

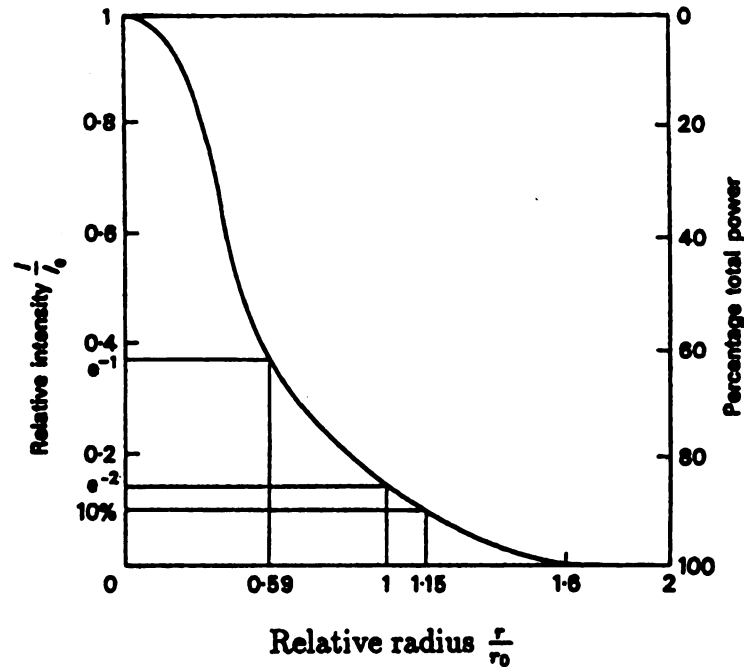


Figure 1.3 Variation of relative intensity and percentage total power with radius for a Gaussian TEM_{00} beam [18]. Note that for the vertical line representing e^{-1} , the value should read 0.71 instead of 0.59.

One of the important characteristics of laser radiation is the highly directional, collimated nature of the beam. The collimation is so important because it means that the energy carried by laser beam can easily be collected and focused to a small area. In terms of diffraction theory of light, for a monochromatic, circular light beam, the angle of divergence θ is given approximately by the equation

$$\theta = 1.22 \left(\frac{\lambda}{D} \right) \quad (1.8)$$

where θ is the wavelength of the light, D the diameter of the aperture through which the light emerges. Equation (1.8) implies that the divergence angle θ is inversely proportional to the beam size. Of all TEM_{mn} modes of laser beam, only Gaussian beam is truly diffraction-limited (the minimum value of the divergence angle θ set by Equation (1.8)) [19]. In other words, the Gaussian beam retains its Gaussian form as the beam transmits through optical systems. This represents the best case. Compared with the Gaussian beam, other TEM_{mn} modes exhibit larger beam divergence angles because they consist of two or more individual beams with different phases.

1.3 Laser Parameters

1.3.1 Laser-Beam Diameter

Laser-beam diameter is one of the two important variables determining the power density for a given incident laser-beam power. Because of the nature of the laser beam and the definition of the beam diameter, it is very difficult to measure the beam diameter for high-power laser beams. As has been stated before, the Gaussian beam diameter can be defined as the diameter where the laser power has dropped to $1/e^2$ or $1/e$ of the central value. The beam diameter defined on the basis of $1/e^2$ of the central value contains almost 86% of the total power, whereas the diameter defined on the basis of $1/e$ of the central value contains slightly over 60% of the total power. Therefore, the $1/e^2$ beam diameter is usually adopted [20].

Because the spatial distribution of energy in the laser beam affects the focusing characteristics of the beam, the laser beam can not be focused to one point on a workpiece surface. The diffraction-limited focal spot size, assuming no aberrations from the optical lens, is expressed by

$$d = 2(1.22 \frac{\lambda}{D})f\sqrt{(2M+1)} = 2.44(\frac{\lambda f}{D})\sqrt{(2M+1)} \quad (1.9)$$

where d is the focused beam diameter, f the focal length of the focusing optics, λ the wavelength of the laser beam, D the unfocused beam diameter, and M the number of oscillating modes.

For a Gaussian beam, $M = 0$, hence

$$d = 2.44(\frac{\lambda f}{D}) \quad (1.10)$$

In fact, the following relation is more commonly used to describe the focused spot diameter of a Gaussian beam

$$d = \frac{4\lambda f}{\pi D} \quad (1.11)$$

The actual value will be larger than the focused beam diameter calculated by Equation (1.11) due to aberrations and other imperfections of the focusing optic system.

1.3.2 Laser-Beam Power

Laser-beam power is one of the main processing variables for laser surface treatment. Incident laser power and laser-beam diameter determine the power density in the interaction zone, and laser power and traverse speed determine the treatable clad volume per unit time for a given powder feeding rate. The total power P of the Gaussian beam is given by following equation

$$P = \frac{\pi r_0^2 I_0}{2} \quad (1.12)$$

1.3.3 Power Density

Power density is defined as the incident laser-beam power per unit area. According to this definition, power density can be expressed by the relationship

$$P_d = \frac{P}{A} \quad (1.13)$$

where P_d is the power density, P is the incident laser-beam power, and A is the irradiation area. For a circular laser beam, for example, the irradiated area $A = \pi r^2$. The power density is a main parameter for laser materials processes since it determines the process functions, efficiency, and quality.

For power density values up to about 10^4 W/cm^2 , the absorbed energy depends on the wavelength λ , the material, and the surface conditions of the interaction zone. In general, this range of power density is suited for solid transformation hardening.

When power density values increase to the order of 10^5 W/cm^2 , the material in the interaction zone begins to melt in a hollow seam. This power density is typically used for the laser processes of conduction welding, surface melting, alloying, and cladding.

The powder density values in the order of 10^6 W/cm^2 leads to the formation of a vapor hole which is approximately focused laser spot size ("keyhole") surrounded by molten material. This situation will correspond to the processes of drilling and deep penetration welding.

Figure 1.4 clearly shows a relationship between power density and laser materials processes.

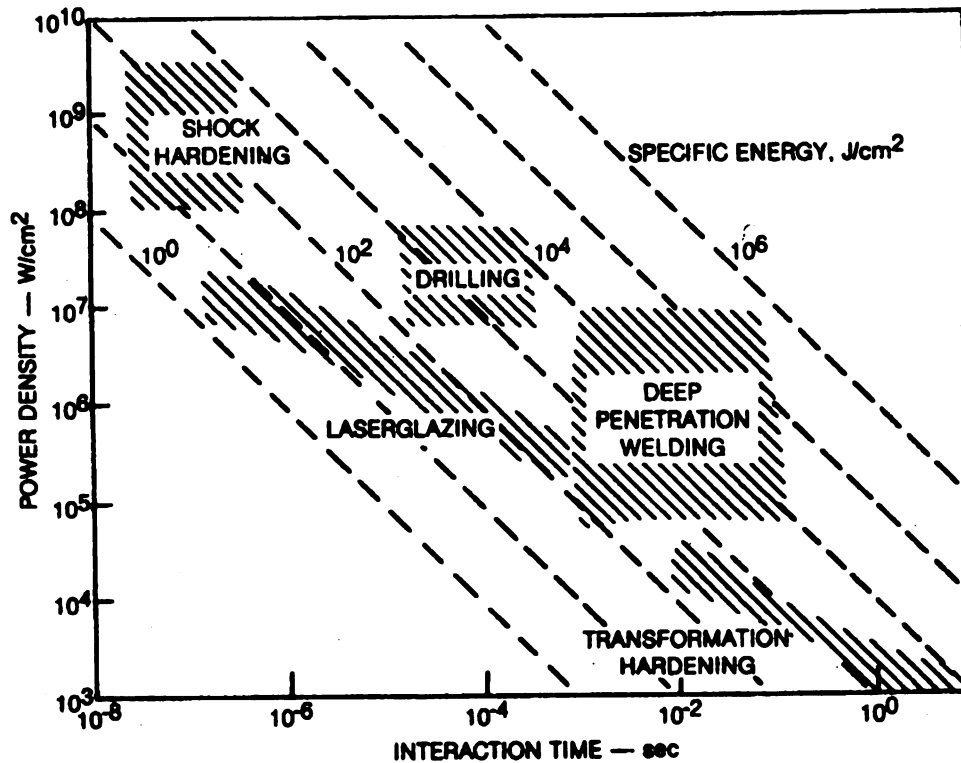


Figure 1.4 Laser materials interaction energy diagram [21].

1.4 Industrial Lasers

Lasers are being used in manufacturing industries ranging from automobile and tooling-die to gas turbines. They can be coupled with CAD/CAM systems to produce functional prototypes and industrial components economically. The various types of lasers commercially available include solid-state lasers (Ruby and Nd: YAG lasers), gas lasers (He-Ne and CO₂ lasers), and semiconductor (diode) lasers (GaAs laser), and so on. Of the various types of laser systems, Nd: YAG and CO₂ laser are widely used in fabrication of industrial components from metals, alloys, and composites.

1.4.1 The Nd:YAG Laser

The most commonly used solid-state laser is the 1.06 μm Nd: YAG (Yttrium aluminum garnet, $\text{Y}_3\text{Al}_5\text{O}_{12}$) laser. Neodymium-doped yttrium aluminum garnet (Nd: YAG) crystal possesses a combination of properties uniquely favorable for laser operation. The YAG host is hard, of good optical quality, and has a high thermal conductivity. Furthermore, the cubic structure of YAG favors narrow fluorescent linewidth, which results in high gain and low threshold for laser operation. In Nd:YAG, about 1% trivalent yttrium is substituted by trivalent neodymium, so charge compensation is not required. While Nd^{3+} ion exhibits a satisfactorily long fluorescence lifetime and narrow fluorescence linewidths, and possesses a terminal state for the laser transition sufficiently high above the ground state so that continuous-wave operation at room temperature is readily feasible. Therefore, this ion is usually incorporated as a dopant, called lasing medium. Due to special properties of trivalent neodymium, a higher power level has been obtained from Nd lasers than from any other four-level material [22, 23].

A simplified energy level diagram of the Nd^{3+} ions in the YAG crystal is illustrated in Figure 1.5, with conventional spectroscopic notations for the energy levels. All the excited higher levels relax non-radiatively to $4\text{F}_{3/2}$ level. The 1.06 μm laser transition is between the $4\text{F}_{3/2}$ and $4\text{I}_{11/2}$ level. The lower laser transition level, $4\text{I}_{11/2}$ is 2000 cm^{-1} above the ground state ($4\text{I}_{9/2}$) and will normally be unpopulated at room temperature. This indicates that the Nd: YAG laser operates on a four -level system and that the threshold for lasing is low.

The Nd: YAG laser is excited by light from an electric discharge lamp. Xenon flash lamps and krypton filled discharge lamps are most commonly used for excitation

purpose. The excited Nd^{3+} ions in the YAG host in a proper optical resonator can cause the stimulated emission at a number of frequencies within three different groups of transitions centered at 0.9, 1.06, and 1.35 μm . The most efficient laser operation is obtained when the optical resonator is designed for 1.06 μm . This is the wavelength used in Nd:YAG lasers for materials interactions.

Recently, Nd:YAG lasers become of interest for materials surface treatments because multi-kilowatt systems now are available on the market. The maximum power for Nd:YAG sources that can be purchased is about 2.5 kW in continuous-wave mode or about 3 kW average power in a pulsed laser system.

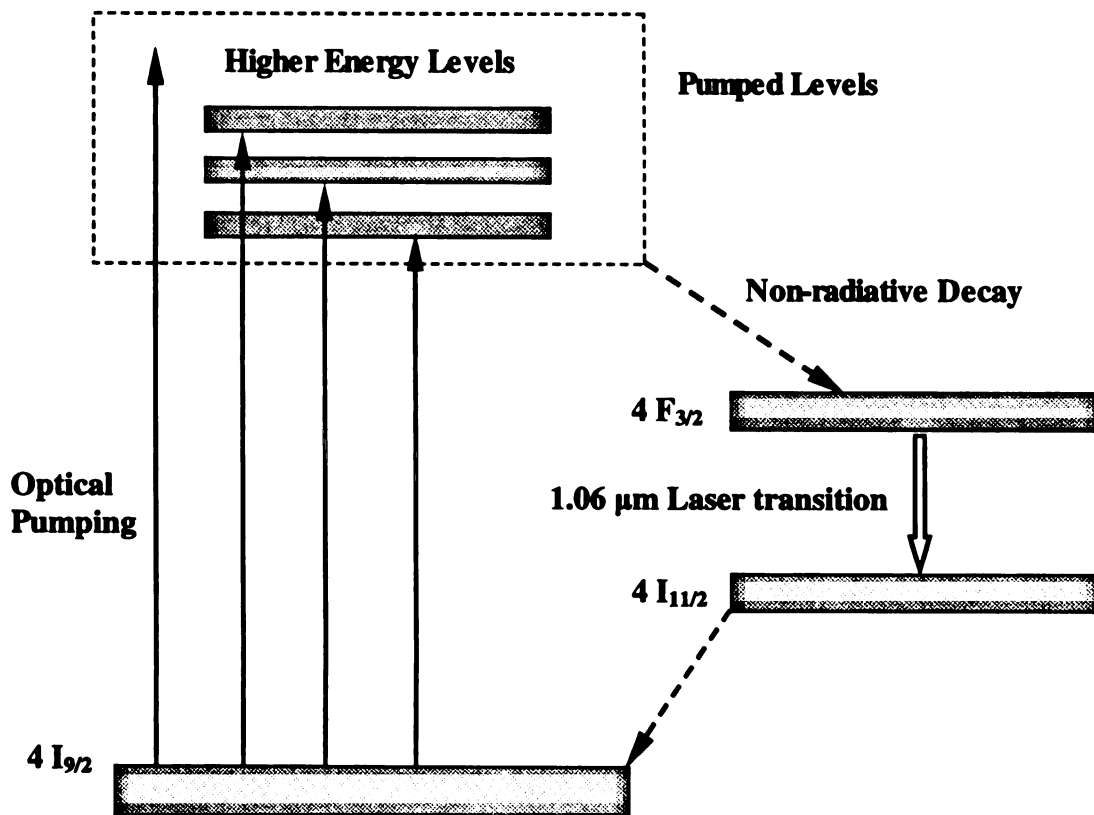


Figure 1.5 Energy level of Nd: YAG laser [24].

1.4.2 The CO₂ Laser

Among many types of gas lasers, the most important molecular laser is carbon dioxide laser. Just as its name implies, the carbon dioxide laser uses CO₂ gas as its active medium. It has been found that the carbon dioxide molecule is a linear molecule, and three atoms lie in a straight line with the carbon atom locating in the middle. Therefore, there are three different types of vibrations which can occur in the carbon dioxide molecules. These vibration modes are called as symmetric vibration, bending vibration and asymmetric vibration respectively, which are illustrated schematically in Figure 1.6 [25].

Symmetric vibration mode V_1 : the carbon atom remains stationary, and the oxygen atoms oscillate about their equilibrium positions as illustrated by the arrows. At any given time, the oxygen atoms are moving in opposite directions along the line of symmetry.

Bending vibration mode V_2 : all the atoms are moving in a plane perpendicular to the line of symmetry. The carbon atom moves in one direction while the two oxygen atoms move in the opposite direction.

Asymmetric vibration mode V_3 : all the atoms move along the line of symmetry. At any given time, the carbon atom is moving in a direction opposite to the two oxygen atoms.

For the different vibration modes mentioned above, the energy associated with them is quantized, based on the principle of quantum mechanics. In the ground vibrational state, there are no vibrational motions. The excited states correspond to excitation of one or more quanta of vibrational energy. The molecule can vibrate in more

than one mode at the same time, and thus it can have more than one quantum of vibration energy in each mode. For convenience, the notation adopted to denote the states is in the form (ijk) , where i, j , and k are integers denoting the quanta of vibrational energy in each of the three modes. The integer i corresponds to the symmetric vibration, j to the bending vibration, and k to the asymmetric vibration.

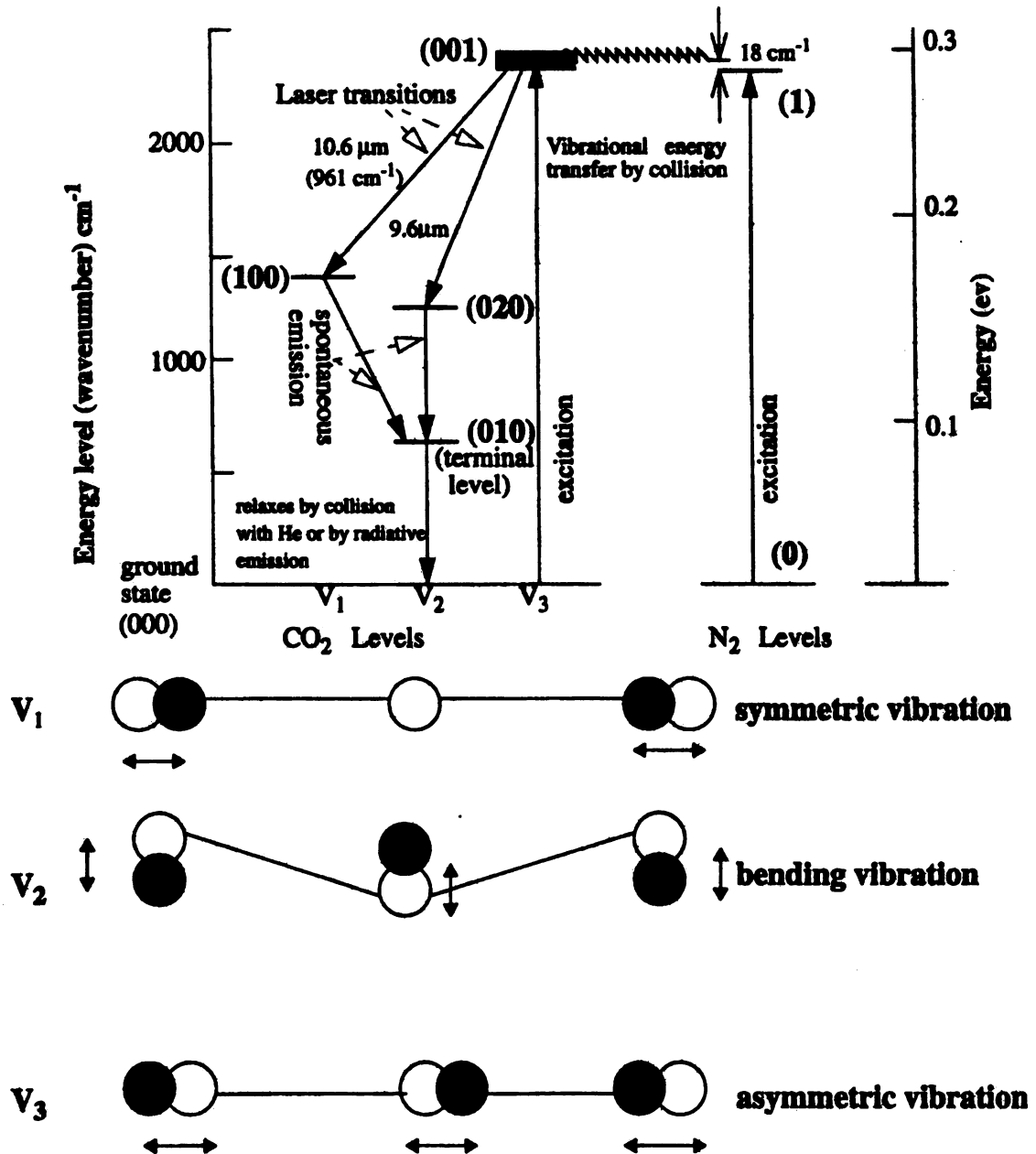


Figure 1.6 Three vibrational modes and various energy levels for CO₂ laser [25].

Figure 1.6 Three vibrational modes and various energy levels for CO₂ laser [25].

In carbon dioxide lasers, carbon dioxide, nitrogen, and helium gases are mixed in the laser tube. The gas tube is placed in an optical resonator. When the gas discharge is induced by applying the electric field to the gas tube, the electronic bombardment and the ionic collision with helium ions excite the nitrogen molecules to their vibrational quantum states (001). When the excited nitrogen molecules collide with ground state (000) CO₂ molecules, the nitrogen molecules transfers their energy from the collisions to CO₂ molecules, and then return to the ground state. The CO₂ molecules in the ground state are excited to the higher energy state by this bombardment. When the excited CO₂ molecules take downward transitions to the lower energy state, the transitions will produce a population inversion between the (001) state and the (100) state, as shown in Figure 1.6. Although there is another state (020), which shares a common upper state with the (001) state, the probability of transition to the (020) state is only about one-twentieth to the (100) state. The most of laser operation in CO₂ laser proceeds at the wavelength of 10.6 μm. The addition of helium to the gas mixture can also increase the output power. Because helium gas tends to deplete the CO₂ population on the lower laser level (010) by collisions and tends to keep the gas mixture cool due to the high mobility of helium atoms. Because of the relaxation effect of helium, carbon dioxide molecules in the lower energy level eventually return to their ground states. This process cools the CO₂ gas and reduces losses due to absorption of 10.6 μm light by lower to upper laser level transitions.

Since the useful transitions in a carbon dioxide laser are based on vibrational molecular quantum states, the transition energies are low. Therefore, carbon dioxide laser operates in the infrared wavelength.

Although the transition energies are low, the transition energy per unit time is large or the operational power is high. Today high power continuous-wave CO₂ lasers are commercially available with output power up to 25 kW.

1.5 Laser Beam-Material Interaction

In metals, the incident laser radiation is predominantly absorbed by free electrons in the conduction band. The photon of the incident laser radiation has relatively low energy. For example, the energy of CO₂ laser photons is only 0.12 eV while the photons obtained from the Nd:YAG laser have about 1.2 eV of energy. When a laser beam strikes a metal surface, heat transfer occurs by photon/electron interactions with free or bound electrons. These interactions raise the energy state of the electrons in the conduction band. The excited electrons collide with other photons and electrons, and give back their radiation by spontaneous emission. In this way, the electronic energy derived from the photons of the incident laser radiation is converted into the heat energy. It is this heat energy that is used for laser materials processes. In practice, most metals behave in this manner for light wavelengths exceeding about 0.5 μm , which includes both YAG and CO₂ lasers. Previous studies have shown that most of this absorption occurs in the shadow surface layer of metals, typically a few atomic layers, so that laser absorption in metals is truly a surface effect.

The interaction of high-power laser radiation with metals is capable of providing a novel and useful processing tool. However, it is difficult to obtain effective energy coupling between the incident laser radiation and workpiece due to the high reflection of metals. At room temperature, most pure metals and alloys absorb the less of the incident laser radiation, about one percent for copper and tens of percent for steels, for example,

so that most of incident laser power is reflected from the metal surface. In order to yield an effective process, it is necessary to obtain the adequate laser energy at the workpiece, and couple a fraction of the incident laser energy as high as possible into the materials.

The efficiency with which a material absorbs the incident laser radiation is defined as the materials absorptivity. It has been found that the absorptivity of a surface is a function of the materials, nature of the surface, the level of oxidation, temperature, and wavelength and power density of the incident laser radiation [26]. Therefore, improving the nature of a metal surface or use of lasers with shorter wavelengths can greatly enhance its absorption. For a CO₂ laser beam with 10.6 μm wavelength at normal incidence, the absorptivity of most metals is less than 10%, while for a Nd:YAG laser beam with 1.06 μm wavelength at the same incident angle, the absorptivity is up to 30%. In addition, increase in the roughness of a metal surface also can enhance the absorptivity by a factor of 1.2 to 1.5 due to surface contamination caused by machining process.

Although metals severely reflect CO₂ laser beams, up to now, the lasers used for material surface modifications mainly are CO₂ lasers due to their high available power level. In order to improve the absorptivity of metals at 10.6 μm wavelength of CO₂ laser beams, surface coatings, such as colloidal graphite coating and paint coating, and surface oxidation by chemical or heat treatment processes [27, 28] are widely used in industry. By these processes, the absorptivity can be increased to the values of 70 to 80%.

Chapter 2

LASER SURFACE TREATMENT

The use of high-power laser beams has opened a novel category of processing opportunities in metal surface treatment and composite material fabrication. Laser materials processing is characterized by concentrating an extremely high power density on a small area of the alloy surface to achieve very rapid heating and cooling of the near surface of materials. During laser irradiation, with or without alloy powder injection, the substrate surface can be modified by changing either its alloy composition and structure, or only its structure. Because laser surface treatment (LST) belongs to a kind of rapid melting and solidifying process, it can extend solid solution, form metastable phases, refine the grain size, and hence improve the wear resistant, corrosion resistant, and oxidation resistant properties of the treated materials.

Depending upon the main processing variables, power density and interaction time, different laser surface treatment processes, such as laser hardening, remelting, surface alloying, dispersing, and cladding, have been developed. The definition and function of laser surface modifications are succinctly described as follows:

2.1 Laser Solid-Transformation Hardening

The laser surface hardening is usually used to harden the selected surface area of iron-base alloys such as mild carbon steel, tool steel, and cast iron, etc. A basic feature of laser-induced transformation hardening is so called self-quenching. Such a process is based on the basic principle similar to the conventional heat treatment: the surface layers of an alloy is heated locally to transform to austenite, and is then rapidly quenched by

conducting heat to the bulk material (self-quenching). This process leads to the formation of a certain volume fraction of the martensitic phase transformation at the surface layers of a substrate. To produce large temperature gradients, short dwell times are necessary in order to avoid too much temperature rise in deeper layers. Determined by laser power input, spot size, and traverse speed, typical dwell times during the process are approximately between 0.1 and 5 seconds. As a result, the total heat input of the workpiece is low, and thus its distortion can be minimized.

Typically, laser heat treatment produces two zones: one is the hardened zone, and the other is the transition zone. The hardened zone is referred as to the area with a desired hardness and a hardened depth. The hardened zone is surrounded by a transition zone, a region of less effectively hardened material. Reduced effectiveness of treatment is caused incomplete heating. Compared with the conventional heat treatment process, laser solid-transformation hardening has following advantages [29]:

- Low energy input to the workpiece results in low distortion upon heating.
- Self-quenching into the cold rigid bulk of the workpiece causes little distortion upon cooling.
- Energy can be more efficiently used due to local heating of the treated surface area.
- Process is more flexible because laser beam can be directed to reach the complex geometric parts of a workpiece.
- Laser heat treatment can often achieve a higher hardness due to rapid heating and cooling.
- External quenchants are not needed due to the process characteristic so that fumes and dirt from heating and quenching can be minimized.

Due to the above advantages, laser heat treatment has been widely used in manufacturing industries to improve the wear resistance and fatigue properties of the treated materials or components [30-34], such as camshaft, crankshaft, extruder shaft, gear, and the like.

2.2 Laser Remelting

Laser remelting can improve the wear resistance and corrosion resistance of the thin surface layers of different alloys by homogenizing and refining the surface microstructure through rapid self-quenching. Through this process, high heating and solidification rates can generate supersaturated solutions, metastable phases, or amorphous structures. For this reason, the properties of the treated surface layers can be improved. Taking tool steels for example, due to the high solidification rates, carbon diffusion is suppressed, and the high temperature phases with their increased solubility limits are quenched down to the room temperature. The resulting fine and homogeneous microstructure of the remelted tool steel leads to the improvement of wear and corrosion resistance. The metallic materials suitable for laser remelting process include cast iron [35-39], aluminum alloys [40, 41], low and medium carbon steels [42, 43], and tool steels [44, 45]. In comparison to laser-induced transformation hardening, the laser remelting process requires a higher power density. This density can be achieved by increasing laser power input at a given laser-spot size.

2.3 Laser Surface Alloying

Unlike laser remelting process, laser surface alloying is usually used to change both chemical compositions and microstructures of the surface layers of a substrate by simultaneous surface melting and injection of alloying elements, and hence creates a new

surface alloy with the novel structures and required properties, such as wear resistance, corrosion resistance, and high-temperature oxidation resistance. The chemical composition of the formed surface alloy not only depends on the composition of the materials involved, but also on the degree of mixture. In other words, the base material and the added materials must be adapted each other to achieve the required structures and properties. By laser alloying process, the high temperature in the melt pool can dissolve the stable phases like intermetallic compounds, and the convection in the melt pool causes a good intermixing of the molten substrate with the alloying elements added, and the rapid solidification leads to the formation of fine and homogeneous structures. Laser surface alloying with alloying elements, such as C, Ni, Cr, Mo, W, Co, Mn, and Ti, is usually used to improve the wear resistance and corrosion resistance of different kinds of steels [46-54], aluminum alloys [55, 56] and titanium alloys [57, 58].

2.4 Laser Dispersing

Laser dispersing is a special type of alloying process. During this process, the carbide particles with a high melting point are injected into the melt pool so that composite layers form after rapid solidification. The formed composite layers mainly consist of the injected hard particles uniformly dispersed in the metallic matrix with a lower melting point. In order to obtain a good wear behavior of the layers produced by laser dispersing, a low dissolution of the injected hard particles is necessary. For laser dispersing, metal carbides, such as WC, TiC, VC, Mo₂C and SiC, are usually used as hard particles. A significant number of publications report that this process has been developed to inject hard carbide particles into different metal substrates, such as steels [59-64], aluminum alloys [65, 66], and titanium alloys [67-69], and wear resistance of the surface

layers has been significantly improved. Because high percentage of carbides may lead to the reduction in ductility of the composite layers, the dispersing process possibly causes cracking [70].

2.5 Laser Surface Cladding

2.5.1 General Description

Laser surface cladding is a process in which an alloy powder or metal/carbide mixtures are allowed to interact with the laser beam on the surface of the substrate to form a rapidly solidified cladding layer with the required properties, such as high hardness, high wear resistance, high corrosion resistance, and high-temperature oxidation resistance, without affecting the performance of the bulk material. Unlike laser alloying, the chemical composition of the clad layer is usually very close to that of the alloy powder used because the dilution of the cladding layer can be controlled by choosing optimized process variables. Generally, a good clad has following characteristics: uniform coating thickness and smooth surface, free of porosity and cracks, minimum dilution and distortion, and good metallurgical bonding with the substrate.

2.5.2 Scope of Laser Cladding

For laser cladding process, different kinds of ferrous and non-ferrous alloys as well as superalloys are usually used as the substrates, and the clad materials used really depend on the application purposes. For example, laser cladding with reinforcement materials, such as Fe-Cr-C-W, Co-Cr-C-W, Ni-Cr-B-Si or Fe-Cr-Ni, is widely used to improve the wear and corrosion resistance of plain and mild carbon steels [71-76]. Laser cladding with nickel base alloys is used to improve the wear resistance of aluminum

alloys [77, 78]. Laser cladding with Ni-Cr-Al-Hf improves the high temperature oxidation resistance of nickel-base superalloys [79, 80].

Laser cladding by carbide/metal composite powder on steels, aluminum, nickel, and titanium base alloys has shown its application potential for becoming a widely used hard-facing technique. Optimized combinations of basic material, metallic binder, and hard material allow the composite layers to be produced. The composite powder is usually made up of hard particles, such as SiC, WC, TiC, and VC, and ductile cobalt or nickel base alloys, and the produced cladding layers display high wear-resistant and corrosion-resistant properties [81-86].

In addition, laser cladding process is being used to produce functionally gradient composites or laminated metal-matrix composites [87, 88]. Such a process is displaying a broad application potentials in manufacturing industries.

2.5.3 Processing Parameters

Both applications and efficiency of laser surface treatments strongly depend on process variables. The main process parameters for laser cladding include incident laser-beam power and spacious energy distribution, laser-beam spot size and shape, laser absorptivity of both substrate and clad materials, traverse speed, powder feed rate, and shielding gas flow rate, and so on. Laser parameters are discussed in Chapter 1, and the remaining processing parameters are described in detail as follows:

2.5.3.1 Absorptivity

As has been stated before, for an optically opaque material, the absorptivity is referred to as the fraction of the laser energy absorbed by the substrate and the clad materials. It has been found that, because the infrared absorption of metals mainly

depends on the conductive absorption by free electrons, the absorptivity is a function of the electrical resistivity of the substrate. It was found that the absorptivity is proportional to the square root of electrical resistivity, and expressed as follows [28]:

$$A = 112.2\sqrt{\rho_r} \quad (2.1)$$

where A is the absorptivity, and ρ_r is the electrical resistivity.

Equation (2.1) shows that the smaller the electrical resistivity, the lower is the absorptivity. That is why most metallic materials, particularly copper and aluminum, have smaller values of intrinsic absorptivity. On the other hand, the apparent (extrinsic) absorptivity at a metal surface is considerably modified by its surface mechanical and chemical properties, such as roughness and oxidation [20, 28]. Therefore, the effective absorptivity also is a function of the surface condition of the substrate. Increased roughness or oxidation of the metal surface can greatly enhance the coupling of laser energy. In addition to the influence of the electrical resistivity and the surface condition, the absorptivity is related to the laser-beam wavelength [20]. In metals, absorptivity increases for shorter-wavelength laser beam. For example, absorptivity of the polished steel surface is about 30% for Nd:YAG laser with 1.06 μm wavelength, and is six times more than that for CO_2 laser with 10.6 μm wavelength. If the surface is oxidized, the absorptivity can increase to the value of 60% for CO_2 laser radiation.

In laser surface alloying and cladding processes, alloy powder has to be used. It is provided by either blowing the powder into the interaction zone or preplacing the powder on the surface of the substrate. In both cases, energy absorption has been observed to be significantly improved.

2.5.3.2 Traverse Speed

Traverse speed is the velocity at which the substrate moves with respect to the stationary laser beam. The ratio of the laser-beam diameter to the traverse speed defines the interaction time. For a given spot size, the reduction in traverse speed increases the interaction time. This will lead to the increase of the dilution, if other variables such as laser-beam power and powder feed rate, are held constant. On the other hand, variation of traverse speed has a marked effect on the dimensions of the cladding tracks. The clad width slightly increases and the clad thickness rapidly increases as the traverse speed decreases. When the power density and powder feed rate are held constant, the traverse speed has an upper and a lower limits. The high speed limit will cause cladding to cease due to insufficient energy input to melt the substrate surface, and low speed limit will lead to the high dilution or even the distortion of the substrate due to the high energy input. Therefore, for laser cladding process, suitable traverse speed has to be selected to ensure the mechanical properties of the cladding layer and the metallurgical bonding between the clad and the substrate.

2.5.3.3 Powder Feeding Techniques

There are two techniques to supply the alloy powder for laser surface alloying and cladding. One is the preplaced powder technique, and the other is the blown powder technique. The former is called the two-step process, while the latter is called the one-step process.

For two-step process, loose or paste-bound powder is preplaced on the substrate surface before laser irradiation [89, 90]. This process was used in the early stages of development of laser surface alloying and cladding. However, two-step process has many

drawbacks, such as weak metallurgical bonding with the substrate, uncontrollable clad thickness, and insufficient operation flexibility, so that it is not suitable for an automatic production environment.

For one-step process, alloy or carbide/metal composite powders are transported by an inert gas stream, usually argon or helium, and injected through a nozzle directly into the center of the laser beam/molten pool on the moving substrate. This method of powder supply is widely used due to its high process quality and flexibility. There are two manners to deliver the alloy powder into the molten pool: laterally injecting the powder into the molten pool [91, 92] or injecting the powder into the molten pool through a coaxial nozzle along with the laser beam [93, 94]. By using the coaxial nozzle, which was designed by researchers at High Energy Laser Processing (HELP) Laboratory, Michigan State University, the efficiency of powder utilization is up to 80% [95], and the localized areas of components of complex geometry can be deposited with better control on clad thickness and dilution by carefully selecting the processing parameters.

Powder feed rate is defined as the total powder amount supplied per unit time. The variation of powder feed rate greatly affects the clad thickness and dilution as well as its quality. If other variables are held constant, the clad thickness increases linearly, and the dilution decreases with the increase of the powder feed rate.

2.5.3.4 Shielding Gas

The shielding gas is usually used to protect the optical components from fume and spatter, and thus to ensure effective transmission of the laser beam to the interaction zone. The shielding gas also protects the molten material from oxidation. For laser surface alloying and cladding process, an inert gas such as helium or argon is usually used as the

shielding gas. However, since helium gas is expensive, argon gas is used as the shielding gas to reduce the production costs for laser cladding process.

Shielding gas flow rate has a great effect on the clad quality. Increasing the cover gas flow rate helps reduce the dilution of the clad by enhancing cooling rate (other processing parameters remaining constant). However, a high cover gas flow rate leads to the formation of porosity inside the cladding layer due to bubble entrapment. Therefore, the optimum shielding gas flow rate has to be selected to ensure the clad quality.

2.5.4 Advantages of Laser Cladding Process

Laser surface modification has many advantages over other competing techniques, such as plasma spraying, flame spraying, and tungsten inert gas (TIG) welding. Compared to plasma spraying, the laser process offers a good bonding between the coatings and the substrate, and a lower level of porosity. Compared to TIG welding, the laser surface cladding has the advantage of smoother coating surface, lower dilution, more economic use of expensive alloys, lower thermal distortion, less machining, higher process flexibility, and better suitability for on-line process control and automatic production.

2.5.5 Limitations of Laser Cladding Process

Laser surface treatment has many advantages, but it has some limitations. A main characteristic of all laser surface treatments is that the treated region is a narrow strip. For this reason, larger surface areas to be treated can be finished only by overlapping tracks. From the point of view of cost-effectiveness, laser surface treatments are just suitable for manufacturing costly and special industrial components. Obviously, it is this reason that limits the wider applications of laser cladding process in consumer product industries.

2.5.6 Applications of Laser Cladding Process

Laser cladding technique was invented more than two decades ago. Since then, many researchers around the world, have been dedicating their investigation. One of such studies is production of surface coating, when laser is the tool for the surface coating work. Due to such great efforts, both theoretical and applicable aspects of interaction between a high energy laser beam and a solid material are approaching closer to the real-world applications. Some real-world applications of laser cladding in manufacturing industries are described as follows:

Mah [96] employed the directed light fabrication (DLF) process to deposit various complicated geometric components by laser cladding. The parts have straight sides, smooth contours, and sharp corners. This novel process is being substituted for the conventional process to fabricate the functional prototype of a newly developed product.

In tooling-die manufacturing industry, Mazumder *et al.* [97] directly deposited H13 tool steel powders by laser cladding to prototype injection molding and trimming dies. It was reported that the production period of such tooling dies was greatly shortened, and thus the production costs were dramatically reduced. Concurrently, Hu *et al.* [10] utilized a similar technique to deposit highly wear-resistant tool steel CPM15V on the mild steel die body to form near-net-shaped cutting blades, and manufactured cutting and stamping dies at a sharply reduced production cost, compared with conventional manufacturing process.

In aerospace industry, it is well recognized that Rolls Royce is a pioneer in taking advantage of the many benefits of laser cladding for production purpose. The first and the most well-known application is the cladding of interlocking edges of turbine blades at

Rolls Royce. A Cobalt-based alloy was deposited on the Nickel-based superalloy blades by laser cladding process using a 2 kW CO₂ laser, and the one-step powder feeding technique [98]. Since then, this new technique has been widely used to rebuild or repair the worn turbine blades and vanes.

In automobile industry, Toyota Motor Company developed a novel laser cladding process for producing engine valve seats [99]. By this process, the valve seats were directly formed on the cylinder head by cladding copper-based alloy powder on the aluminum substrate. It was reported that the temperature of the valves and their seats was reduced, the overall engine performance was improved, and the durability of the engine was enhanced three times in comparison to the conventional process of the valve seat preparation.

Now laser cladding process has demonstrated a great application potential in various manufacturing industries. The combination of laser cladding technique and advanced CAD (computer-aided design)/CAM (computer-aided manufacturing) system can be employed for rapidly prototyping industrial components, manufacturing tooling dies with required geometric shapes and larger dimensions, and repairing both aerospace and industrial turbine blades and vanes.

Chapter 3

EXPERIMENTAL PROCEDURES

3.1 General Description

This research mainly consists of the following parts: (1) design an integrate coaxial powder feeding system; (2) develop a simple but realistic process model which governs various relationships between the maximum clad thickness and the process variables; (3) direct fabrication of 3-D components with different geometric patterns by laser cladding; (4) measure the temperature distributions of molten pool, heat-affected zone, and substrate during laser cladding process.

A combination of CAD (computer-assisted design)/CAM (computer-assisted manufacturing) systems and an integrated laser cladding system were used in this experiment. Thus, the reinforced materials can be precisely deposited onto metallic substrates in a preprogrammed geometric patterns, in order to reach the above-mentioned research goal.

3.2 Choice of Materials

The aim of laser surface cladding is to deposit reinforced materials with the required mechanical and physical properties onto different metallic substrates in order to alter their surface properties, such as wear resistance, corrosion resistance, and high-temperature oxidation resistance. Typically, cost-effective structural materials like plain or mild carbon steel, and aluminum alloy are used as substrates. The clad materials used depend on the application purposes.

3.2.1 Substrate Materials

As has been stated in INTRODUCTION, in the conventional manufacturing process of rotary cutting die, the entire die body and cutting blades are made of an expensive tool steel D2 or M2. However, in practical application, only cutting blades are used for cutting functions. Therefore, the die body made of tool steel is not necessary, and completely wasteful. In addition, the heat treatment cost of tool steel die body is also extremely expensive. In order to greatly reduce the costs of material itself and production, AISI 1045 medium carbon steel plates and rollers were used as the substrates in this study. The steel plates were used in modeling work and prototype of 3-D components, and its dimension was 100 mm x 50 mm x 6.35 mm. In addition, the steel roller was used for fabrication of the patterned rotary cutting die, and its dimension was 305 mm in length, and 101.6 mm in diameter. For all research projects, the substrate surfaces were polished by using a sandpaper to remove the oxidation layer and also to roughen the surface for improving coupling rate of the laser energy before laser cladding process. For convenience, the chemical compositions of AISI 1045 and 4140 steels, and Inconel 738LC (IN-738LC) nickel-based superalloy as well as reinforced materials are listed in Table 3.1.

In the investigation of measuring temperature distribution, AISI 4140 steel plates were used as the substrate, which had dimensions of 75 mm x 50 mm x 6.35 mm.

Table 3.1 Chemical compositions of substrates and clad materials (wt. pct)

<i>Materials</i>	<i>Fe</i>	<i>Cr</i>	<i>V</i>	<i>C</i>	<i>Mn</i>	<i>Mo</i>
1045 steel	bal.	---	---	0.43-0.5	0.6-0.9	---
4140 steel	bal.	0.8-1.1	---	0.38-0.43	0.75-1.1	0.15-0.25
AISI 304L	bal.	18.5	---	0.024	1.44	---
CPM10V*	bal.	5.25	9.75	2.45	0.50	1.30
CPM15V*	bal.	5.25	14.5	3.40	0.50	1.30
IN 738LC	0.50 max	15.70-16.30	---	0.09-0.13	0.20 max	1.50-2.00

<i>Materials</i>	<i>Si</i>	<i>Ni</i>	<i>S</i>	<i>P</i>	<i>Co</i>	<i>W</i>
1045 steel	---	---	0.05	---	---	---
4140 steel	0.15-0.3	---	0.04	0.035	---	---
AISI 304L	0.55	9.5	0.019	---	---	---
CPM10V	0.90	---	0.09	---	---	---
CPM15V	0.90	---	0.07	---	---	---
IN-738LC**	0.30 max	bal.	0.015 max	---	8.00-9.00	2.40-2.80

<i>Materials</i>	<i>Al</i>	<i>Ti</i>	<i>Ta</i>	<i>Nb</i>	<i>B</i>	<i>Zr</i>
1045 steel	---	---	---	---	---	---
4140 steel	---	---	---	---	---	---
AISI 304L	---	---	---	---	---	---
CPM10V	---	---	---	---	---	---
CPM15V	---	---	---	---	---	---
IN-738LC	3.20-3.70	3.20-3.70	1.50-2.00	0.60-1.10	0.007-0.012	0.03-0.08

* The chemical compositions of CPM 10V and CPM 15V clad materials are provided by *Crucible Materials Corporation*.

** The chemical compositions of IN-738LC clad material are provided by *Praxair Surface Technologies*.

3.2.2 Clad Materials

In order to significantly improve the wear resistance of cutting blades and prolong the service life of tooling dies, the clad materials used in this research were commercially available tool steel powders, CPM10V and CPM15V, which are made by the Crucible Particle Metallurgy (CPM) process. The particle size for CPM10V was -270/+325 mesh (44 - 55 μm), and for CPM15V was -140/+200 mesh (74 - 100 μm). The chemical compositions

of CPM 10V and CPM15V are listed in Table 3.1. For convenience, morphology of clad materials is shown in Figure 3.1.

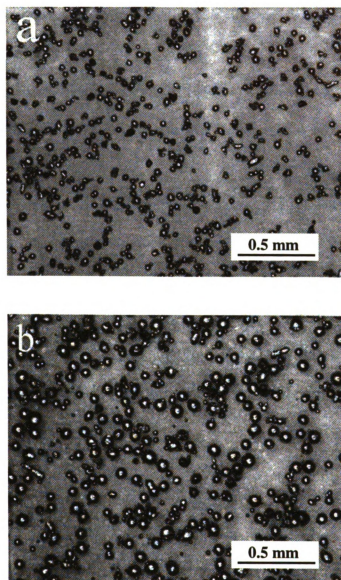


Figure 3.1 An overview of powder morphology. (a) CPM10V tool steel. (b) 304L stainless steel.

CPM10V was designed as a tough, air hardening alloy with added high carbon and vanadium for superior wear resistance, toughness, and strength for cold and warm tooling applications. It is these properties that make it an excellent candidate to replace other conventional wear-resistant materials in cold work tooling applications, particularly where tool toughness is a problem.

CPM15V contains 50% more hard vanadium carbides in its microstructure than CPM 10V, to provide even higher wear resistance. Therefore, it is intended for applications requiring exceptional wear resistance.

As a result of pronounced ingot segregation, conventional tool steels often contain a coarse, non-uniform microstructure accompanied by inferior mechanical properties along the transverse direction. However, tool steels CPM10V and CPM15V produced by the CPM process exhibit very homogeneous microstructures with uniformly dispersed spherical carbides. These steels are characterized by exceptional wear resistance and relatively good impact toughness in comparison with conventional tool steels, such as D2 and M2, as shown in Figures 3.2 and 3.3 [100].

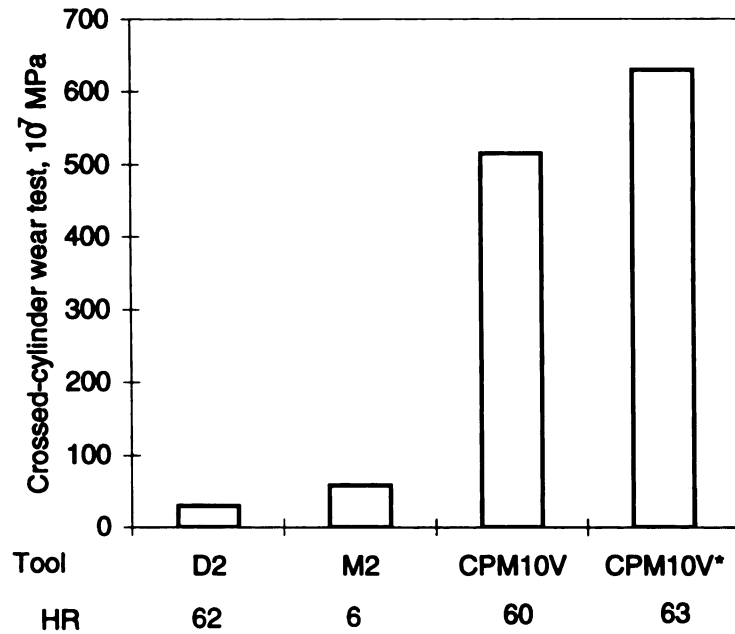


Figure 3.2 Wear resistance of CPM10V and conventional tool steels at indicated hardness [100]. CPM10V* (hardened) is subjected to quenching, which increases its hardness, and thus the extra wear resistance.

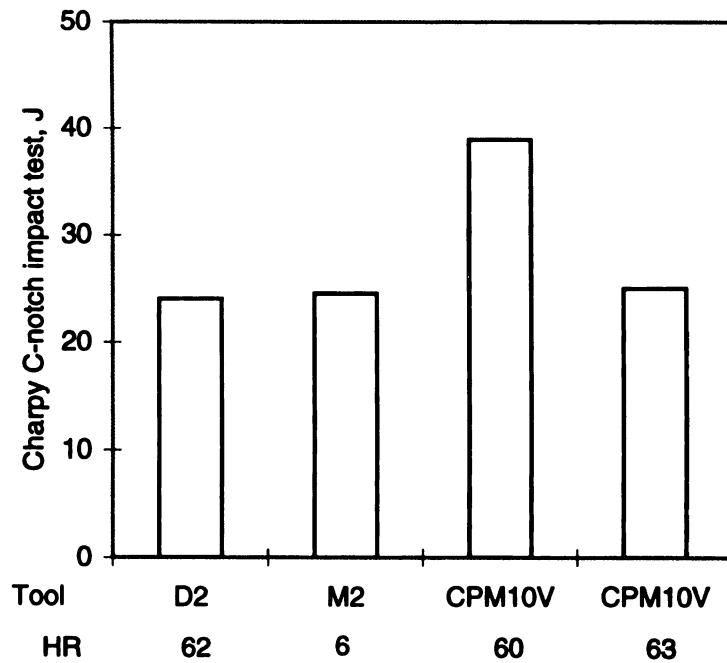


Figure 3.3 Charpy C-notch impact properties of CPM10V and conventional tool steels at indicated hardness [100].

AISI type 304L stainless steel is an austenitic Cr-Ni stainless steel. It has good corrosion resistance, and high ductility. 304L stainless steel also has excellent drawing, forming, and spinning properties. In addition, its low carbon content means less carbide precipitation in the heat-affected zone during the welding process and a lower susceptibility to intergranular corrosion.

A laminated metal matrix composite (LMMC) is defined as a composite material with alternate layers of a high-modulus, high-strength material as the strengthener, and a deformable ductile material as the matrix. Such a composite material can be directly deposited by laser cladding technique. In this study, 304L stainless steel and CPM10V tool steel have been used as clad materials. The particle size for 304L stainless steel powder ranges from -140/+325 mesh (44 - 100 μm). Its chemical compositions are listed in Table 3.1, and powder morphology is shown in Figure 3.1. The composite materials have been produced in such a way that the laminates consist of alternating stainless steel and tool steel layers or one stainless steel and two tool steel layers. Thus, the composite materials are characterized by hard surface, wear-resistance, and tough core, and possibly used to fabricate cutting blades of cold tooling dies, which require to withstand imposed service loads without premature deformation, fracture, and excessive wear.

The reinforced material used for repairing industrial and aviation gas turbine blades was commercially available IN-738LC superalloy thermal spray powder. Its particle size falls between -200 and +325 mesh (44 - 74 μm). IN-738LC filler material was produced by *Praxair Surface Technologies*. The chemical compositions provided by the manufacturer are given in Table 3.1.

3.3 Laser Cladding System

Laser cladding system mainly consists of a continuous-wave CO₂ laser, a set of optical mirrors, a powder feeding system, and a computer-assisted manufacturing (CAM) system. The experimental setup is shown in Figure 3.4.

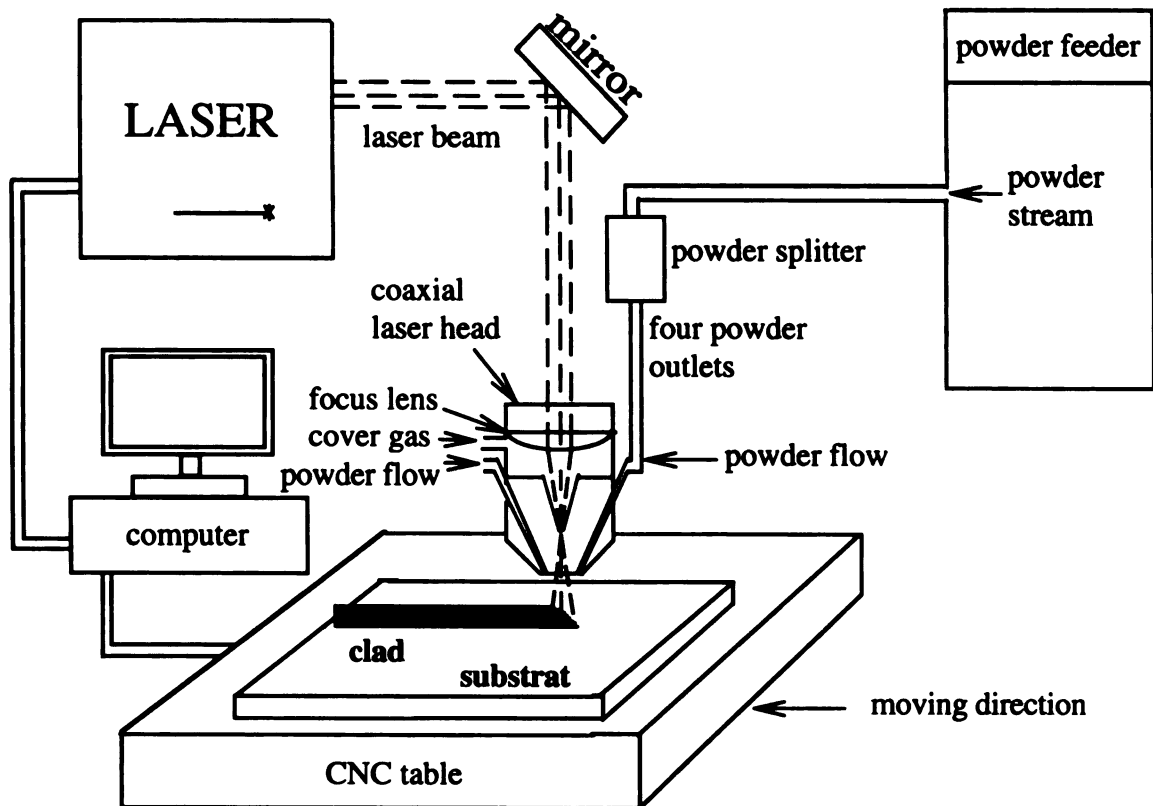


Figure 3.4 A schematic drawing of the laser cladding process [4].

3.3.1 CO₂ Laser

A continuous wave CO₂ laser operating in the TEM_{01*} mode, with an output power range of 200 to 2500 watts was used for laser cladding experiments. The characteristics of a 2500 L model Triumph (*Triumph Industrial Lasers Inc.*) laser are given in Table 3.2. For the purpose of this research, the CO₂ laser was operated in a continuous wave (cw) mode.

Table 3.2 Characteristics of the RF excited CO₂ laser

Parameters	Value/Type
Type of Laser	Fast flow coaxial CO ₂ laser
Mode of the beam	TEM _{01*}
Output stability	±2%
Beam diameter (raw)	≈ 18 mm
Excitation	RF excited
Temporal mode	Continuous and pulsed (1-10 kHz)
Maximum output power	2800 watts (continuous)
Wave length	10.6 μm
Gas consumption	He: 64 l/hr
	N ₂ : 12 l/hr
	CO ₂ : 3 l/hr

3.3.2 Beam Delivery System

Optical devices mainly consist of a beam bender mirror and a transmissive ZnSe focal lens with a focal length of 190.5 mm. Laser beam generated by laser machine travels along its optical axis to a beam bender mirror, then vertically reflects down to a focusing lens, and finally reaches the surface of a substrate for laser treatment process.

3.3.3 Powder Feeding System

The quality of laser cladding tracks depends upon the processing variables, and position, stability, continuity, and accuracy of the powder feeding. Even a small deviation of the powder flow rate, and the location of powder delivered with respect to laser beam

center, will lead to a significant variation of the geometry, thickness, and smoothness of cladding tracks [101].

Lateral powder feeding system, as shown in Figure 3.5(a), has been commonly used for laser surface alloying and cladding [91, 92]. However, in terms of our laser alloying, and cladding experience, such a feeding system has many drawbacks. First, it is difficult to align the location of the powder delivery with respect to the laser beam center. This positioning is very critical, and a small deviation will greatly decrease the powder utilization efficiency, and lead to a poor quality cladding tracks. Generally, the powder utilization efficiency for lateral feeding system is rather low, and falls between about 0.3 and 0.5, depending on the positioning accuracy of powder delivered with respect to laser beam center, and the divergence of powder stream. With side powder feeding systems, preheating or premelting of powder does not occur, as a result, cladding tracks are generally rough, and both thickness and width of tracks are not uniform. Second, side feeding system, once set up, might work reasonably well for a linear cladding track, but does not work for complex geometric patterns requiring bidirectional motions. Third, typically, the inclination angle between the delivery tube and horizontal plane is 25-35°, and the distance from the delivery tube tip to the interaction zone is about 12-15 mm, so the distance from the laser nozzle tip to workpiece requires a clearance of at least 20 mm. This gap is so large that the shielding gas is not fully able to protect the cladding surface from oxidation. If the cover gas flow rate is increased to overcome this problem, the powder is blown away. For these reasons, it is necessary to design a new powder feeding system, which produces high stability, continuity, and accuracy of powder flow, while, avoiding oxidation, under an actual production condition.

The integrated powder delivery system designed in this research, includes a close-loop powder feeder, a powder splitter, and a coaxial nozzle, as shown in Figure 3.5(b).

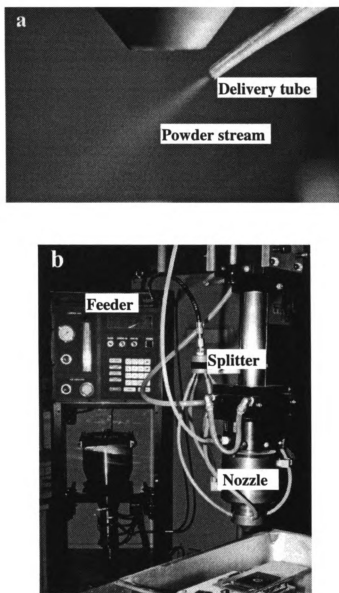


Figure 3.5 An overview of powder feeding systems. (a) Lateral powder feeding system. (b) Integrated coaxial powder feeding system.

3.3.3.1 Powder Feeder

A close-loop powder feeder (*METCO* Model 9MP) was used for providing a stable, continuous, and accurate powder feeding rate. The heart of the 9MP powder feeder is the proven fluidized-bed, powder regulating concept in which a carrier gas pressure differential is used to deliver the powder at precise flow rates. A microprocessor based weight-loss metering system continuously closed-loop monitors and controls powder feed rates. This system is capable of consistently delivering alloy powder at rates as low as 0.07 gm/sec.

3.3.3.2 Powder-Flow Splitter

The powder feeder transports the alloy powder, through a hose, to the powder splitter by using pressurized argon gas (called carrier gas). The powder stream is split into four streams of powder flow. These four streams are then carried through four tubes to the circumferential channel between the middle and the external nozzles.

3.3.3.3 Coaxial Nozzle

Figure 3.6 is a schematic diagram of the transverse section of our coaxial nozzle. The specifications of this design, however, were developed by researchers in *High Energy Laser Processing* (HELP) Laboratory, Michigan State University, based on our extensive preliminary investigations.

The coaxial nozzle consists of an inner nozzle, a middle nozzle, an external nozzle, and a water jacket for cooling. The inner nozzle has a channel, through which the focused laser beam passes, and a shielding gas flows. Positive pressure of this shielding gas prevents the particles from flowing up to the lens. As shown in Figure 3.6, the focal point of laser beam is positioned at the tip of the inner nozzle to allow minimum opening for most

effective protection of the lens. The shielding gas also protects the cladding layer from oxidation.

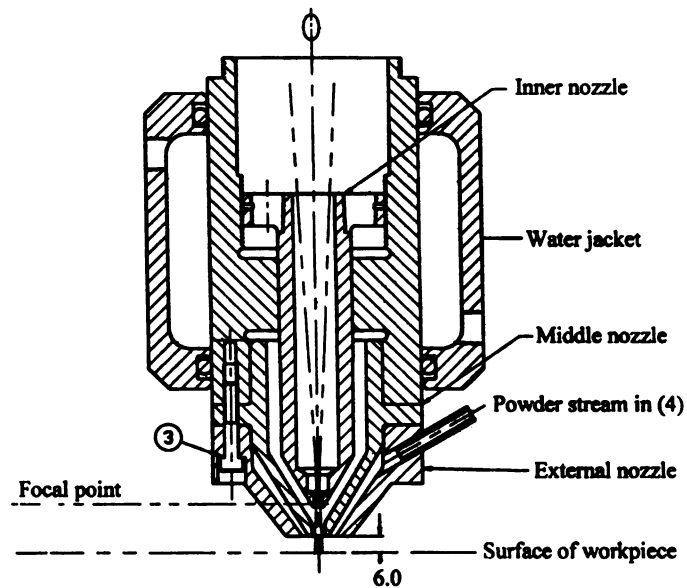


Figure 3.6 A schematic drawing of the transverse section of a coaxial nozzle [10].

The middle and the external nozzles form a cone-shaped circumferential channel, with 27° cone angle, where four parts of powder streams meet and converge to form a cone-shaped powder stream with the same central axis as the laser beam. Figure 3.7 shows the nature of powder flow through the coaxial nozzle. This cone of powder finally interacts with the laser beam on the surface of a workpiece to form cladding tracks. As a result of precise deposition of the powder with respect to the center of the laser beam, the powder utilization coefficient for our coaxial feeding system is up to about 80%. More details about

measuring the powder utilization coefficient are discussed in Chapter 4. Since the working distance, from the bottom surface of the coaxial nozzle to the specimen surface, is fixed at about 6-8 mm, spacers (each is 5 mm thick) are inserted between the middle nozzle and the nozzle block for adjusting defocus distance, which controls laser spot diameter on the work piece. Therefore, the range of spot diameter is between 1.8 mm and 3.4 mm.

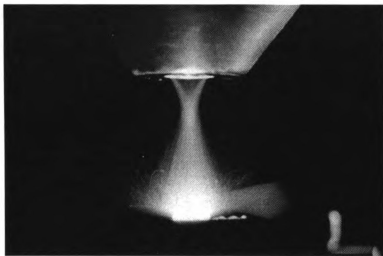


Figure 3.7 A view of cone-shaped powder stream irradiated by laser beam.

During laser cladding process, a considerable amount of laser radiation is reflected to the bottom surface of the nozzle, which heats it to a relatively high temperature. Therefore, a circulating-water cooling system is necessary to prevent overheating of the nozzle. From our study, this nozzle, equipped with cooling system, can work very well for a continuous long-time use, for manufacturing patterned cutting-dies via laser cladding.

This integrated powder delivery system avoids all of the drawbacks of a lateral powder feeding system. It can provide a highly stable, continuous, and accurate powder feed

rate, and deliver the powder stream precisely into the molten pool on the substrate to form high quality cladding tracks. Also, this system allows deposition of complex geometric patterns on a planar, or a curved surface for different applications, such as fabrication of cutting and stamping dies, repair of turbine blades, and rapid prototyping of industrial components. By adjusting the pressure of the coaxial cover gas, the amount of preheating of powder can also be controlled.

3.3.4 CAM System

Computer-assisted manufacturing (CAM) system was used for laser cladding experiments. CAM system consists of a high precision X-Y motion tables with a computer controller (General Numeric Inc.), and its specifications are given in Table 3. The specimen mounted on X-Y tables was translated under a stationary laser beam. The combination of CAM system with two linear axes and step motor was utilized to fabricate various 3-D components.

Table 3.3 CNC machine specifications

Description	Value
Range of motion	1.27 m x 1.27 m
Maximum traverse speed	0.254 m/sec
Maximum contour speed	0.127 m/sec
Accuracy	0.0166 cm/m
Resolution	0.0127 cm
Repeatability	0.00254 cm

3.4 Laser Cladding

Laser cladding experiments were carried out in three separate sets of experiments: (1) deposit tool steel CPM10V on AISI 1045 medium carbon steel plates for modeling work; (2) alternatively deposit stainless steel 304L and CPM10V on the 1045 steel plate to

fabricate 3-D components; (3) coat CPM10V on AISI 4140 steel plate for measuring temperature distribution during laser cladding.

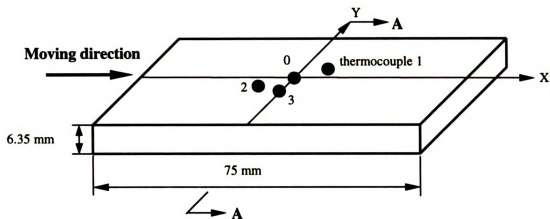
To date, no published literature has reported that tool steels, CPM10V and CPM15V, are used as hard-facing materials for manufacturing tooling dies by laser cladding process. Therefore, wide ranges of experiments were accomplished to fully develop such a brand-new and cost-effective process. The powder utilization coefficient was measured. The correlations between the clad width and process parameters were determined. Various relationships between the maximum clad thickness and process parameters were developed. And optimal process variables were investigated for fabricating 3-D components for real-world application.

In addition, the process parameters used in this research covered a wide range: Laser power varied from 1.1 to 2.4 kw; laser spot diameter from 1.8 to 3.4 mm; traverse speed from 3 to 14.3 mm/sec; and powder feed rate from 0.1 to 0.25 gm/sec. Argon was used as the shielding gas, and its flow rate was fixed at 0.85 m³/hr, which ensured to prevent the deposited coatings from oxidation during laser cladding. The detailed process parameters are given in different sections in order to clearly explain and discuss different relationships.

3.5 Temperature Measurement

Two types of thermocouples were utilized for measuring temperature distributions during laser cladding process [102]. One is Tungsten-Rhenium thermocouple (C type), and the other is Platinum-Rhodium thermocouple (R type). The upper limits for temperature measurement of C-type and R-type thermocouples, respectively, are about 2400 °C and 1480 °C. Both types of thermocouples have 0.127 mm diameter.

Liu *et al.* [103] used k-type thermocouple to measure the temperature distributions beyond welding zone, that is, heat-affected zone and base material. For convenience, we have adopted some part of his experimental setup. Four small holes with 1.88-mm diameter, were drilled from its bottom almost through top surface of a specimen in order to measure the temperature of clad zone. The top thin layer (10 μm) is very important for the temperature measurement of clad zone because, without this thin layer, laser beam will directly irradiate the thermocouple junctions, and thus easily burn the thermocouples out. The specimen dimension, and thermocouple layout and location are shown in Figure 3.8. The C-type thermocouple is located at the laser beam center, and three R-type thermocouples at the indicated positions. In addition, the thermocouples were inserted into ceramic tubes, which have 1.59 mm outside diameter and 0.40 mm inside diameter, to prevent the contact between two thermocouple wires. The thermocouple junctions were welded to the bottom of the blind holes using a capacitive discharge welding facility. Finally, the ceramic tubes were fixed to the workpiece using OMEGABOND 200 in order to strengthen the connection between the thermocouples and the specimen.



Thermocouple 0: $X=0$, and $Y=0$, Thermocouple 2: $X=-5$ mm, and $Y=-2$ mm,
 Thermocouple 1: $X=5$ mm, and $Y=1$ mm, Thermocouple 3: $X=0$, and $Y=-4$ mm (remelting),
 or $X=0$, and $Y=-5$ mm (cladding).

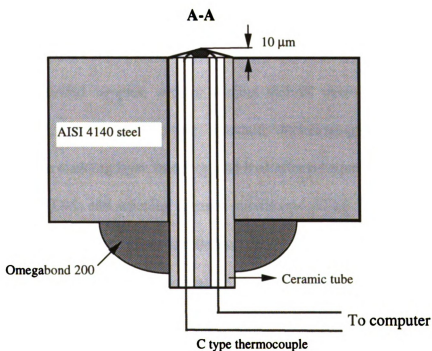


Figure 3.8 An overview of specimen dimension, thermocouple layout and location [102].

3.6 Post-Clad Treatment

Tempering treatment was carried out in a bench-top Lindberg 58114 wire element furnace with a microprocessor-base controller. It has a 1473 K temperature rating, and a stability of $-5/+5$ K at steady state. In terms of the heat treatment specification of tool steel CPM 10V, laser-deposited samples were tempered at 813 K (540 °C) for 15 minutes, and then cooled to the room temperature. This process repeated one more time (so called “double tempering”). The aim of tempering treatment in this study was to release the thermal stresses caused by laser cladding process.

Subzero treatment was carried out in liquid nitrogen. The tempered sample was dipped into liquid nitrogen for 15 minutes. This treatment led to the transformation of the retained austenite to martensite, and therefore the hardness was obviously increased.

3.7 Microstructural Characterization

The laser-cladded samples, with or without thermal treatments, were sectioned, mounted, polished, and etched using standard metallographic techniques. The microstructures of the cladding layer, interface, and heat-affected zone were characterized by optical microscope (OM) and scanning electron microscope (SEM). The facilities used for microstructural observation was given as follows:

- Olympus PM-10AK optical microscope.
- Olympus PME-3 optical microscope.
- Hitachi scanning electron microscope.

In order to reveal the microstructural feature for each clad and base materials, several chemical and electrolytic reagents were used to prepare the specimens for

microstructural observation. Table 3.6 lists the procedure used for specimen preparation and chemical reagents.

Table 3.6 Chemical reagents and specimen preparation procedures

Technique	Procedure	Reagent	Material	Feature
	Mechanical polish			
Optical Microscopy	Chemical etch (2% Nital)	#1 98 ml methanol 2 ml H ₃ PO ₄	Mild and tool steels	General microstructure
Scanning Electron Microscopy	Chemical etch (Marble)	#2 10 g CuSO ₄ 50 ml HCl 50 ml H ₂ O	304L stainless steel	General microstructure
	Chemical etch (Kalling)	#3 1.5 g CuCl ₂ 33 ml ethanol 33 ml HCl 33 ml H ₂ O	IN 738LC superalloy	General microstructure

3.8 Hardness Measurements

The microhardness measurements of laser cladding samples under different treatment conditions were carried out using a LECO M-400-G1 microhardness tester. Different loads were used for the hardness measurement, and the indentation time was set at 15 seconds. The hardness measurements were taken across the cladding layer, heat-affected zone, and substrate at increments of 0.1 mm.

Chapter 4

RESULTS AND DISCUSSION

4.1 Characteristics of Cone-Shaped Powder Stream

In the past few years, coaxial powder feeding method has been used in laser cladding process. Due to great changes in powder feeding mechanism, laser beam-materials interaction results have been improved. This interaction has a great effect on the temperature of clad zone. Therefore, it is necessary to discuss the characteristic of the powder stream first. Figure 4.1(a) shows the nature of powder flow through the nozzle without laser beam irradiation. The powder stream is uniformly distributed on the cone surface. As a result of special design of our coaxial nozzle, cone-shaped powder stream interacts with laser beam at about 3.5 mm from the nozzle exit, and is preheated to rather high temperature, or even partially or fully molten before reaching the molten pool of a substrate, as shown in Figure 4.1(b). It was reported that after the powder stream interacts with the laser beam during its motion from the nozzle exit to the workpiece surface, only approximately 40% of the laser energy is transmitted to the workpiece [104]. This process is very complex, and involved in many factors, such as spatial distribution of laser beam and power density, velocity and density distribution of the powder stream, powder property, interaction time between the laser beam and the powder stream, and cover gas flow rate, etc [102, 105].

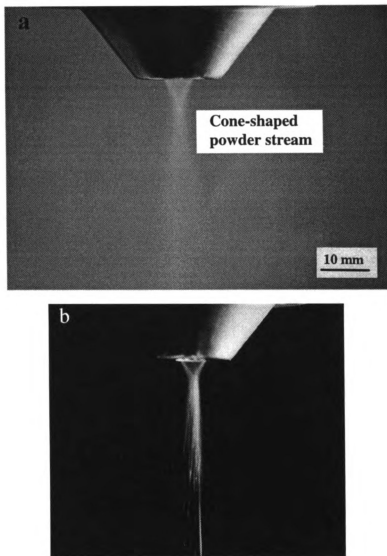


Figure 4.1 A view of cone-shaped powder stream. (a) Without laser beam. (b) With laser beam. Process parameters are as follows: laser power is 2.1 kw, laser spot size 2.9 mm, powder feed rate 0.25 g/sec, and cover gas flow rate 0.85 m³/hr.

Cover gas flow rate has a great effect on cone-shaped powder stream. When cover gas flow rate is increased from 0.85 to 3.4 m³/hr, it exerts a larger force on cone-shaped powder stream along its central axis, and squeezes the powder stream out, as shown in Figure 4.2(a). On the other hand, with higher cover gas flow rate, a larger impact force develops, and more powder bounces up from a workpiece surface in all directions, as displayed in Figure 4.2(b). This can lead to decrease in powder utilization efficiency, and

formation of poor quality cladding tracks. Circular cladding track 2 in Figure 4.3 is an example of poor quality clads due to higher cover gas flow rate. It has been found that, for our specially designed coaxial powder feeding system, the upper limit of cover gas flow rate for laser cladding process is about $1.7 \text{ m}^3/\text{hr}$.

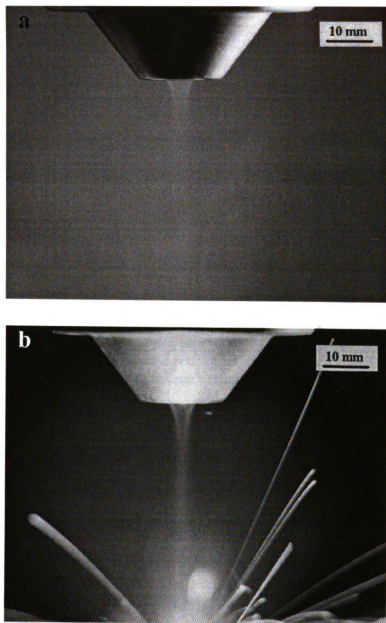


Figure 4.2 Effect of cover gas flow rate on cone-shaped powder stream. (a) Without laser beam irradiation. (b) With laser beam irradiation. Cover gas flow rate $3.4 \text{ m}^3/\text{hr}$. Other processing parameters are the same as those of Figure 4.1.

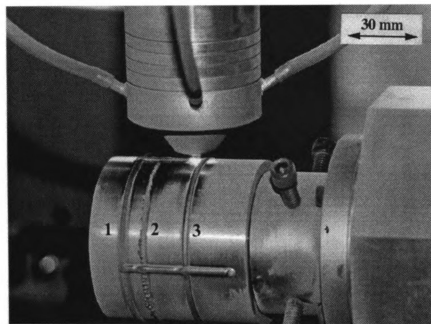


Figure 4.3 A view of circular cladding tracks on a solid cylinder. Cladding track 2 is an example of poor quality clads due to higher cover gas flow rate.

4.2 Desirable Powder Morphology and Particle-Size Distribution

Material factors can be divided into intrinsic and extrinsic properties of the clad and the substrate materials. Intrinsic properties include thermal conductivity and diffusivity, specific heat, latent heat, reflectivity, and mass density of the powder and the substrate. These intrinsic properties affect the molten-pool temperature, and temperature distribution in the substrate and thereby affecting clad formation. The extrinsic properties include particle size, particle-size distribution, particle shape, and the surface condition of the substrate. A powder suitable for laser cladding must have a proper particle-size distribution and particle shape for it to efficiently absorb laser energy and form a molten pool. Spherical particles are preferable for smooth powder delivery.

Figure 4.4 shows a spherical powder morphology. To the best of our knowledge, this is a desirable powder, and best suited for laser cladding process. The particle-size distribution for the powder falls between a range of 53 to 125 μm .

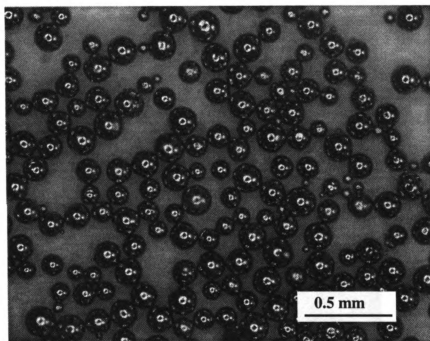


Figure 4.4 A view of desirable powder morphology for laser cladding process.

4.3 Effect of Powder Feeding Systems on Clad Quality

Figure 4.5(a) shows an overview of single cladding tracks with rectangular contours (x and y translations) on an AISI 1045 steel plate. The cladding track, which is 2.3 mm in width, and 1.3 mm in height, is smooth in appearance, and upon testing, found to be metallurgically sound. Figure 4.5(b) displays a macrograph of cladding tracks perpendicular each other, which were produced by using lateral powder feeding system. As seen in Figure 4.5(b), cladding tracks look very rough. When the powder delivery direction was perpendicular to the substrate-moving direction, no clad was formed because no molten pool

on the substrate was produced during laser cladding process. It is this drawback of the side powder feeding system that limits the real-world applications of laser surface alloying and cladding in consumer product industries.

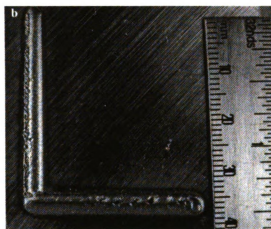
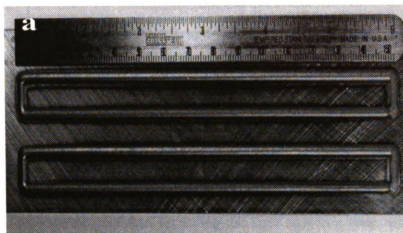


Figure 4.5 Effect of powder feeding systems on cladding quality. (a) Rectangular cladding tracks with smooth surface. (b) Perpendicular cladding tracks with rough surface via lateral powder feeding system.

4.4 Measurement of Powder Utilization Coefficient

Powder utilization coefficient α is defined as the ratio of the amount of powder participating in cladding to the total amount of powder provided by the feeding system within the duration of laser irradiation on the substrate. The value of α is not only related

to the type of feeding mechanism, such as side feeding system or coaxial feeding system, but also to material characteristics like the type, particle size, and particle shape of powders, and the nature and dimension of substrates, etc. Generally, the α value for coaxial feeding system is much higher than that for side feeding system (for side feeding, typically, α value falls between about 0.3 and 0.5 in comparison with about 0.8 for coaxial case) due to the precise deposition of the powder with respect to the center of the laser beam.

Many experiments with various process conditions, were carried out to measure the powder utilization coefficient α . The powder utilization coefficient α was computed by setting a powder feed rate, and then recording the laser scanning time, and weighing the sample before and after laser treatment.

If W_1 is weight of the substrate, and W_2 total weight of the substrate and the clad, then $W_c = W_2 - W_1$ is the net clad weight within scanning time t . If F_p is power feed rate, then $W_p = F_p t$, is the total weight of powder delivered within the scanning time t . The powder utilization coefficient α is then obtained from this ratio: $\alpha = W_c / W_p$. Based on experimental results, a few relationships have been observed:

- For a given laser power, spot size, and powder feed rate, when traverse speed varies in a range of ~ 5 to ~ 10.5 mm/sec, α value is approximately equal to 0.7 and 0.8 for each process condition, as shown in Figure 4.6. This shows that α value is not related to traverse speed.
- For a given laser power, spot size, and traverse speed, when powder feed rate varies from 0.1 to 0.25 gm/sec, α value is also rather close to 0.8, shown in Figure 4.7. This

means that the ratio W_c/F_p is a constant when scanning time t is fixed because the net clad weight increases with the increase of powder feed rate.

- Figure 4.8 shows that α value is related to spot size. The smaller the laser-beam diameter, the less amount of powder laser beam catches, and therefore the lower the powder utilization efficiency. When laser-beam diameter $D = 1.8$ mm, average $\alpha \cong 0.71$. While $D \geq 2.3$ mm, average $\alpha \cong 0.80$.

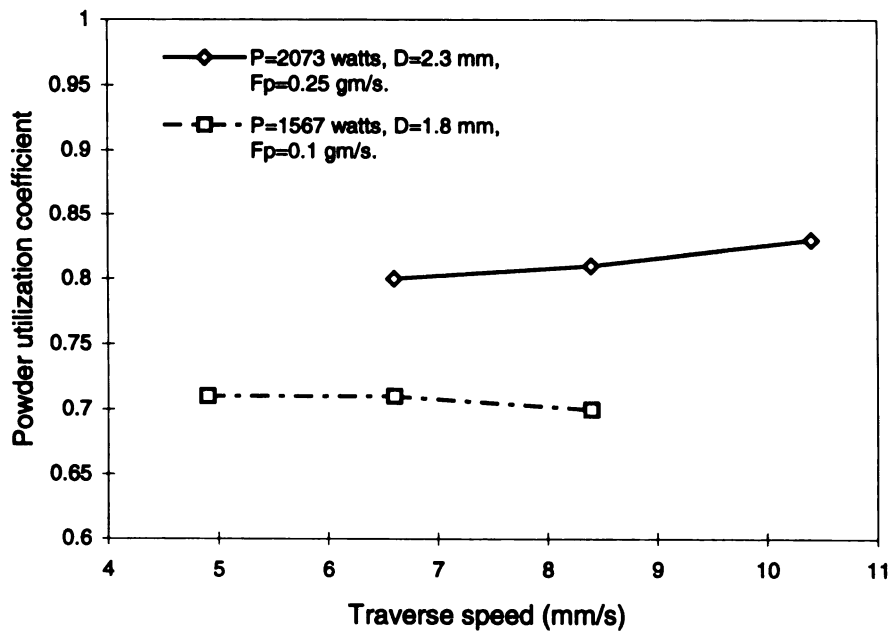


Figure 4.6 Plot of powder utilization coefficient vs. traverse speed.

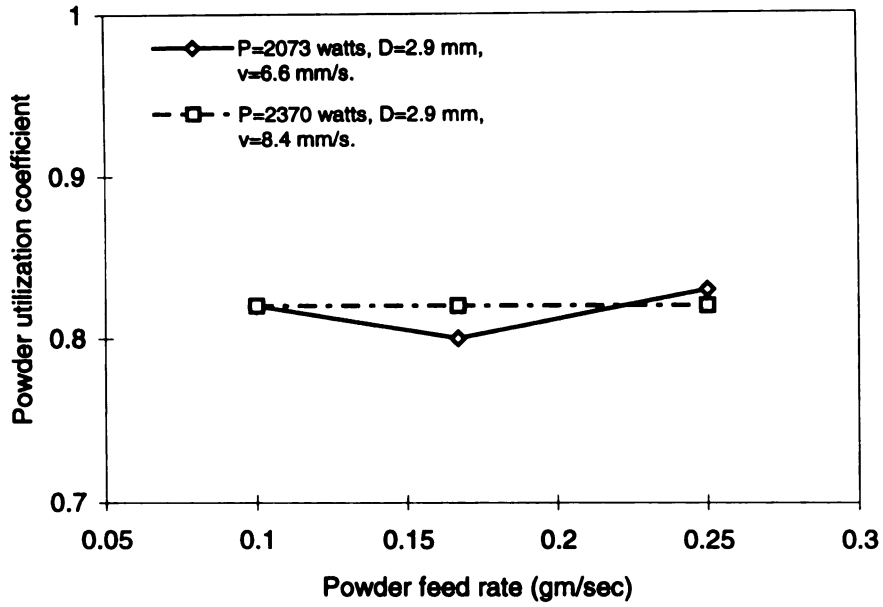


Figure 4.7 Plot of powder utilization coefficient vs. powder feed rate.

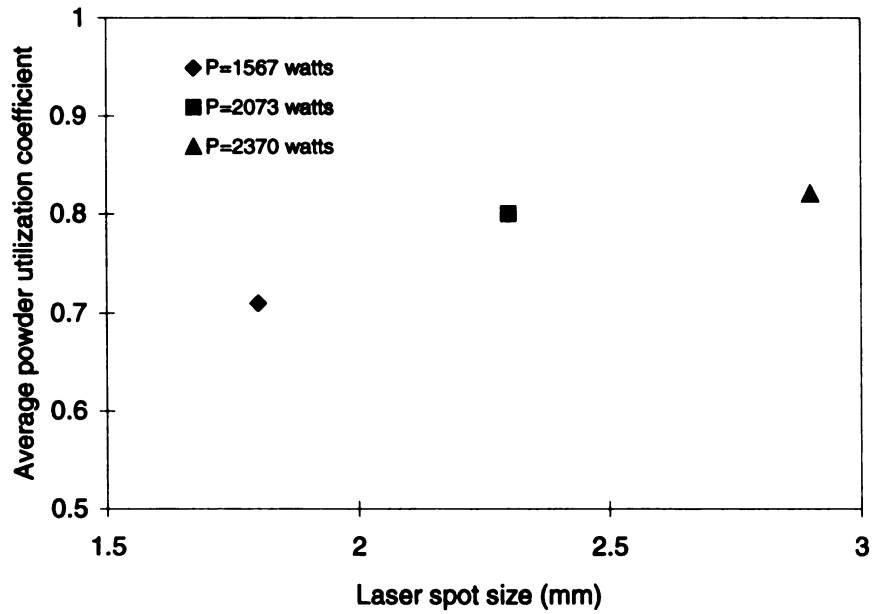


Figure 4.8 Plot of average powder utilization coefficient vs. laser spot size.

4.5 Relationships between Clad Width and Process Parameters

Theoretically, clad width is primarily dictated by the laser-beam diameter, the integrated beam diameter or the scanning beam amplitude. However, the clad width is also related to traverse speed, energy density ($E_d = AP/\pi Dv$), and powder feed rate. In order to determine the relationships between the clad width and processing parameters, several experiments were carried out under various processing conditions. Based on experimental results, the following points can be made:

- With other variables held constant, clad width linearly decreases as the traverse speed increases, as shown in Figure 4.9. When traverse speed accelerates to about 8.5 mm/sec, clad width is approximately equal to laser-beam diameter for each process condition. This speed is called threshold traverse speed under experimental conditions. Below threshold traverse speed, cladding track is wider than laser-spot size. Lines (1), (2) and (3) in Figure 4.9 are governed by the following equations respectively,

$$w = -0.19v + 4.64 \quad (4.1)$$

$$w = -0.19v + 4.25 \quad (4.2)$$

$$w = -0.20v + 3.93 \quad (4.3)$$

- Figure 4.10 is a diagram of clad width versus energy density. When laser power, spot size, and powder feed rate are kept constant, clad width increases with increase in specific energy. This is because sufficient energy is available to melt clad material situated at a distance wider than the beam itself.

- Figure 4.11 shows that, with other variables held constant, cladding track gently widens as powder feed rate increases. If the energy input is sufficient, the large powder feed rate will lead to a wider cladding track.

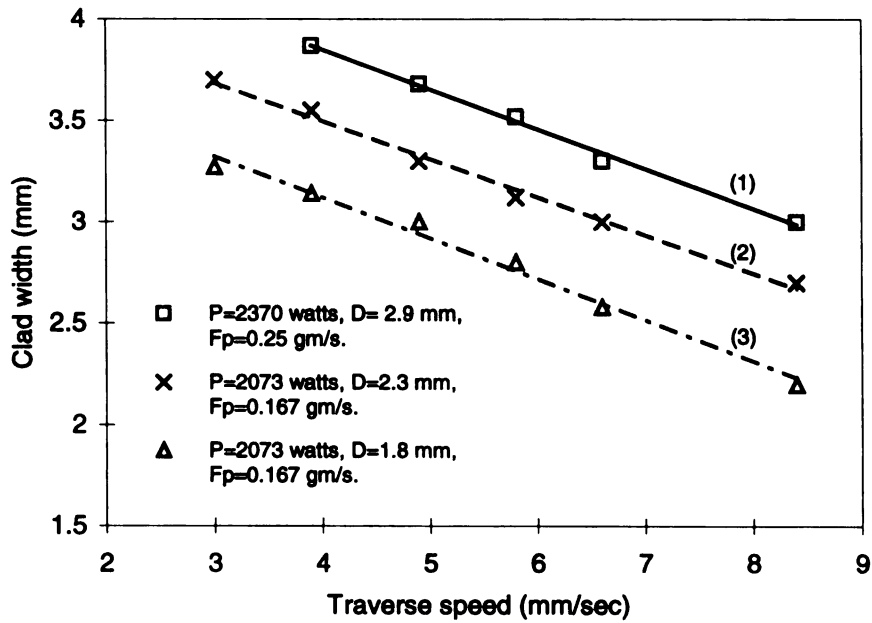


Figure 4.9 Clad width as a function of traverse speed.

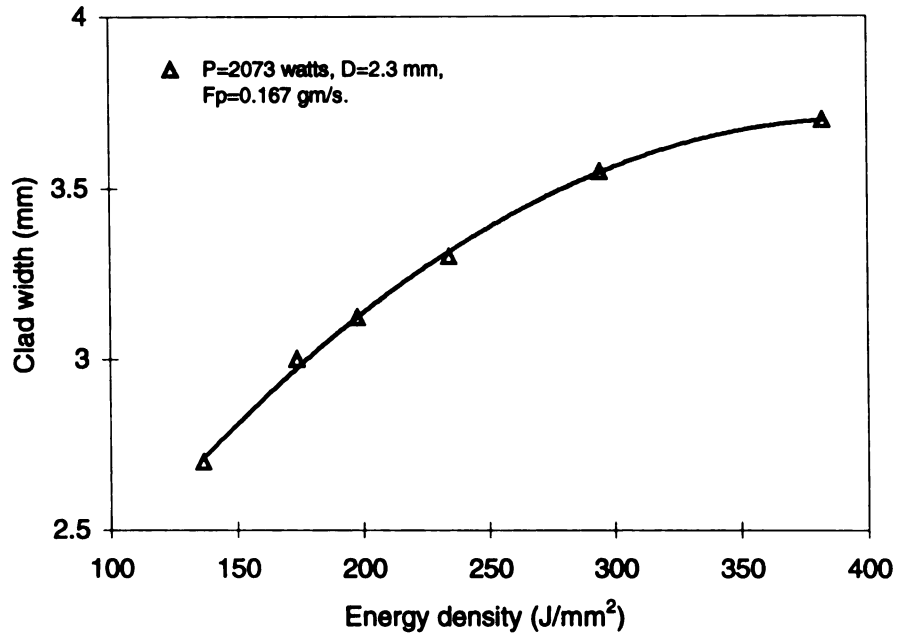


Figure 4.10 Clad width as a function of energy density.

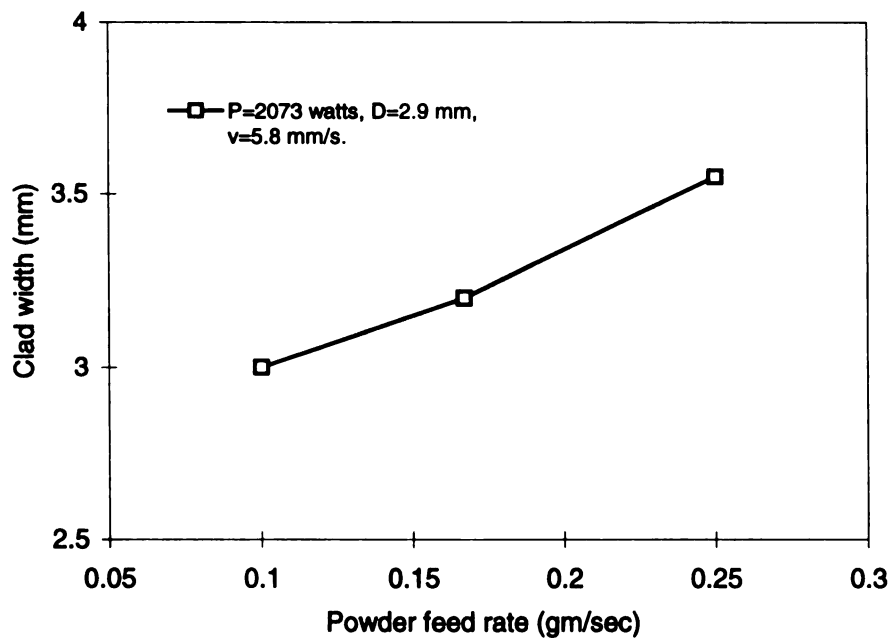


Figure 4.11 Clad width as a function of powder feed rate.

4.6 Process Modeling

The laser cladding is a very complicated process involving the following physical and metallurgical phenomena: (1) laser-beam energy and material interaction, (2) heat transfer in the clad, and the substrate, (3) rapid melting and solidification, and (4) clad material and substrate material reaction and inter-diffusion. For this reason, process modeling of the laser-cladding process is a difficult task. A few models for laser cladding process have thus far been developed by other authors [106-108]. These models involved various physics concepts and complicated mathematical calculations, and help understand phenomena and mechanisms during laser cladding, but were not suited for rapidly evaluating optimized processing parameters. The following model is developed based on the geometric features of the transverse section of single cladding tracks, physical properties of alloy powder itself, and processing parameters. Due to a simple, but realistic approximations, this process model can be easily used to evaluate the optimal processing conditions for on-line production and manufacturing.

4.6.1 Assumptions

The model is based on the following assumptions:

1. Power density is suitable for laser cladding process, where the clad track is sound and free of cladding defects, such as porosity, microcracks, poor metallurgical bond, and high dilution.
2. Geometry of the transverse section of single cladding tracks is parabolic arch.
3. When traverse speed $v < \sim 8.5$ mm/sec, Equations (4.1), (4.2) and (4.3) are used to calculate the clad width, which is inserted into related formula to calculate the

maximum clad thickness. While traverse speed varies from ~8.5 to ~14.5 mm/sec, laser-beam diameter is substituted for the clad width in the model.

4. Laser-spot diameter $D = 1.8$ mm, $\alpha \cong 0.70$, while $D \geq 2.3$ mm, $\alpha \cong 0.80$.

4.6.2 Basic Equation

Net clad weight is a function of powder utilization coefficient, powder feed rate, and irradiation time, so it can be expressed as

$$W_c = \alpha F_p t \quad (4.4)$$

where W_c is net clad weight (gm), α powder utilization coefficient, F_p powder feed rate (gm/sec), and t irradiation time (sec) (related to scanning speed).

According to assumption 2, the cross-section is approximately represented by a parabolic arch, as shown in Figure 4.12, and its area A is expressed as

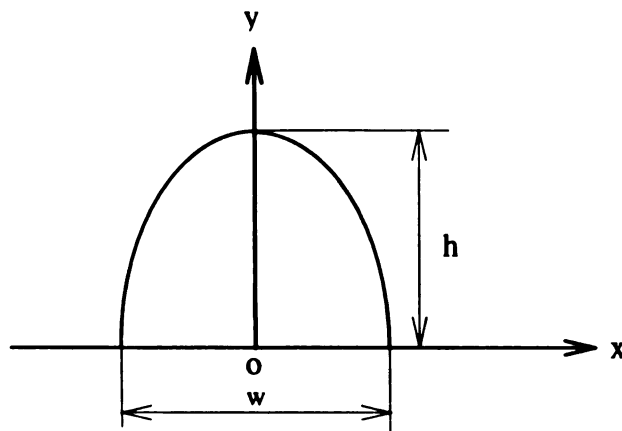


Figure 4.12 Parabolic shape of the cross-section of a single cladding track.

$$A = \frac{2}{3} wh \quad (4.5)$$

where w is clad width (mm), and h the maximum clad thickness (mm).

From geometric shape of a clad track, and physical properties of the alloy itself, the net clad weight can be written as

$$W_c = \frac{2}{3} wh(vt)\rho \quad (4.6)$$

where v is traverse speed (mm/sec), and ρ alloy density (gm/cm³). For tool steel CPM 10V, $\rho = 7.418$ gm/cm³. The term, $\frac{2}{3} wh(vt)$, is actually the volume of a single cladding track.

Combining Equations (4.4) and (4.6), we can get

$$\frac{2}{3} whv\rho = \alpha F_p \quad (4.7)$$

Equation (4.7) is a basic equation, relating the maximum clad thickness and various process parameters.

4.6.3 Energy Density Equation

Energy density is defined as [21]

$$E_d = P_d \tau \quad (4.8)$$

where E_d is energy density (J/mm²), P_d power density (watts/mm²), and τ time (sec) required to move a distance of the laser beam diameter along the traverse direction.

Power density is expressed as

$$P_d = \frac{P}{A_l} \quad (4.9)$$

where P is laser power (watts), and A_l irradiation area (mm²).

For simplicity, assume that the shape of laser spot is circular (for our TEM₀₁ mode laser beam, the shape actually is doughnut), then irradiation area $A_l = \pi D^2/4$, where D is laser beam diameter (mm).

Substituting A_l into Equation (4.9), we can obtain

$$P_d = \frac{4P}{\pi D^2} \quad (4.10)$$

The scanning time τ can be expressed as

$$\tau = \frac{D}{v} \quad (4.11)$$

Substituting Equations (4.10) and (4.11) into Equation (4.8), one has

$$E_d = \frac{4}{\pi} \frac{P}{Dv} \quad (4.12)$$

The above equation shows that the energy density is directly proportional to laser power, and inversely proportional to spot size or traverse speed.

4.6.4 Clad Thickness-Energy Density Equation

Equations (4.7) and (4.12) can be rewritten as, respectively,

$$h = \frac{3\alpha F_p}{2wv\rho} \quad (4.13)$$

$$\frac{1}{Dv} = \frac{\pi E_d}{4P} \quad (4.14)$$

Based on assumption 3, when $v \geq 8.4$ mm/sec, $w = D$. Then substituting Equation (4.14) into Equation (4.13), we can obtain

$$h = \frac{3\pi}{8} \frac{\alpha F_p}{P\rho} E_d \quad (4.15)$$

For a particular alloy powder, if laser power and powder feed rate are fixed, the clad thickness is directly proportional to energy density, which depends on the spot size and traverse speed.

4.7 Relationships Derived from Basic Equation

Equation (4.13)

$$h = \frac{3\alpha F_p}{2wv\rho}$$

shows that clad thickness is related to powder feed rate, spot size ($w = D$, when $v \geq 8.4$ mm/sec), and traverse speed, while the laser power is held constant.

4.7.1 Relationship between Clad Thickness and Traverse Speed

In Equation (4.13), for a given powder (fixed mass density ρ), if laser power, spot size, and powder feed rate are kept constant, then Equation (4.13) can be simplified as

$$h = \frac{C_1}{v} \tag{4.16}$$

where C_1 is a constant depending upon process variables and alloy density.

Equation (4.16) shows that the clad thickness is inversely proportional to traverse speed. The faster the traverse speed, the less is the powder input per unit length, and therefore the thinner the cladding track. For example, substituting $\alpha = 0.70$, $F_p = 0.167$ gm/sec, and $\rho = 7.418 \times 10^{-3}$ gm/mm³ into Equation (4.13), it becomes: $h = 23.59/wv$. When traverse speed varies from 3 to 6.6 mm/sec, the corresponding clad thickness can be calculated using Equation (4.3) and this simplified relationship. Figure 4.13 displays the calculated and experimental plots, which show that clad thickness is inversely

proportional to traverse speed in both cases. Also, experimental and calculated results match very well.

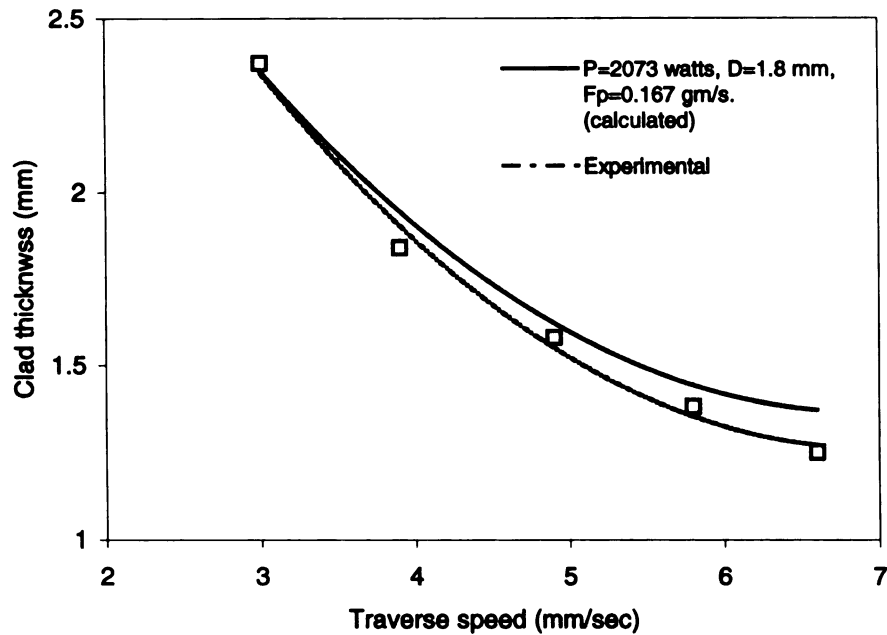


Figure 4.13 Clad thickness as a function of traverse speed.

4.7.2 Relationship between Clad Thickness and Powder Feed Rate

If laser power, spot size and traverse speed are kept constant, Equation (4.13) becomes

$$h = C_2 F_p \quad (4.17)$$

where C_2 is a constant which is related to process parameters and alloy density.

Equation (4.17) reveals that clad thickness and powder feed rate have a linear relation. The larger the powder feed rate, the more is the powder input per unit length, and higher will be the clad thickness. However, for a fixed energy density, if the powder feed rate is too high, it is possible to cause lack of fusion in cladding layer, or produce poor metallurgical bonding between the cladding layer and the substrate.

Inserting $\alpha = 0.8$, $w = D = 2.9$ mm, $v = 8.4$ mm/sec, and $\rho = 7.418 \times 10^{-3}$ gm/mm³ into Equation (4.13), then it becomes $h = 6.64 F_p$. Theoretical and experimental results are displayed in Figure 4.14. As shown in Figure 4.14, clad thickness linearly increases as powder feed rate increases.

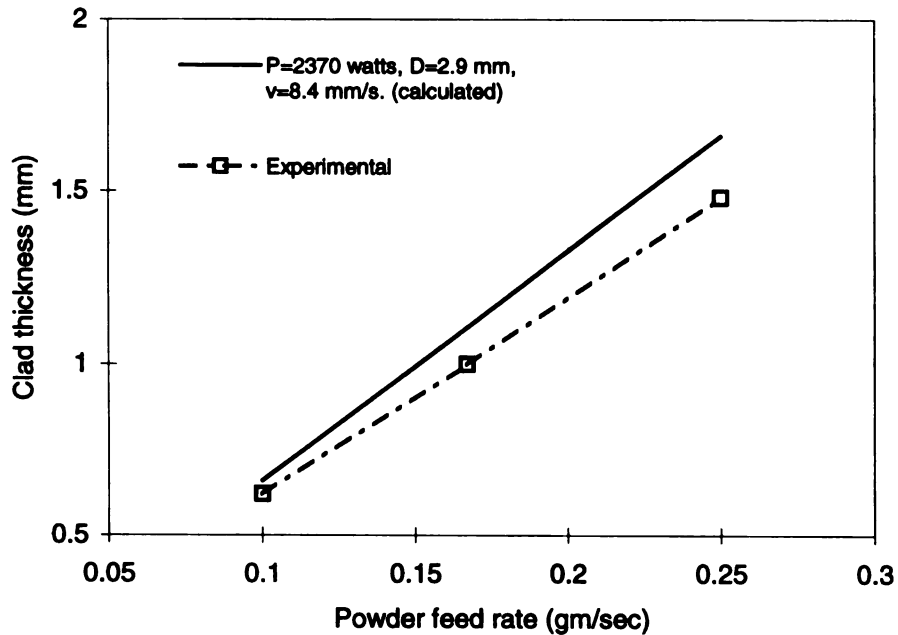


Figure 4.14 Clad thickness as a function of powder feed rate.

4.8 Correlation Derived from the Energy Density Equation

Equation (4.12) displays that the energy density is related to spot size, laser power, and traverse speed.

4.8.1 Relationship between Energy Density and Spot Size

The laser power and traverse speed are kept constant, and then Equation (4.12) is simplified as

$$E_d = \frac{C_3}{D} \quad (4.18)$$

where C_3 is a constant.

Equation (4.18) displays that energy density is inversely proportional to spot size. In other words, energy density and the reciprocal of the spot size have a linear relation, as shown in Figure 4.15. For very low values of energy density, it is possible to create cladding defects, such as lack of fusion and poor metallurgical bonding, or even debonding. This is because insufficient energy is available to melt the substrate surface after melting powder particles.

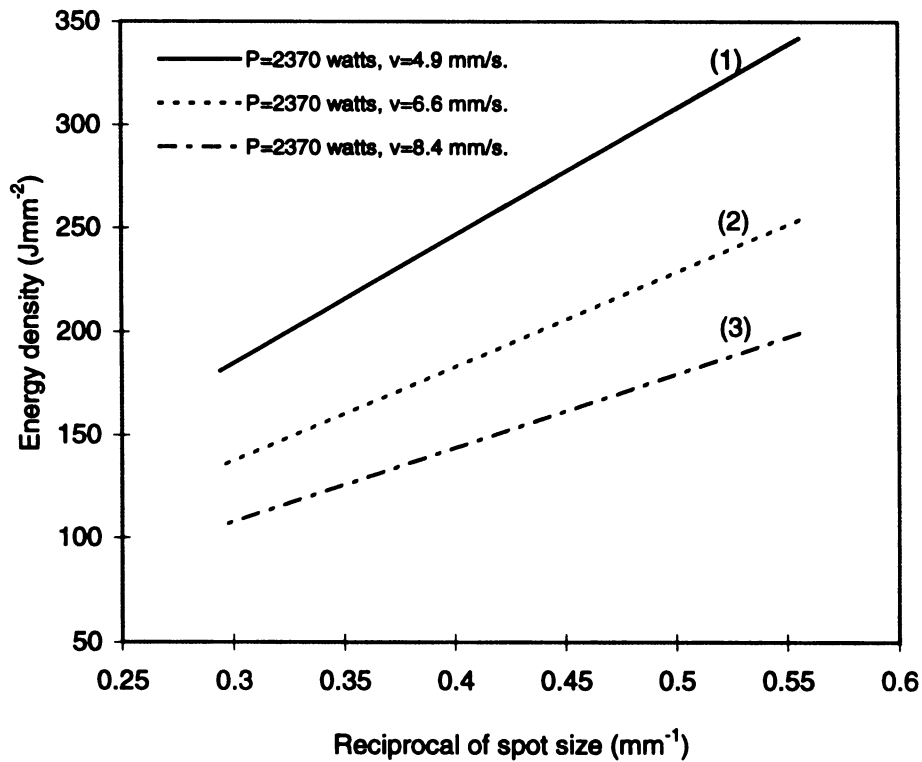


Figure 4.15 Energy density as a function of reciprocal of spot size.

4.8.2 Relationship between Energy Density and Traverse Speed

When the laser power and spot size are fixed, Equation (4.12) is reduced to

$$E_d = \frac{C_4}{v} \quad (4.19)$$

where C_4 is a constant.

The above equation demonstrates that the energy density is inversely proportional to traverse speed. The faster the traverse speed, the less the interaction time or dwell time, and the smaller the energy density. The relation between energy density and the reciprocal of traverse speed is displayed in Figure 4.16. It shows that energy density linearly increases as the reciprocal of traverse speed increases.

In terms of Equation (4.10), when laser power is fixed, power density is related to spot size, and not related to traverse speed. Therefore, it is more reasonable to use energy density to explain phenomena that happen during laser cladding than power density.

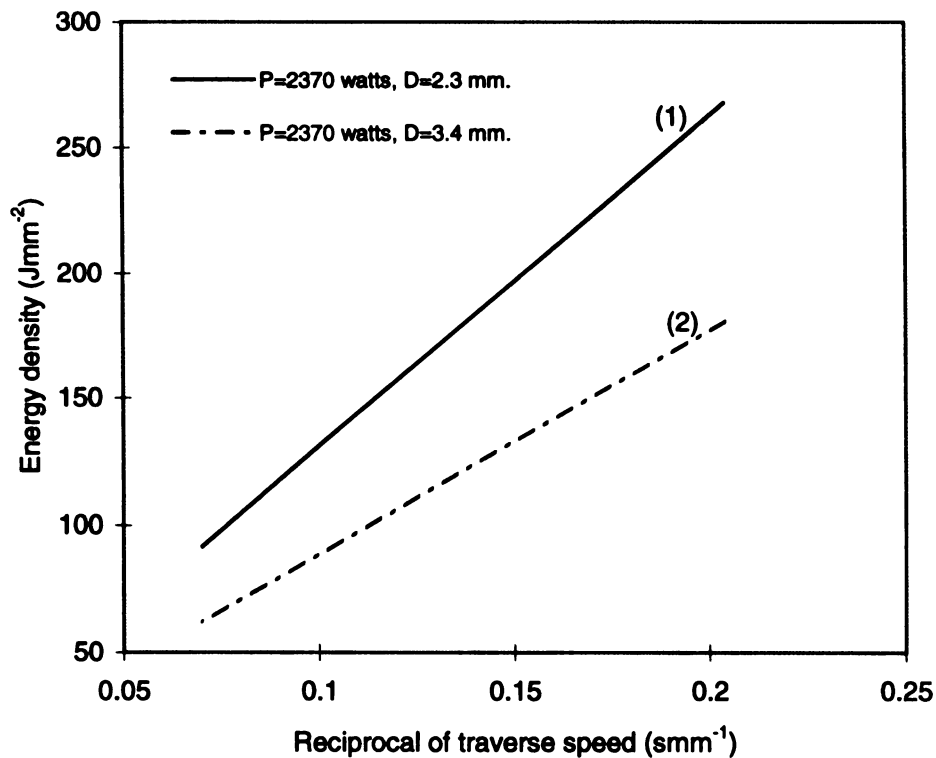
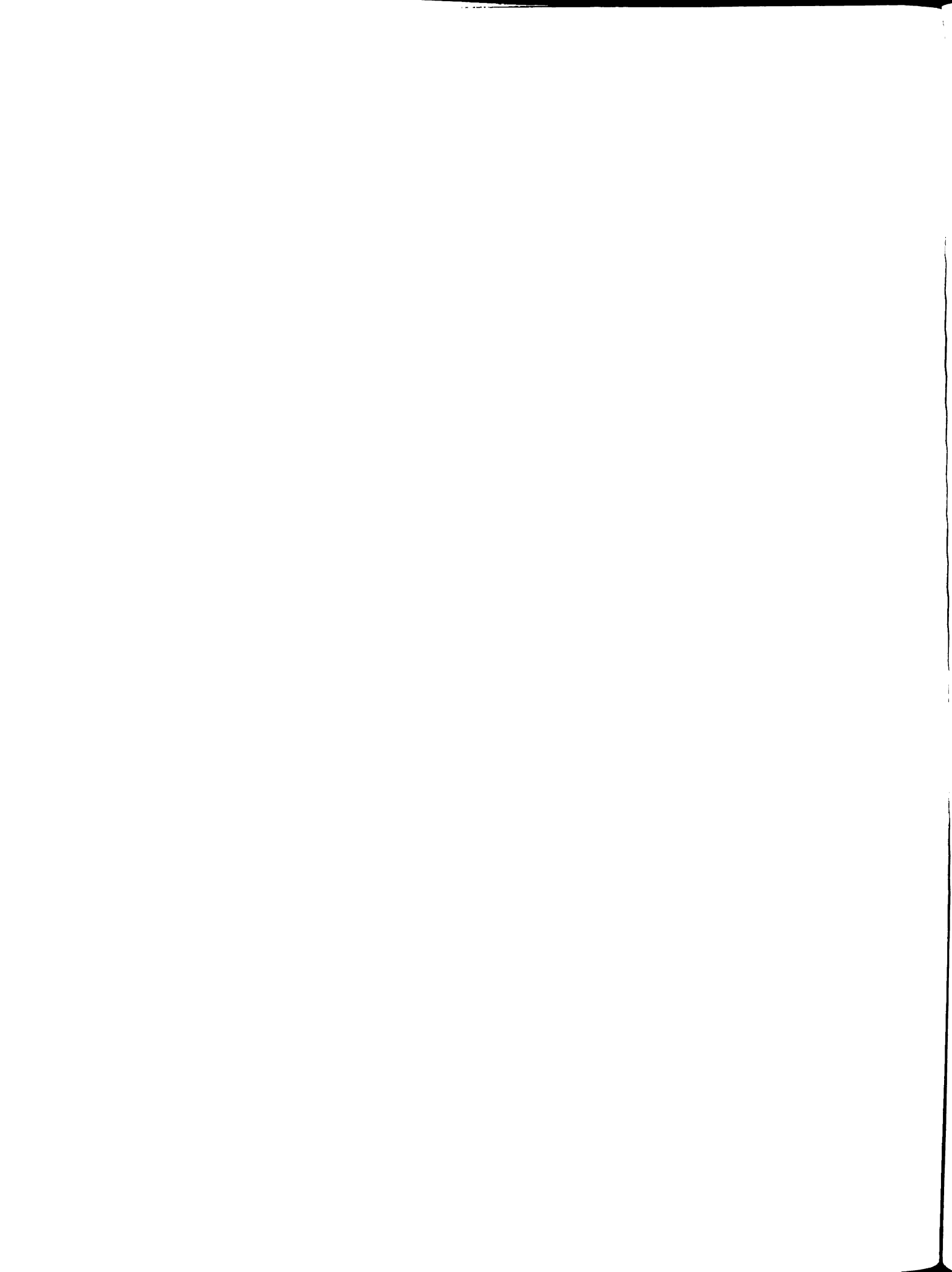


Figure 4.16 Energy density as a function of reciprocal of traverse speed.

4.8.3 Relationship between Energy Density and Laser Power

If spot size and traverse speed are held constant, then Equation (4.12) becomes



$$E_d = C_5 P \quad (4.20)$$

where C_5 is a constant.

Equation (4.20) shows that energy density and laser power have a linear relation. The higher the laser power, the larger the energy density, as shown in Figure 4.17. If the energy density is too high, it is possible to create high dilution which can change the properties of cladding layer. This is because, for a given powder feed rate, greater energy delivered per unit area causes greater substrate melting and change in clad alloy composition.

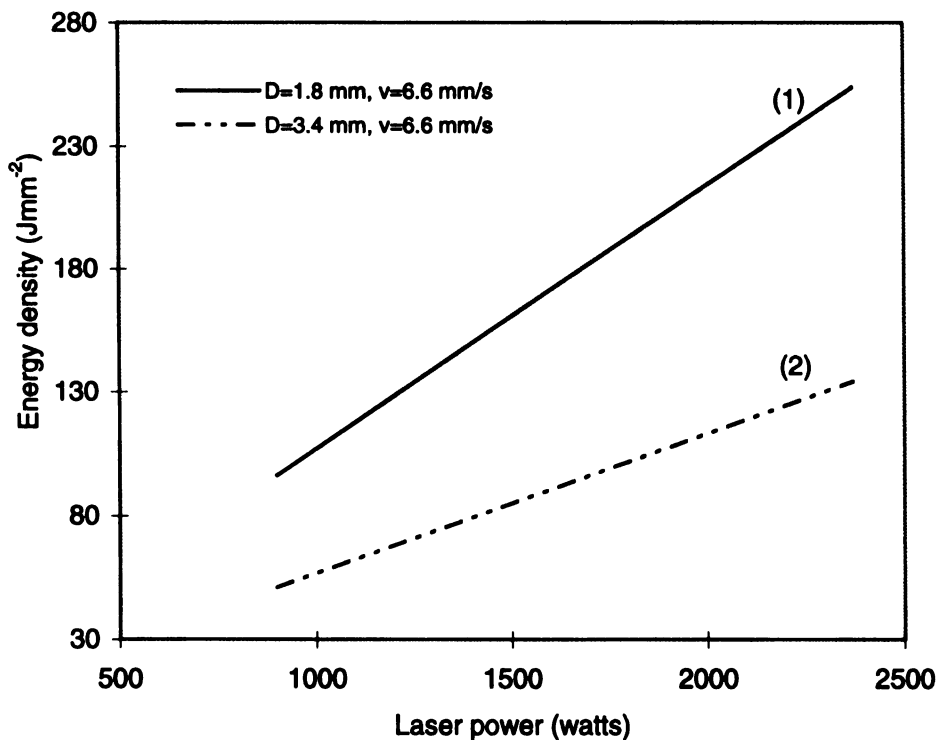


Figure 4.17 Energy density as a function of laser power.

4.9 Relationship between Clad Thickness and Energy Density

From Equations (4.12) and (4.13), we know that, for fixed laser power and spot size, energy density is only a function of traverse speed. While, for fixed laser power, spot size, and powder feed rate, clad thickness is also a function of traverse speed. Therefore, both clad thickness and energy density are inversely proportional to traverse speed. The faster the traverse speed, the lower the energy density, and thinner the clad track.

Substituting $\alpha = 0.8$, $P = 2370$ watts, $D = 3.4$ mm, $F_p = 0.25$ gm/sec, and $\rho = 7.418 \times 10^{-3}$ gm/mm³ into Equations (4.12) and (4.15), respectively, we obtain: $E_d = 887.5/v$ and $h = 0.0134 E_d$. When traverse speed varies from 8.4 to 14.3 mm/sec, the corresponding clad thickness can be calculated using the above two simplified relationships. Figure 4.18 represents calculated and experimental results between the clad thickness and the specific energy, respectively. They show that the clad thickness and energy density have a linear relationship. Also, the calculated result is in good agreement with the experimental result.

4.10 Relationship between Penetration Depth and Energy Density

If traverse speed and spot size in Equation (4.12) are kept constant, energy density is only a linear function of laser power. For a given powder feed rate, the higher is the laser power, the higher is the energy density, thus more energy is transferred to the substrate, and therefore deeper is the heat-affected zone. The plot of penetration depth versus energy density is shown in Figure 4.19 The penetration depth linearly increases with increase in energy density.

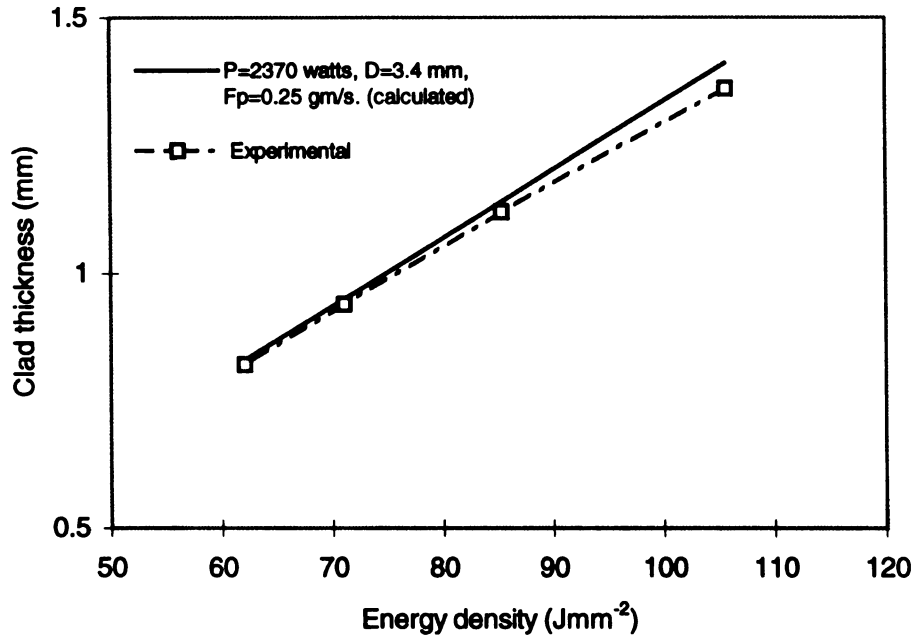


Figure 4.18 Clad thickness as a function of energy density.

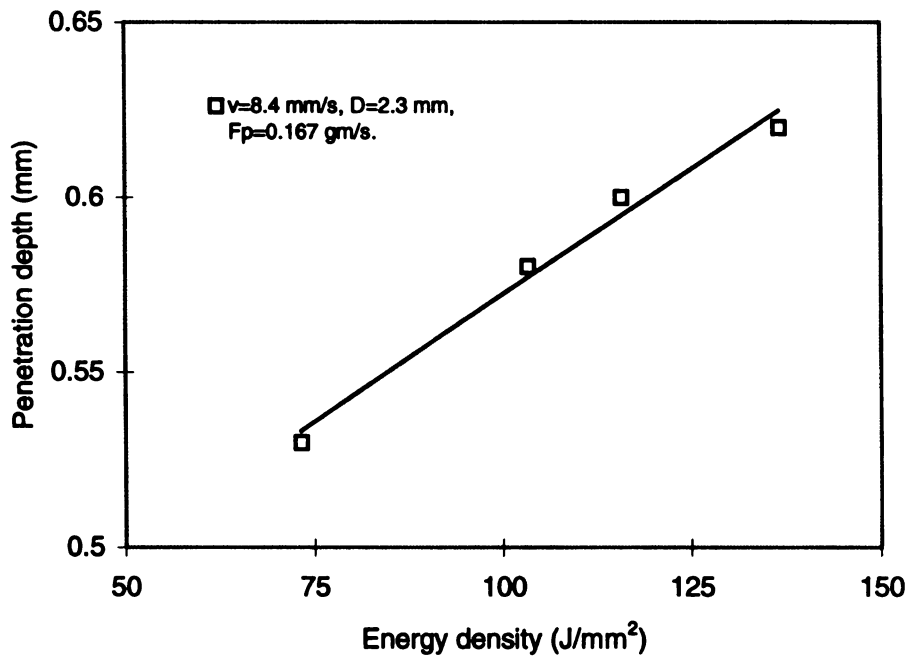


Figure 4.19 Penetration depth as a function of energy density.

4.11 Evaluation Standards of Laser Cladding Quality

The main processing parameters for laser cladding include laser power and spatial distribution, laser spot diameter, traverse speed, powder feed rate, cover gas flow rate, and overlapping percentage for multi-track buildup. Each parameter plays an important role in laser cladding processing. Only if all these parameters harmonically work together, high quality cladding track or layer can be produced.

General criteria for evaluating laser cladding quality is setup as follows: clad has a smooth surface and an uniform width, it is free of porosity, crack and inclusion, and has a good metallurgical bonding with the substrate but a low dilution. In addition, a good clad has three zones: clad zone, interface zone, and heat-affected zone (HAZ). Clad zone is a solidified molten alloy. Interface zone is an inter-diffusion zone between the clad and the substrate. And heat-affected zone is produced by transferring laser energy to the substrate during the process.

Due to higher laser energy input, clad in Figure 4.20(a) is sunk into the substrate so that both chemical composition and mechanical and physical properties of reinforcement material have been changed. Thus, buildup with a high dilution is not desirable. As seen in Figure 4.20(b), the buildup meets the above evaluation criteria. Therefore, this is an optimized processing condition. Figure 4.20(c) clearly shows that there are a lot of pores inside the clad. Such a defect will adversely affect the mechanical strength of cladding layer. Because of low laser energy input, cladding track did not metallurgically fuse with the substrate, as shown in Figure 4.20(d). This phenomenon is called lack of fusion. Optimized shielding gas flow rate has a great effect on cladding quality. If cover gas flow rate is too high, then it is highly possible to produce porosity

because some inert gas is entrapped in the clad due to high cooling rate. On the other hand, if it is too low, cladding zone is not completely protected. Therefore, oxides or inclusion form inside the clad during the process, as shown in Figure 4.20(e).

For multi-layer deposition, both molten pool temperature and temperature distribution of the buildup have to be well controlled by gradually reducing laser power input if other process parameters are kept constant. Otherwise, it is easy to create cracking inside the clad or heat-affected zone due to overheating and thermal cycle fatigue. Figure 4.20(f) clearly display such a defect.

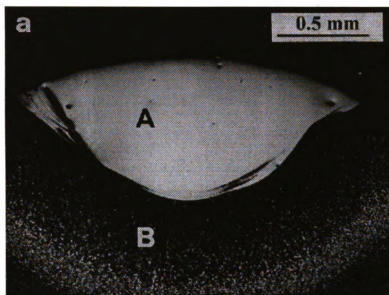
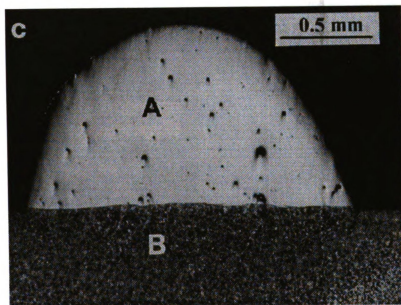
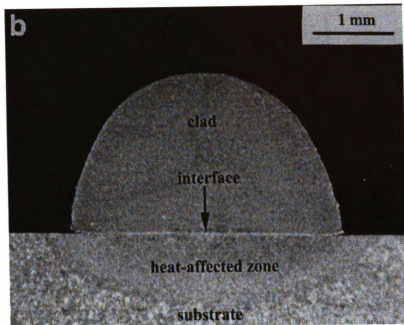
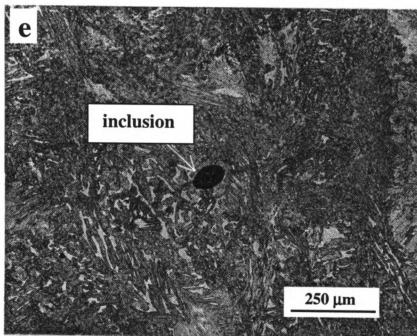
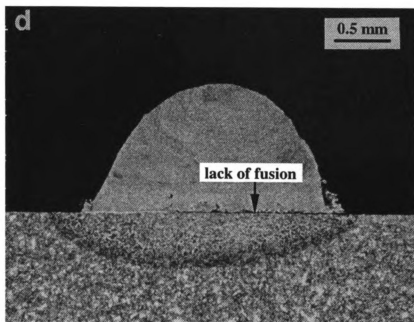


Figure 4.20 Overview of the transverse section of cladding tracks or layers. (a) High dilution. (b) Optimized condition. (c) Porosity. (d) Lack of fusion. (e) Inclusion. (f) Cracking. A: Clad. B: Base metal.

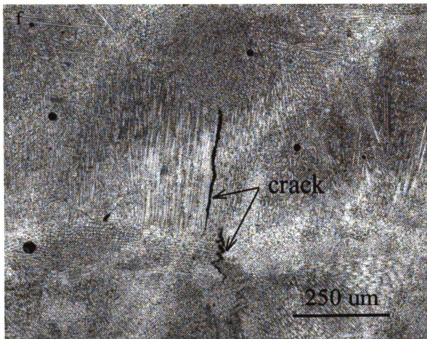
(continued)



(continued)



(continued)



4.12 Overlapping Rate

Required dimensional buildup consists of multi-tracks or layers. For convenience, it is necessary to define the term "overlapping rate". Schematic drawing of cladding track overlapping is displayed in Figure 4.21. Just as it implies, overlapping rate R_O between two adjacent tracks is defined as follows:

$$R_O = \frac{D - D_l}{D} \times 100\% \quad (4.21)$$

where D is laser spot diameter on the substrate surface (mm), D_l the distance CNC table moves with respect to the laser beam center (mm).

For example, if laser spot size $D = 2$ mm, and moving distance $D_l = 1$ mm, and then R_O is 50%.

Overlapping rate plays a very important role in multi-track deposition because this parameter affects laser cladding quality. When other processing parameters are kept constant, for example, too small overlapping rate often creates such a defect as lack of fusion between two adjacent tracks during laser cladding. Based on our experimental data, 50% of overlapping rate is most suited for multi-track deposition. This point will be explained in the section of prototype of 3-D components.

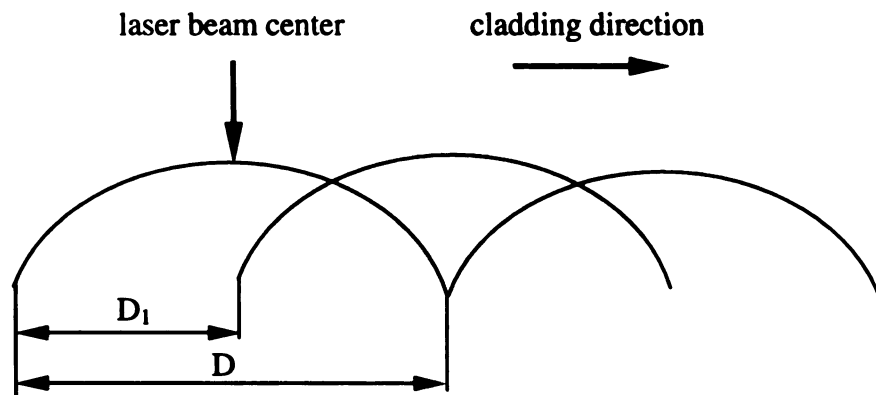


Figure 4.21 Schematic drawing of the transverse section of multi-track overlapping.

4.13 Dilution

By definition, laser cladding process is to deposit a reinforced material onto a metallic substrate without changing its chemical composition and properties. In order to get a good metallurgical bonding between the clad and the substrate, there must be an interface zone or inter-diffusion zone. Theoretically, from the point of view of physical metallurgy, a few atomic-layer inter-diffusion zone is thick enough to ensure a solid bonding between the deposit and the base material. In practice, it is very difficult to control laser energy input to get that ideal interface zone. For simplicity, the term dilution is introduced here. Figure 4.22 presents the concept of dilution ratio. Dilution can be

defined as the change in chemical composition of the reinforced material caused by intermixing of the melted substrate and deposit. Based on this definition, it is easy to express the dilution R_d by the following relation:

$$R_d = \frac{h_d}{h_c + h_d} \times 100\% \quad (4.22)$$

where h_c is clad thickness without change in composition (mm), and h_d intermixing thickness between the deposit and the substrate (mm).

For laser cladding process, dilution ratio has to be controlled as low as possible in order to maintain both composition and properties of reinforced material. To the best of our knowledge and experimental data, tens of microns of inter-diffusion zone is practically an ideal interface zone, as shown in Figure 4.23.

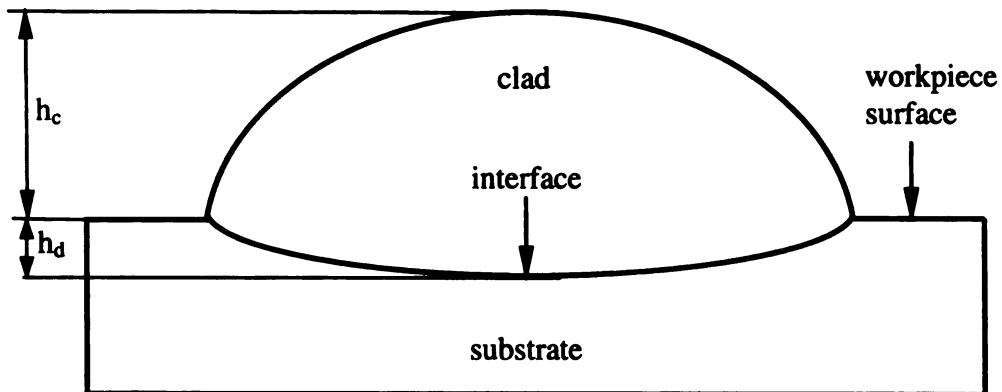


Figure 4.22 Schematic drawing of cladding and intermixing zones for calculating dilution ratio.

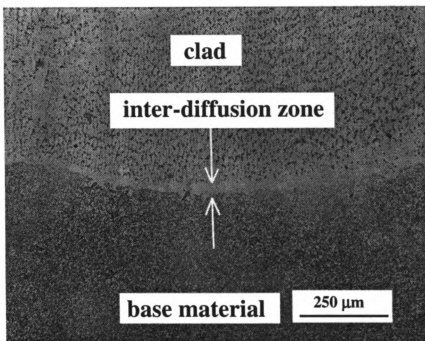


Figure 4.23 Optical microstructure of the transverse section of a cladding track, showing a low intermixing zone.

4.14 Calculation of Deposition Rate

Assume that a cubic coupon is directly deposited from metallic powder by laser cladding process, then its volume V can be expressed as follows:

$$V = LWH \quad (4.23)$$

where L , W , and H are length, width and height of the coupon, respectively. Due to the characteristic of laser cladding, such a coupon can be produced only by overlapping multi-tracks and multi-layers. For this reason, the term deposition rate is introduced to describe the processing productivity. Just as its name implies, the deposition rate is defined as the volume produced within a unit time (mm^3/sec). Figure 4.24 clearly shows how multi-tracks overlap to produce a platform layer.

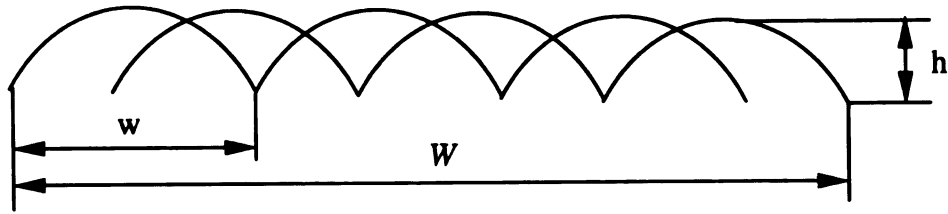


Figure 4.24 Schematic drawing of multi-track overlapping to produce a platform layer by laser cladding process.

For 50 percent of overlapping rate between two adjacent tracks, and based on Equation (4.23) and Figure 4.23, it is easy to get following relationships:

$$L = l = v\tau$$

$$W = [n - 0.5(n - 1)]w \quad (4.24)$$

$$H = mh$$

where l , w and h are length, width and height of a single cladding track (mm), respectively. v is traverse speed (mm/s), and τ time required for producing a single cladding track (s). n is the number of multi-tracks, and m the number of deposited layers.

Substituting the above equation into Equation (4.23), one can have

$$V = 0.5m(n + 1)whl \quad (4.25)$$

Equation (4.25) is divided by total deposition time t , then deposition rate R_d is given by

$$R_d = \frac{0.5m(n + 1)whl}{t} \quad (4.26)$$

The above equation can be used to roughly calculate the deposition rate.

4.15 Geometric Characteristics of Single Cladding Tracks

The clad bead geometry is related to process parameters, such as power density, traverse speed, and powder feed rate. There are three basic single clad bead geometries:

deep penetration bead in Figure 4.20(a), parabolic clad bead in Figure 4.20(b), and clad bead with a low dilution and a reasonable aspect ratio of width to height. As has been discussed before, clad bead with high dilution rate is not desirable because both chemical composition and properties of the reinforced material have been changed. In our newly developed process for producing tooling dies, because the cutting blades on the rotary cutting die is 1.5 mm high, only parabolic clad track can meet the height requirement for the sake of cost-effectiveness.

When multi-tracks overlap to produce larger coating area, transverse geometry of single cladding tracks, overlapping percentage, and aspect ratio are very important parameters. In terms of our experimental results, for multi-track laser deposition, the aspect ratio is at least 2 in order to make coating layer with a smooth surface and no defects. Within a certain range of the aspect ratio, the larger this value is, the more it is suited for multi-track buildup. Figure 4.25 shows two types of transverse geometric shapes of single cladding tracks. The aspect ratio in Figure 4.25(a) is small; while the aspect ratio in Figure 4.25(b) is reasonably large. When two adjacent tracks with a small aspect ratio overlap, because laser energy hardly transmits through the first track to fuse two tracks together, and then it is highly possible to create lack of fusion in marked L region during the laser cladding. Figure 4.26 clearly exhibits such a defect.

Based on our processing model, there are two ways to control the aspect ratio. One way is to increase traverse speed to reduce clad thickness. In this way, the aspect ratio can be increased. The other way is to decrease powder feed rate to increase aspect ratio.

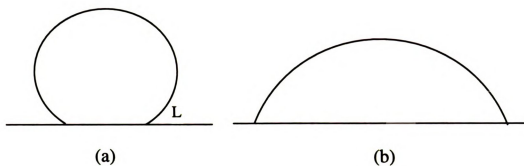


Figure 4.25 Schematic drawing of transverse geometric shapes of single cladding tracks. (a) Small aspect ratio. (b) Desirable aspect ratio.

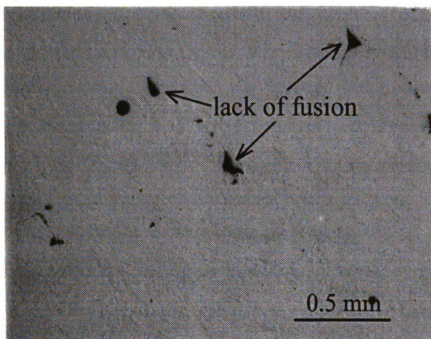


Figure 4.26 An overview of lack of fusion forming under the following condition: two adjacent tracks with a small aspect ratio overlap. Unetched.

4.16 Laser Direct Fabrication of 3-D Components

Now laser cladding process is demonstrating a great application potential in various manufacturing industries. The combination of laser cladding technique and advanced CAD/CAM system can be employed for rapidly prototyping industrial components, and tooling dies with required geometric shapes and larger dimensions. This section will present some foremost-mentioned applications of laser cladding process in manufacturing industries.

4.16.1 Tooling Dies

4.16.1.1 Fabrication of Tooling Dies

Figure 4.27(a) displays a view of rectangular hard-facing tracks on an AISI 1045 steel roller with 101.6 mm diameter [4]. High wear-resistant tool steel CPM15V was laser deposited on the steel roller to form near-net-shaped cutting blades. By using optimized processing parameters, it just took 45 minutes to deposit 12 pieces of near-net-shaped cutting blades by laser cladding. Compared with the conventional production process (it takes 7 days to finish the whole process, including both heat treatment and machining), this new process is so efficient that production costs can be significantly reduced. For the sake of cost-effective production, parabolic clad bead was chosen for this particular application purpose. The cladding tracks are 1.8 mm in height and 3 mm in width. They are subsequently machined, sharpened and honed into cutting blades, as shown in Figure 4.27(b). Fully functional prototype of industrial rotary cutting dies, for pilot testing, has been successfully produced by this newly developed process. The experimental result has also demonstrated that the curvature of a substrate can be accommodated, in our laser cladding system, to produce high quality curved cladding

tracks. Thus, this new technique has opened a novel application field of laser-assisted die manufacturing, through which required geometric patterns on steel substrates can be deposited for manufacturing cutting and/or stamping dies.

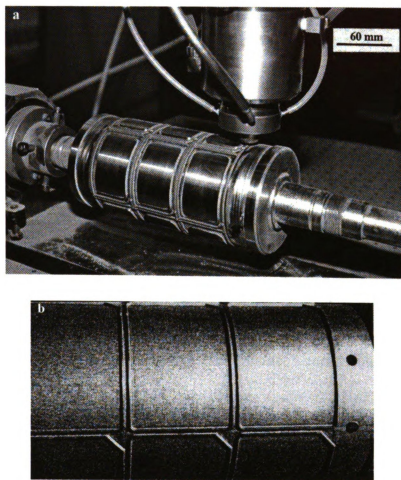


Figure 4.27 An overview of near-net-shaped cutting blades deposited on a steel roller by laser cladding process. (a) As-cladded condition. (b) After machining [4].

The optimized processing parameters for directly fabricating the cutting dies are listed in Table 4.1.

Table 4.1 Processing parameters of producing rotary cutting dies

Samples	Material	Power P (watts)	Traverse speed v (mm/sec)	Spot size D (mm)	Powder feed rate F _p (gm/sec)
1	CPM 15V	2370	4.7	2.3	0.25

Samples	Energy density E _d (J/mm ²)	Cover gas flow rate (m ³ /hr)	Carrier gas flow rate (m ³ /hr)
1	279.2	1.27	0.62

4.16.1.2 Microstructure of Clad Bead

Vanadium contents in CPM 10V and CPM 15V are up to about 10 and 15 wt. %, respectively. Its major influence is the formation of highly wear-resistant carbides. Vanadium carbide is one of the hardest carbides found in high speed steels. These carbides also help maintain a very fine grain size at the high heat treating temperatures used for high speed steels because vanadium carbide is a thermodynamically stable intermetallic compound. That is why highly wear-resistant tool steel CPM15V was used to form near-net-shaped cutting blades by laser cladding process. Figure 4.28 (a) displays that fine spherical vanadium carbide particles are uniformly dispersed in the matrix, which consists of martensite and retained austenite. High magnification SEM micrograph in Figure 4.29 clearly shows the morphology of vanadium carbide. Due to high cooling rate, laser cladding process refines microstructures, and forms supersaturated solid solutions. Therefore, strength, hardness, and ductility of deposited tracks can be greatly improved. In comparison, the morphology of coarse eutectic chromium carbides and precipitated Cr₇C₃ and Cr₂₃C₆ carbides in D2 alloy [109] is shown in Figure 4.28(b). The coarse chromium carbides segregate along transverse direction in D2 tool steel ingot, and lead to poor mechanical properties.

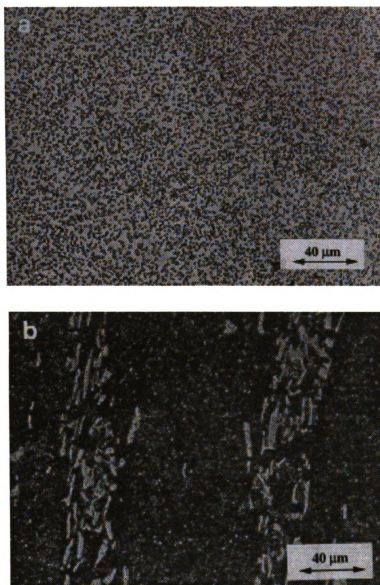


Figure 4.28 Overview of carbides in CPM 10V and D2 alloys. (a) Fine vanadium carbide uniformly dispersed in the matrix in CPM 10V tool steel. (b) Segregation and flake morphology of coarse chromium carbides in D2 alloy.

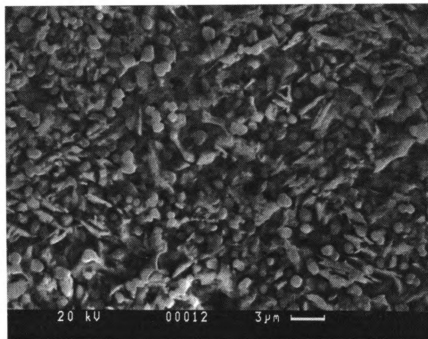


Figure 4.29 SEM micrograph of clad bead, showing morphology of vanadium carbides.

4.16.1.3 Microhardness of Clad Bead

Figure 4.30 shows Vickers hardness measured from the CPM10V clad bead to the substrate under different treatment conditions. The sample used to measure the hardness was made by the following processing parameters: laser power P is 2073 watts, laser spot diameter D is 2.3 mm, traverse speed v is 3 mm/sec, and powder feeding rate F_p is 0.167 gm/sec.

The hardness of the as-clad sample is about 650 Hv, which is approximately equal to that of conventional tool steel D2 after standard heat treatment, as shown in Figure 4.30 (a).

Because retained austenite in high-alloy steels is extremely stable, it must be destabilized by tempering above 500°C, and transformed to martensite. Also, the

tempering treatment can further increase the hardness of steel by secondary hardening and the formation of hard martensite [110, 111]. For this reason, after the sample is “double tempered” at 540°C for 15 minutes each, the hardness increases to about 700 Hv, as shown in Figure 4.30 (b).

After the tempered sample is dipped in liquid nitrogen for 15 minutes, the hardness increases to 850 Hv due to the transformation of the retained austenite to martensite, as shown in Figure 4.30 (c).

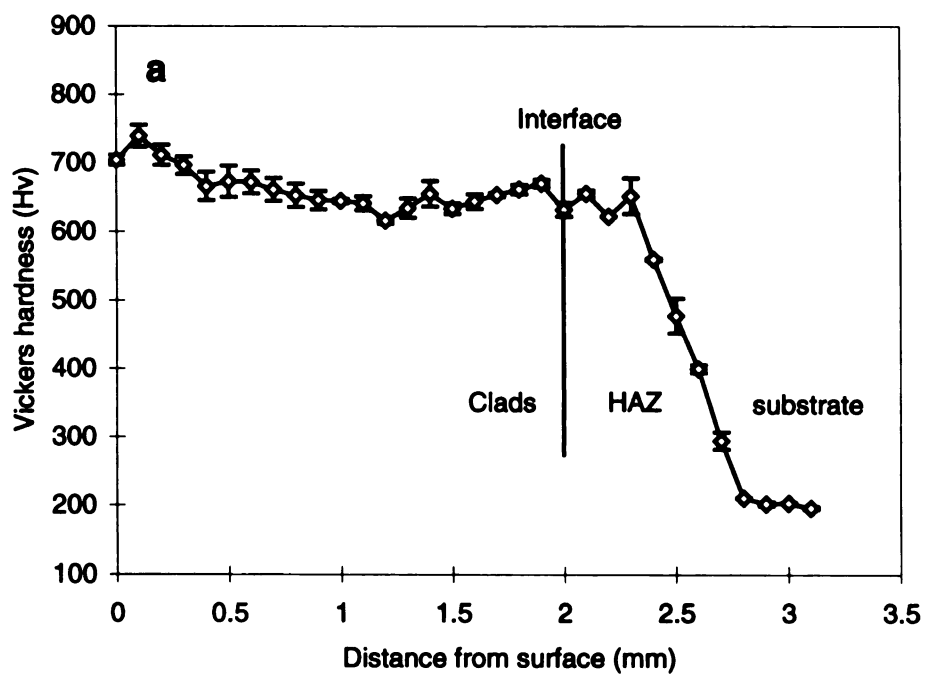
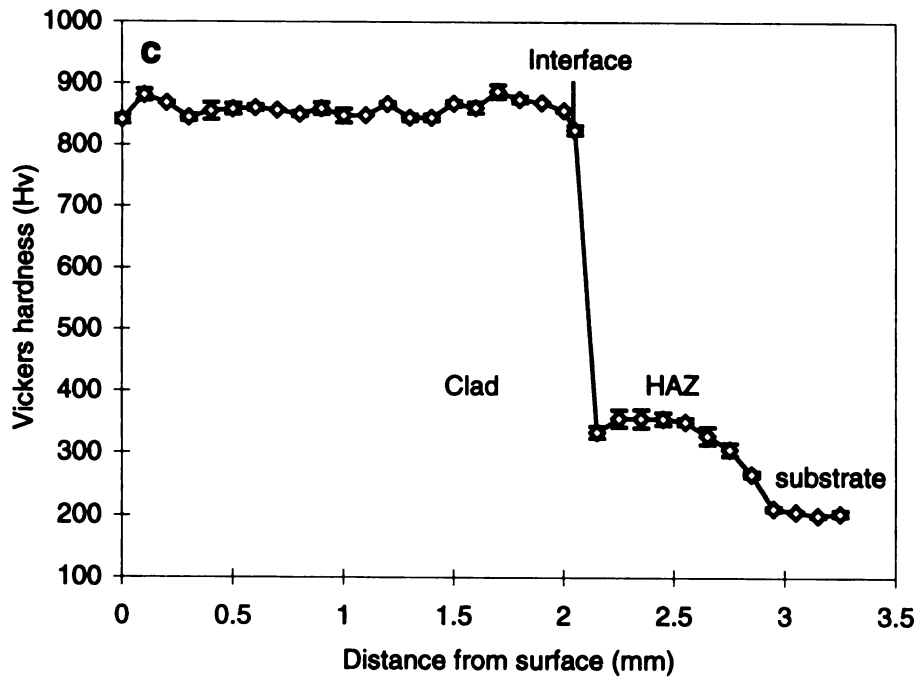
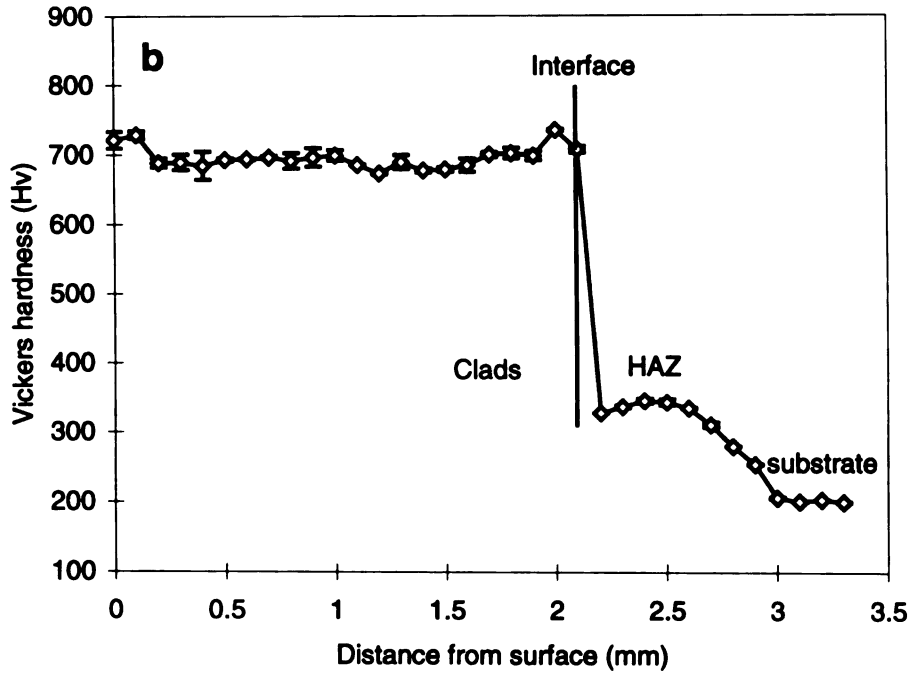


Figure 4.30 Microhardness profiles of the cladding track. (a) As-clad. (b) As-clad + tempering. (c) As-clad + tempering + liquid nitrogen treatment.

(continued)



4.16.2 Laminated Metal Matrix Composites (LMMCs)

A laminated metal matrix composite (LMC) is defined as a composite material with alternate layers of a high-modulus, high-strength material as the strengthener, and a deformable ductile material as the matrix. To the best of our knowledge and experience in laser cladding process, such a composite material can be directly deposited from the metallic powder by laser cladding technique. In this study, 304L stainless steel and CPM10V tool steel have been used as clad materials. The composite materials have been produced in such a way that the laminates consist of alternating stainless steel and tool steel layers or one stainless steel and two tool steel layers. Each a composite material is characterized by hard surface, wear-resistance, and tough core, and could possibly be used to fabricate cutting blades of cold tooling dies, which are required to withstand imposed service loads without deformation, fracture, and excessive wear. I have conducted a series of experiments, and succeeded in producing various geometric laminated 3-D components. The laminated composites have relatively smooth surface and a good planer interface, are free of pores and cracks, and good bonding between two layers.

4.16.2.1 Direct Fabrication of LMMCs

For convenience, the processing parameters used for producing samples 2-7 are listed in Table 4.2. For samples 2-5, the laminated orders from the bottom to the top are ABBABB and the like, and the processing parameters from the second layer through the top layer are the same.

Table 4.2 Processing parameters used for the laser cladding operations

Samples	Laminated Layers	Power (watts)	Traverse speed (mm/sec)	Powder feed rate (g/sec)	Overlapping percentage (%)
2, 3, 4, 5	1 st 304L	1970	5	0.1	50
	2 nd CPM 10V	1260	5	0.1	50
	3 rd CPM 10V	1260	5	0.1	50
6	1 st 304L	1914	3	0.12	25
	2 nd CPM 10V	1326	4.9	0.08	50
	3 rd 304L	1326	4.9	0.08	50
	4 th CPM10V	1326	4.9	0.08	50
7	1 st 304L	1914	3	0.12	25
	2 nd CPM 10V	2073	4.9	0.12	25
	3 rd 304L	1914	3	0.12	25
	4 th CPM10V	2073	4.9	0.12	25

Figure 4.31(a) is a view of a laminated metal matrix composite (LMMC) coupon, alternating 304L stainless steel and two CPM10V tool steel layers. The LMMC sample has a smooth surface. The overlap between two adjacent tracks is about 50%. Two separate powder hoppers and metering systems were used to fully automate to produce the LMMC layers.

Figure 4.31(b) and (c) are an overview of square and saddle contours produced by laser cladding process, respectively. The prototypes are 6 mm in height. The square is 38 mm in inner length, and the saddle is 26 mm and 34 mm in diameter and in length, respectively. The deposited components consist of alternating one 304L stainless steel and two CPM10V tool steel layers. On each layer, three cladding tracks overlapped. They have relatively smooth surface and no macro cladding defects.

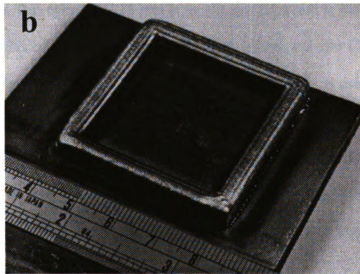
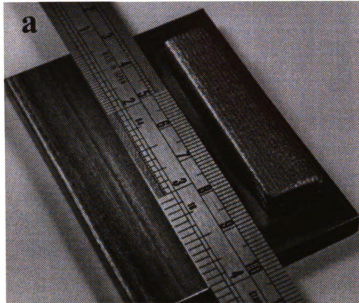


Figure 4.31 Photos of LMMC samples. (a) Buildup coupon (sample 2). (b) Square (sample 3). (c) Saddle prototype (sample 4) with smooth surface via laser cladding.

(continued)



Figure 4.32(a) is an overview of a rapid prototype of a hollow cylinder by laser cladding process. This cylinder is 16 mm in height, and 25.4 mm in inner diameter. It has 18 laminated layers of alternating one 304L stainless steel and two CPM10V tool steel layers. On each layer, four tracks overlapped. Stainless steel 304 is used as the transition layer due to its good ductility and toughness. This thin transition layer plays a key role in direct deposition of tool steel for making 3-D components with laser. Experimental results have shown that, without this transition layer, cladding layers either debond from the substrate or have macrocracks from the top through the bottom. Figure 4.32(b) and (c) clearly show such defects.

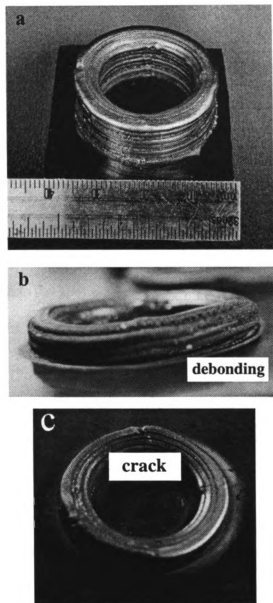


Figure 4.32 A view of LMMC cylinder prototype produced by laser cladding (sample 5). (a) is a good sample, and (b) and (c) show some forming defects as discussed in this section.

In all cases displayed above, the dimension tolerance for the components produced in such a way is not accurate enough to be directly used, and they still need post-clad machining. Based on our best understanding, the tolerance for the deposited

parts is a function of deposition rate (buildup volume per unit time), which is controlled by laser power input, laser spot diameter, powder feed rate, and traverse speed. The higher the deposition rate is, the worse is the tolerance, and vice versa. For samples 1-4, the deposition rate is $30 \text{ cm}^3/\text{hr}$. This deposition rate is much higher than $8.2 \text{ cm}^3/\text{hr}$ [96], but the dimension tolerance is worse than that of components. There is a tradeoff between the deposition rate and the dimension tolerance. If traverse speed is kept constant, and power density (the ratio of incident laser power to irradiated area) is high enough, then both powder feed rate and laser spot size play critical roles in both deposition rate and tolerance control. Smaller the spot size, the lower powder feed rate, better will be the tolerance control. For the consideration of both deposition rate and dimension tolerance, all processing parameters for laser cladding technique have been optimized to directly deposit industrial components at a relatively high deposition rate, and with smooth surface, and good dimension tolerance. In order to reach this goal, there is still a lot of research work to do in the future.

4.16.2.2 Microstructure of the Cross Section of LMMCs

Figure 4.33 is an optical macrograph of the cross section of laminated metal matrix composites. It consists of alternating one 304L stainless steel layer and one CPM10V tool steel. Figure 4.33(a) shows that laminated metal matrix composite is free of pores and cracks, and has smooth and discrete interfaces. From C layer, laser power input is reduced to ~ 1320 watts from ~ 1900 watts due to large increase of the energy coupling rate after depositing the first layer. In this way, a minimum intermixing between two layers can be maintained. In comparison, Figure 4.33(b) shows a macrograph of the cross section of sample 7 with high dilution. Due to higher laser energy input from C

layer to A layer, compared with the corresponding layers in sample 6, stainless steel and tool steel layers intermixed too much (that is what high dilution means), and thus changed chemical compositions and properties of each layer to some extent. In addition, the overlapping rate between two adjacent tracks is approximately 25 percent. So sample 7 has a relatively rough surface. The experimental results have shown that 50 percent overlapping rate is best suited for depositing LMMCs.

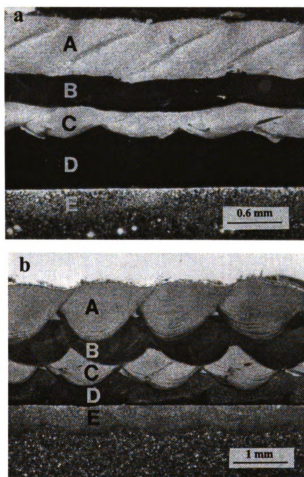


Figure 4.33 An overview of the cross section of LMMC samples 6 and 7. A and C are tool steel CPM10V layers, while B and D are stainless steel layers. E is heat-affected zone [87].

The microstructure of CPM10V layer is shown in Figure 4.27 (a). Figure 4.34 is a magnified optical micrograph corresponding to B layer in Figure 4.33(a). Figure 4.34(a) shows cellular dendrite structure due to high cooling rate. It was reported that a duplex structure of γ - and δ -ferrite existed, and the latter is finely dispersed in the austenitic matrix [112]. In addition, the top tool steel layer was built up on B stainless steel layer, and then the latter was tempered at high temperature during the process. Thus, some precipitated carbides are dispersed in an austenite matrix, as shown in Figure 4.34(b).

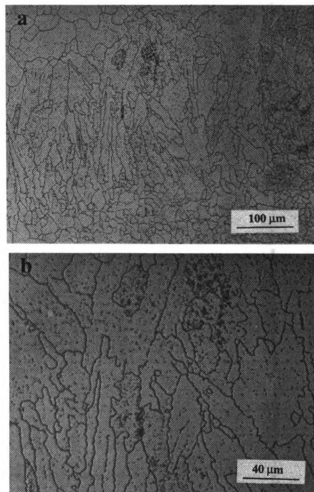


Figure 4.34 Higher magnified optical micrographs of laser clad stainless steel 304L layer. (a) Cellular dendrite structure. (b) The same sample, but higher magnified micrograph shows the precipitated carbides dispersed in the austenite matrix.

4.16.2.3 X-Ray Dot Mapping

One of important issues related to laser cladding process is the metallurgical bonding and its strength. Surface melting condition and compatibility between the cladding and base materials have a great effect on the quality of bonding. In order to maintain both chemical composition and properties of cladding material, the intermixing zone between the clad and the substrate has to be controlled as small as possible by adjusting processing parameters. X-ray dot mapping or EDXS analysis can reveal the alloying element distribution in the interface zone.

The laminated metal matrix composite consists of alternating 304 stainless steel (SS304) and CPM10V tool steel layers, and its base metal is 1045 plain medium carbon steel. The main alloying elements for SS304 are chromium (18.5 wt.%) and nickel(9.5 wt.%); while the alloying elements for CPM10V are vanadium (9.75 wt.%) and chromium (5.25 wt.%). The 1045 steel does not contain these alloying elements. Figure 4.35(a) is a SEM micrograph of the interface zone between the SS304 layer and the 1045 substrate. It clearly shown a sharp but discrete interface. Figure 4.35(b) and (c) display chromium and nickel distributions near the interface zone. The existence of both chromium and nickel elements in the interface zone has proved that laser energy melts a substrate surface, and chromium and nickel atoms penetrate into the substrate forming a sound metallurgical bonding with a low dilution.

Figure 4.36(a) is a SEM micrograph of the inter-diffusion zone between the CPM10V and the SS304 layers. Figure 4.36 (b), (c) and (d) shows chromium, nickel, and vanadium element distribution near the inter-diffusion zone, respectively. During laser

cladding, these alloying element atoms inter-diffuse each other, and form a strong metallurgical bonding.

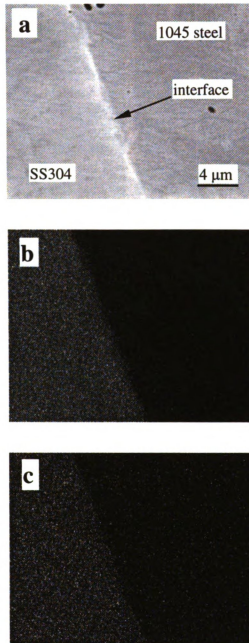


Figure 4.35 Overview of X-ray dot mapping of sample 6. (a) SEM micrograph of 304 stainless steel-1045 steel interface zone. (b) Chromium distribution in the inter-diffusion zone. (c) Nickel distribution in the inter-diffusion zone.

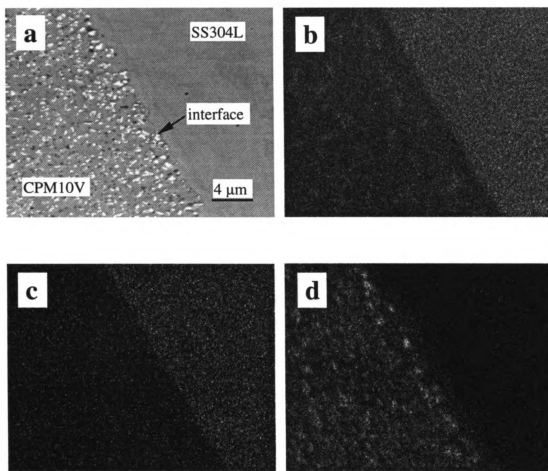


Figure 4.36 X-ray dot mapping of sample 6. (a) SEM micrograph of CPM10V tool steel and SS304L stainless steel interface zone. (b) Chromium distribution in the inter-diffusion zone. (c) Nickel distribution. (d) Vanadium distribution.

4.16.2.4 Microhardness Measurement of LMMCs

Figure 4.37 is a microhardness profile of LMMC sample 6, measured from the top layer through other three layers and interface to the substrate. 100-g and 500-g loads, respectively, were used for the measurement of 304L stainless steel and CPM10V tool steel layers in order to reduce the indentation area. Vickers hardness for stainless steel 304L and tool steel CPM10V layers, respectively, is about 300 Hv and 750 Hv. 304L stainless steel is austenitic type stainless steel, so it does not transform to martensite during the laser cladding. That is why the hardness of 304L stainless steel layer is low. In addition, hardness distribution on each cladding layer is quite uniform.

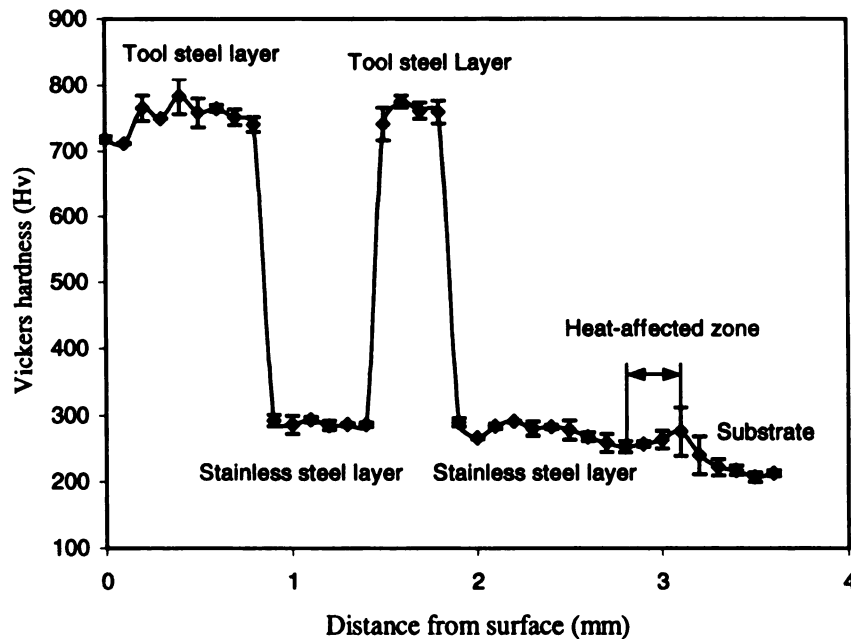


Figure 4.37 Vickers hardness profile of LMMC sample 6.

4.17 Temperature Measurement

One of the characteristics of laser cladding process is rapid melting and solidification. Due to high cooling rate, this process can refine microstructures, form metastable phases, and extend supersaturated solid solutions. Therefore, strength, hardness, and ductility of deposited layers can be greatly improved. It is challenging to accurately measure the temperature distributions of the clad zone, heat-affected zone, and substrate. Conventionally, optical pyrometer has been widely employed to measure a thermal cycle during laser cladding [113, 114]. It was reported that, during laser cladding experiments, the temperatures of the molten pool were all the same at approximately 1700 °C [113]. Recently, charge coupled device (CCD) camera has been used in laser cladding process to perform temperature measurements of the melt pool [115].

So far, few reports have been published which present other new experimental methods to measure the clad-zone temperature. It is this observation that encourages me to utilize Tungsten-Rhenium high-temperature thermocouples to do so. In our study, a wide range of processing parameters and various clad materials have been used in laser cladding experiments to measure temperature distributions [102]. The clad-zone temperatures under various processing conditions fall between 1650 °C and 1800 °C. In this section, this experimental method will be described to determine the thermal cycle and temperature distributions for laser cladding process. The processing parameters and the pertinent technical issues will also be discussed in detail.

4.17.1 Temperature Distributions Without Powder Feeding

Figure 4.38 is a temperature distribution for laser remelting AISI 4140 steel plate. Thermal cycles 0-3 were measured by thermocouples 0-3, respectively. When the laser

beam irradiates the steel plate at some distance away from the thermocouple, the temperature gradually rises due to good thermal conductivity of the workpiece. As the laser beam approaches closer to the thermocouple, then the surface temperature suddenly increases, and quickly reaches the highest point. After that, the laser beam travels away from the thermocouple, and the temperature of the workpiece surface immediately decreases. This is a typical thermal cycle for laser beam-materials interaction. Under the processing condition, the peak temperature for thermocouple 0, located in the center of the laser beam, is about 1550 °C, which is 80 °C higher than the melting temperature 1470 °C of AISI 4140 steel. In the case of the laser cladding process, this experimental data can help understand how much laser energy is required to be transmitted to the workpiece, in order to get a good metallurgical bonding between the clad and the substrate.

Figure 4.39 shows the distribution of the thermal gradients on the workpiece surface along y-direction under each processing condition. The experimental results clearly show that the temperature distribution (the peak temperature for each thermal cycle) is a function of the distance away from the laser beam center, if other parameters are kept constant. The temperature gradients gradually decrease at points farther from the laser beam center. When the distance is about 4 mm away from the laser beam center, the temperature reaches to ~150 °C under all processing conditions.

During laser materials processing, the workpiece temperature at the laser beam center is a function of laser power input if other processing parameters are kept constant, as shown in Figure 4.40. The temperature increases with the increase of laser power input. When the laser power input is ~760 watts, the surface temperature reaches up to ~1800 °C.

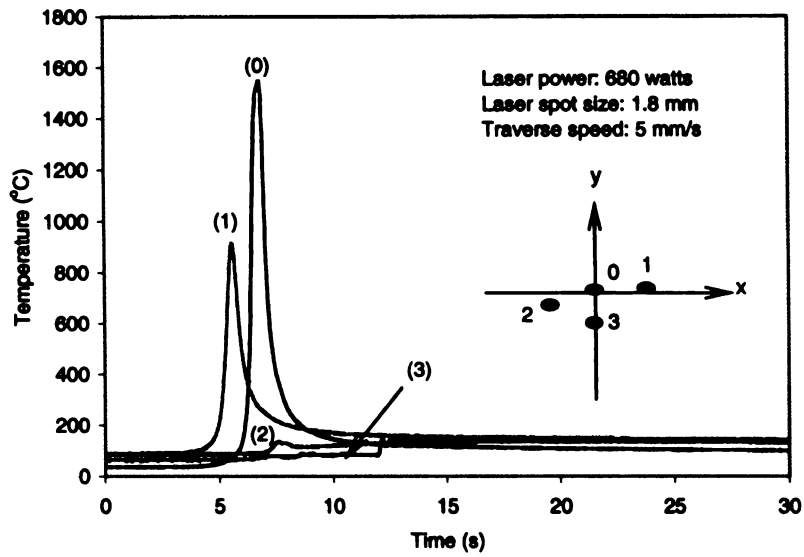


Figure 4.38 A temperature distribution of a laser beam and substrate interaction without powder feed [102].

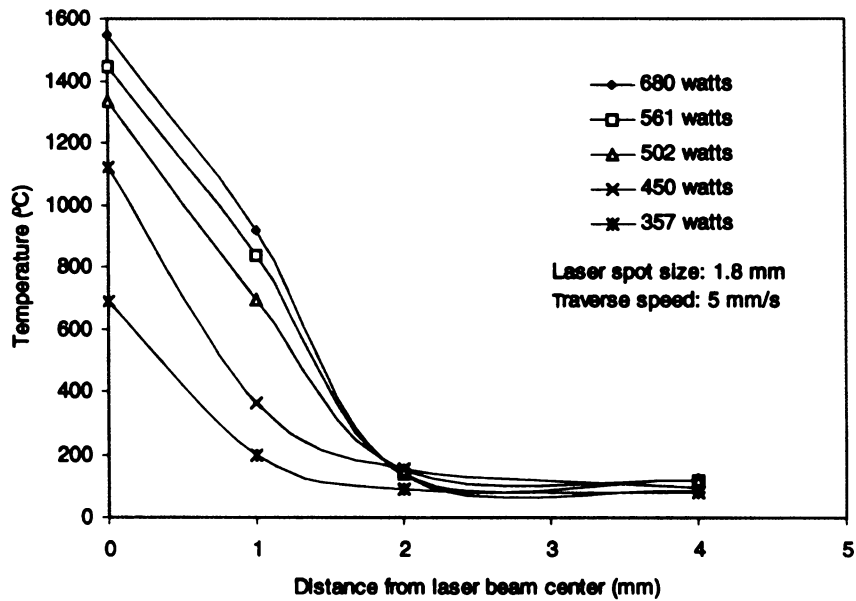


Figure 4.39 Temperature distributions on the surface of the substrate as a function of the distance from laser beam center along y direction [102].

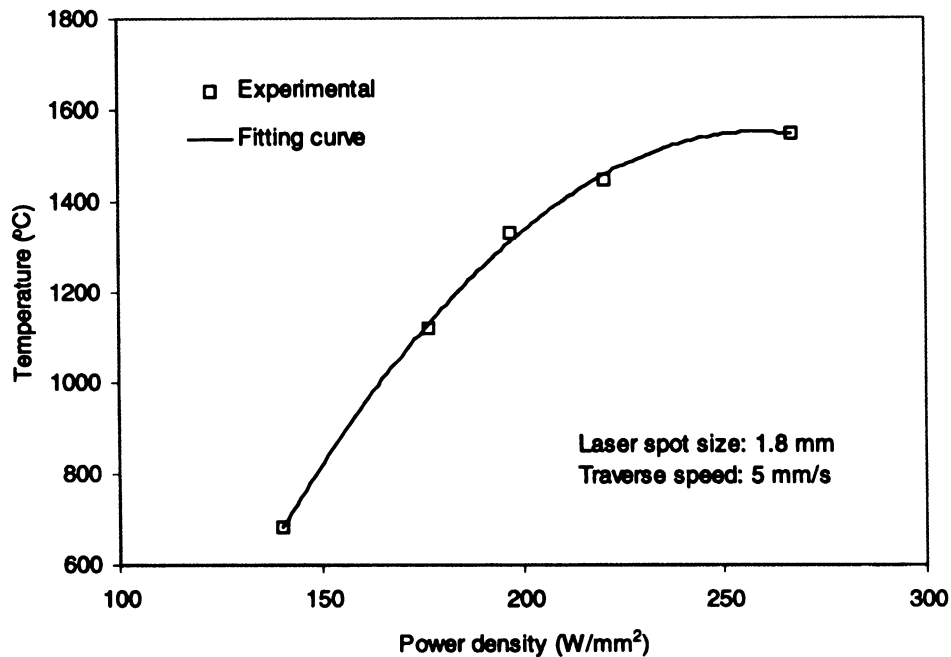


Figure 4.40 Surface temperature at laser beam center as a function of laser power input [102].

4.17.2 Temperature Distribution for Laser Cladding Process

Laser cladding is a process, which involves many metallurgical and physical mechanisms. For example, interaction between the laser beam and the material(s), rapid melting and solidification, and inter-diffusion between the clad and the substrate materials are the dominant mechanisms. During the laser cladding, the interaction of a laser beam with the materials includes the processes of reflection, absorption, and transmission. Thus, the energy balance equation governing laser cladding process may be expressed as:

$$P_l = P_p + P_w + P_r \quad (4.27)$$

where P_l is the total laser power input, P_p the laser power absorbed by powder particles, P_w the laser power absorbed by workpiece, and P_r the laser power reflected by the workpiece and the powder. When P_l is fixed, the magnitudes of P_p and P_w control the energy coupling rate. It was found that the energy coupling rate strongly depends on several factors, such as powder supply methods (pre-placed or coaxial methods), laser parameters (laser-beam mode, and laser-beam wavelength), and absorptivity of both substrate and filler materials (material type and workpiece surface condition) [113].

The thermal cycles for the laser cladding process were, as shown in Figure 4.41, measured from thermocouples 0-3. Under this processing condition, the temperature of clad zone is ~ 1660 °C. The temperatures drop to ~ 1420 °C and ~ 500 °C at 1 mm and 2 mm from the laser beam center, respectively.

Our data acquisition board just has four channels to receive voltage signals during the process, so two sets of data (the peak temperature for each thermal cycle in Figure 4.41) have been superimposed to plot a diagram of temperature versus. distance from the laser beam center, as shown in Figure 4.42. The temperature gradients have Gaussian-like distribution.

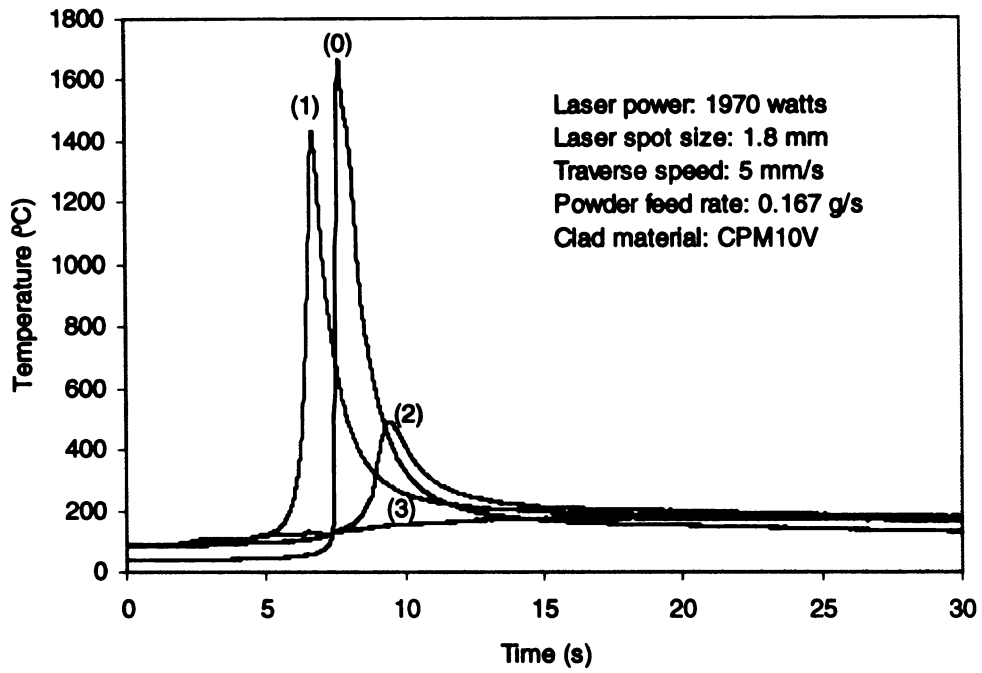


Figure 4.41 Temperature distributions of laser cladding process under given process conditions [102].

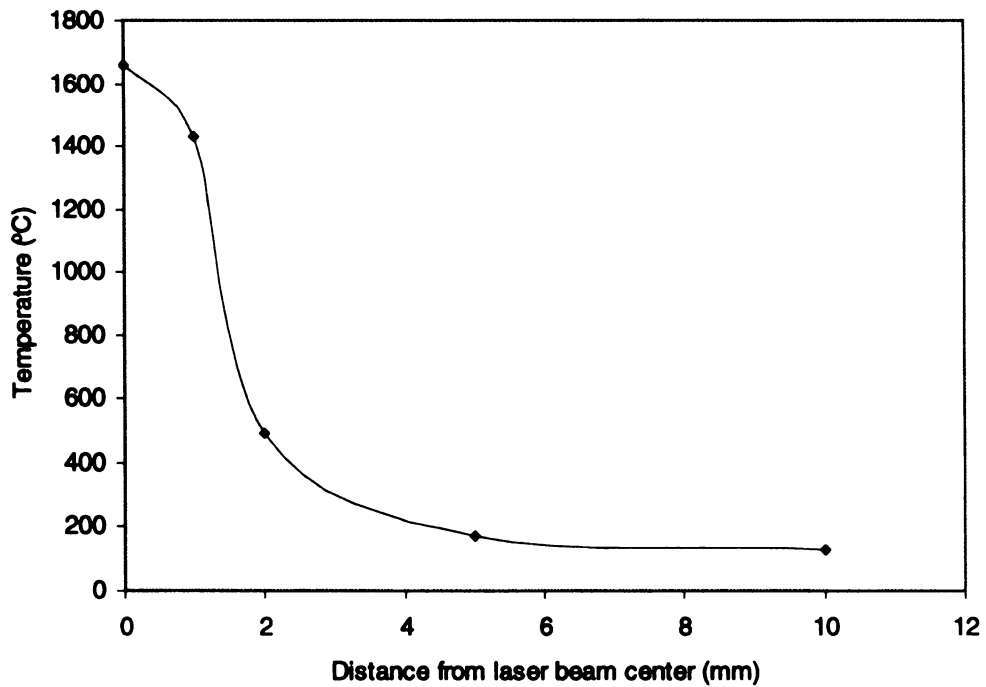


Figure 4.42 Temperature gradients along y direction [102].

The main processing parameters for the laser cladding technique include laser power, laser spot size, traverse speed, powder feed rate, and shielding gas flow rate and so on. Within optimized operation window (except extreme cases), all these variables have some effect on the temperature of clad zone. A wide range of parameters, and various clad materials were used for laser cladding to measure the temperature of the clad zone. Figure 4.43 displays a few thermal cycles for different filler materials, measured at the laser beam center under the same processing conditions. Even if the filler materials are different, the molten-pool temperatures fall between 1650 °C and 1800 °C. These results are in good agreement with those measured by using an optical pyrometer and CCD technique [113, 115].

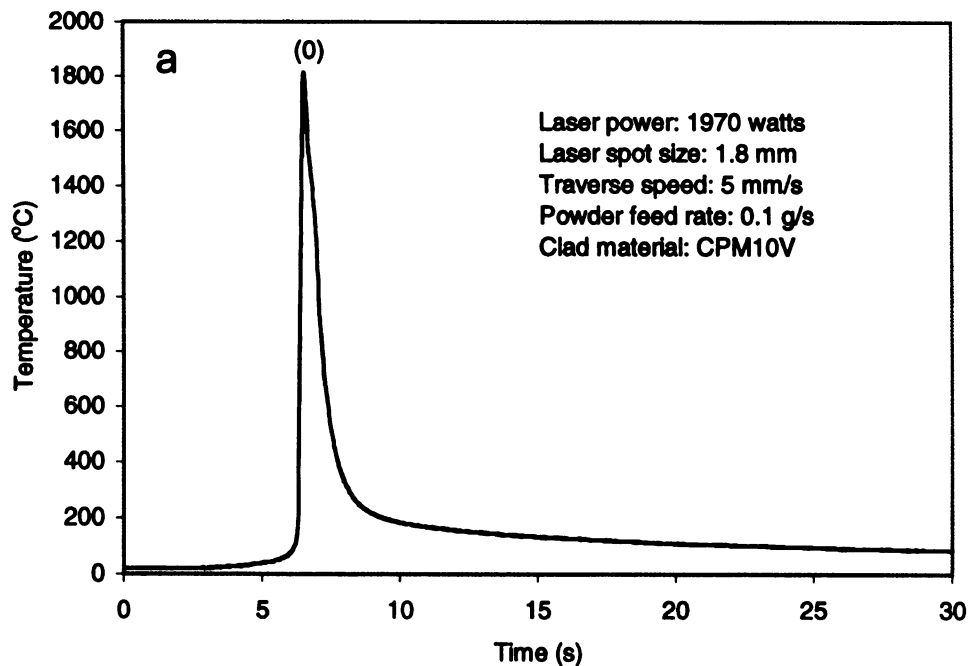
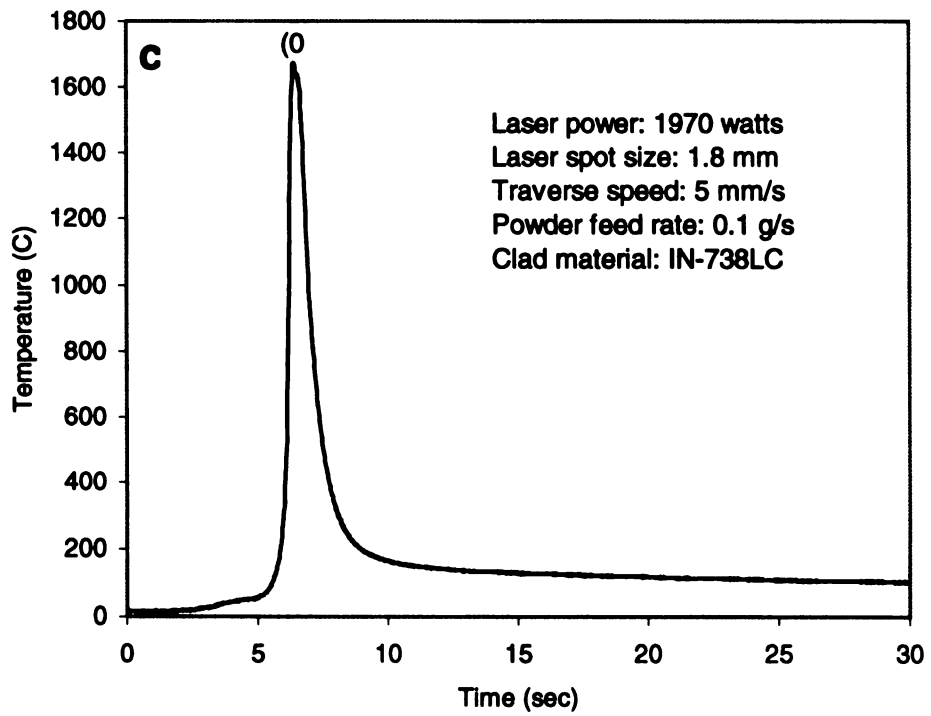
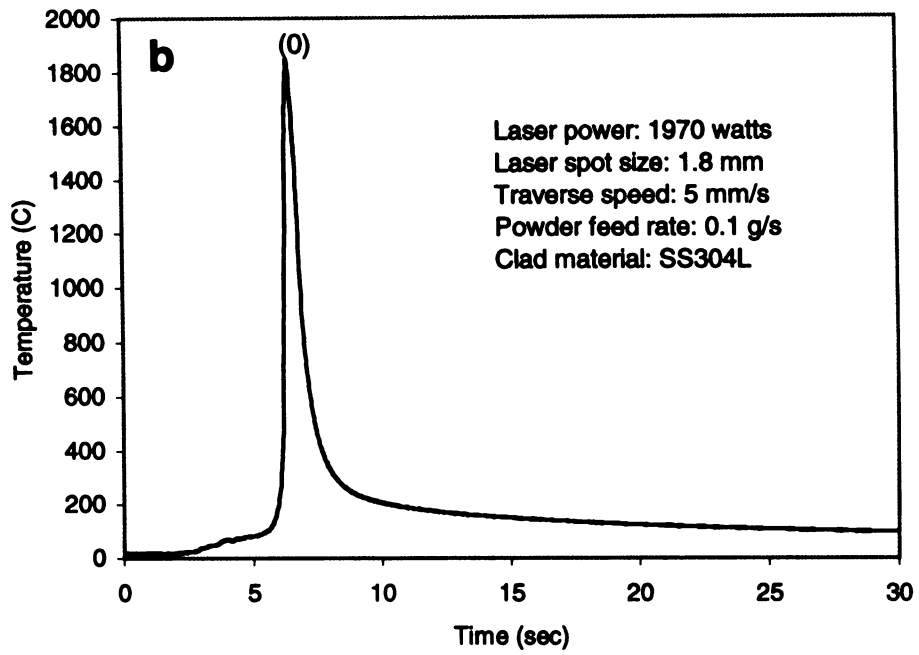
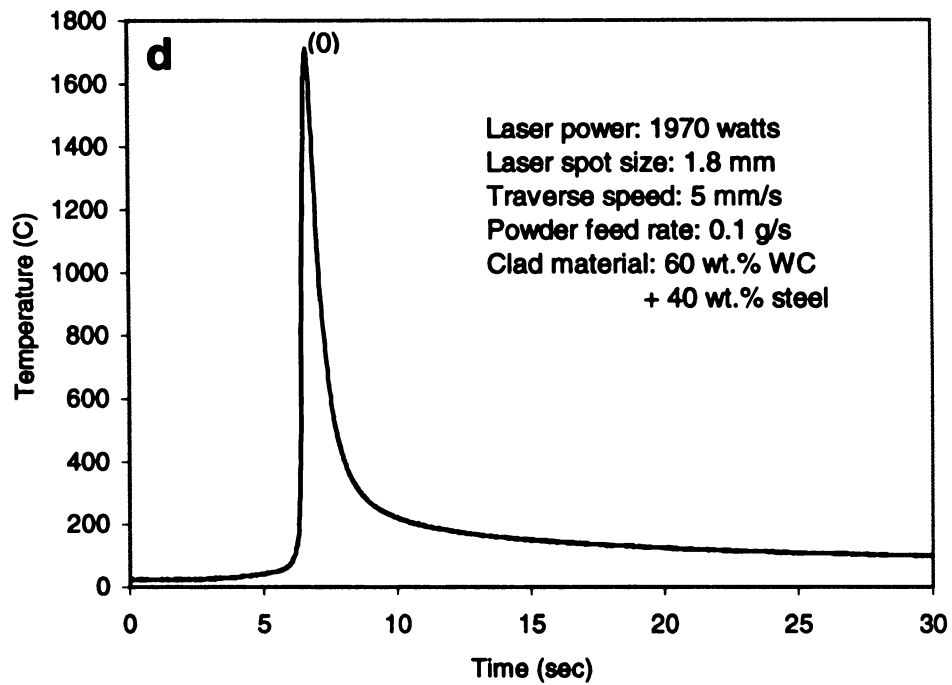


Figure 4.43 Temperature distribution of laser cladding process under laser beam center. (a) CPM10V tool steel. (b) SS304L stainless steel. (c) IN-738LC nickel-base superalloy. (d) Carbide blend.

(continued)



(continued)



The optical macrograph of the cross section of as-cladded sample with a thermal couple is shown in Figure 4.44. It is very difficult to place both thermocouple wires and their junctions inside the clad. Due to our experimental design, the thermocouple junction is located in the middle of the clad. Therefore, the temperature measured this way has to be the molten-powder temperature. This macrograph strongly supports the accuracy of our experimental results. In addition, the clad is free of pores and cracks.

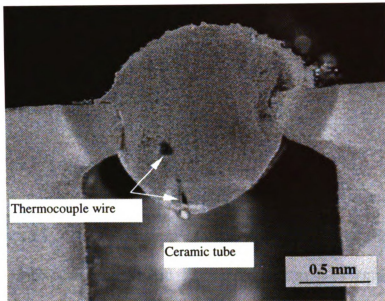


Figure 4.44 Optical macrograph of the cross section of a single cladding track, and its processing conditions are given in Figure 5.43(a) [102].

Chapter 5

CONCLUSIONS

Based on experimental results, the following conclusions can be drawn from this research:

- The new integrated powder delivery system designed for laser cladding process avoids all the drawbacks of the lateral powder feeding systems. It can provide highly stable, continuous, and accurate powder feed rate, and deliver the powder stream coaxially into the molten pool with the laser beam to form high quality cladding tracks or layers, with smooth surfaces, and uniform thickness and width. Also, this system is suited for deposition of complex geometric patterns on a flat plate or a curved surface for different applications, such as fabrication of rotary cutting dies, prototyping of forging dies, and repair of turbine blades. Most importantly, the new powder feeding system is suitable for on-line industrial production.
- Cover gas flow rate has a great effect on cone-shaped powder stream. When cover gas flow rate is increased from 0.85 to 3.4 m³/hr, it exerts a larger force on cone-shaped powder stream along its central axis, and squeezes the powder stream out. Under this condition, more powder bounces up from a workpiece surface in all directions. This will lead to decrease in powder utilization efficiency, and formation of poor quality cladding tracks. It has been found that, for our specially designed coaxial powder feeding system, the upper limit of cover gas flow rate for laser cladding process is about 1.7 m³/hr.
- For a given laser power and spot size, when the traverse speed varies from ~5 to ~10.5 mm/sec, and the powder feed rate varies from 0.1 to 0.25 gm/sec, powder

utilization coefficient, α , is constant for each process condition. In other words, the value of α is a constant function of traverse speed, and powder feed rate under experimental conditions. However, it is related to the laser spot size. When the laser-beam diameter D was 1.8 mm, the average value of α was 0.71. For $D \geq 2.3$ mm, average value of α was 0.80.

- With other variables held constant, clad width linearly decreases as traverse speed increases. When traverse speed accelerates to 8.4 mm/sec, clad width is almost equal to laser-beam diameter. This speed is called the threshold traverse speed for this laser cladding system. Below the threshold traverse speed, the clad is much wider than the laser spot size. Clad width gently increases with the increase of energy density when other parameters are kept constant. The clad gently widens as powder feed rate increases with other variables held constant.
- A simple but realistic process model is developed, relating the maximum clad thickness and various process parameters. For a given alloy powder, if the powder feed rate and spot size are kept constant, the clad thickness is inversely proportional to traverse speed. While traverse speed and spot size are held constant, the clad thickness is directly proportional to powder feed rate. In each case, the calculated results of this model are in good agreement with experimental results.
- An energy density equation, suitable for a TEM_{01} beam mode, is developed. When laser power and traverse speed are kept constant, the energy density is inversely proportional to spot size. While laser power and spot size are held constant, the energy density is inversely proportional to traverse speed. If traverse speed and spot size are constant, the energy density is directly proportional to laser power.

- Thermal penetration depth is a linear function of energy density. For fixed traverse speed, spot size, and powder feed rate, the higher laser power, the higher is the energy density, and more energy is transferred to the substrate, and therefore the deeper is the heat-affected zone.
- Overlapping rate, dilution, and deposition rate for laser cladding process have been defined, respectively. Based on each definition, a simple but useful formula has also been developed.
- A novel process for manufacturing tooling dies, with required geometric patterned cutting blades, has been successfully developed directly by laser cladding process. Fully functional prototype of an industrial rotary cutting die, for pilot testing, has been produced. Compared with the conventional manufacturing process, this new technique can dramatically reduce the production costs due to the elimination of costly heat treatment, and no or greatly reduced demand for electric discharge machining (EDM). In addition, the durability of cutting and stamping dies can be significantly improved because the wear resistant property of CPM15V clad material is much better than that of the tool steel D2, currently used in industry. This new process has been implemented in tooling-die manufacturing industry.
- Within optimized process parameters, various geometric 3-D components have been directly deposited by laser cladding technique. Laser deposited 3-D prototypes on steel substrates are found to be relatively smooth and metallurgically sound. Optical micrographs displayed that they are free of pores and cracks, and have a good metallurgical bonding with the substrate, but with low dilution. Laminated layers have

planner interfaces to maintain both original chemical compositions and mechanical properties of each cladding layer.

- The measurement of the thermal cycle and the temperature distributions for laser cladding process has been developed. Within optimized operation window, a wide range of processing parameters, and various clad materials have been used in laser cladding experiments. The clad-zone temperatures under various processing conditions lies between 1650 °C and 1800 °C. These results are in good agreement with those obtained by optical pyrometer and CCD technique. In addition, in both cases of laser remelting and cladding processes, the temperature gradients along y-direction have Gaussian-like distribution.

BIBLIOGRAPHY

BIBLIOGRAPHY

- [1] M. Cadenas, R. Vijande, H.J. Montes, and J.M. Sierra, "wear behavior of laser cladded and plasma sprayed WC-Co coatings," *Wear*, vol. 212, no. 2, pp. 244-253, 1997.
- [2] Niklas Axen, "Abrasion resistant laser composite layers on tool steels," *Tribologia*, vol. 17, no. 1, pp. 15-18, 1998.
- [3] W. Cerri, R. Maryinella, and G. P. Mor, "Laser deposition of carbide-reinforced coatings," *surface and Coatings Technology*, vol.49, 1991, pp. 40-45.
- [4] Y. P. Hu, C. W. Chen, and K. Mukherjee, "Laser cladding of wear-resistant tool steel," *Advanced Materials & Processes*, vol.152, no. 2, pp. 31-32, 1997.
- [5] Hiro Iwamoto *et al.*, "High temperature oxidation behavior of laser clad NiCrAlY layer," *Materials Science & Engineering A*, vol. A241, no. 1-2, pp. 251-258, 1998.
- [6] J. De Damborenea and A. J. Vasquez, "Laser cladding of high-temperature coatings," *Journal of Materials Science*, vol. 28, no. 17, pp. 4775-4780, 1993.
- [7] Y. P. Hu, C. W. Chen, and K. Mukherjee, "Laser cladding of copper-based composites on 6061 aluminum alloy," (invited) in *The Third Pacific Rim International Conference On Advanced Materials and Processing* (M.A. Imam, R. DeNale, S. Hanada, Z. Zhong, and D.N. Lee, Eds.), vol. 2, pp. 2169-2176, published by TMS, 1998.
- [8] W. M. Steen, "Laser surface cladding," in *Laser Surface Treatment of Metals* (C.W. Draper and P. Mazzoldi, Eds.), pp. 369-387, Martinus Nijhoff Publishers, 1986.
- [9] O. D. D. Soares, "Applied laser tooling," in *Applied Laser Tooling* (O. D. D. Soares and M. Perez-Amore, Eds.), pp. 1-24, Martinus Nijhoff Publishers, 1987.
- [10] Y. P. Hu, C. W. Chen, and K. Mukherjee, "Development of a new laser cladding process for cutting and stamping die manufacturing," *Journal of Materials Science*, vol. 33, pp. 1287-1292, 1998.
- [11] Leon-Fong, "The physics of lasers," in *Applied Laser Tooling* (O. D. D. Soares and M. Perez-Amore, Eds.), pp. 43-53, Martinus Nijhoff Publishers, 1987.
- [12] J. F. Ready, *Industrial Applications of Lasers*. New York: Academic Press, 1978

- [13] J.T. Luxon, D.E. Parker, and P.D. Plotkowski, *Lasers in Manufacturing*. New York: IFS (Publications) Ltd. and Springer-Verlag, 1987.
- [14] W.W. Duley, *CO₂ Lasers-Effects and Applications*. New York: Academic Proess, 1976.
- [15] J. T. Verdeyen, *Laser Electronics*. Prentice-Hall, Inc., 1989.
- [16] D. C. Winburn, *Lasers*. Marcel Dekker, Inc., 1987.
- [17] S.S. Charschan, *Lasers in Industry*. Van Nostrand Reinhold Company, 1972.
- [18] J.E. Harry, *Industrial Application of Lasers*. Mcgraw-Hill, U.K., 1974.
- [19] B. A. Lengyel, *Introduction to Laser Physics*. John Wiley and Sons, Inc., 1967.
- [20] W. M. Steen, *Laser Material Processing*. Springer-Verlag London Limited, 1991.
- [21] A. Belmondo and M. Castagna, "Wear-resistant coatings by laser processing," in *Source Book on Applications of the Laser in Metalworking*, pp. 310-317, ASM International, 1981.
- [22] W. Koechner, *Solid-State Laser Engineering*. New York: Springer-Verlag, 1988.
- [23] D.C. Brown, *High-peak-power Nd: glass laser systems*. New York: Springer-Verlag, 1981.
- [24] A. Sona, "Lasers for surface engineering: Fundamentals and types," in *Lasers in Surface Engineering* (N.B. Dahotre Eds.), pp. 1-34, ASM International, 1998.
- [25] S. Kudapa, *Laser Beam Processing of Metal Matrix Composites*. Ph.D. thesis, Michigan State University, 1996.
- [26] W.M. Steen, and J.N. Kamalu, "Laser cutting," in *Laser Materials Processing* (M. Bass, Eds.), pp. 15-112. North-Holland Publishing Company, 1983.
- [27] R. C. Crafer and P. J. Oakley, "Process and physical aspects of continuous wave laser processing," in *Applied Laser Tooling* (O. D. D. Soares and M. Perez-Amore, Eds.), pp. 55-79, Martinus Nijhoff Publishers, 1987.
- [28] Y. Arata and I. Miyamoto, "Some fundamental properties of high power laser beam as a heat source," in *Plasma, Electron & Laser Beam Technology* (Y. Arata, Ed.), pp.233-262, ASM International, 1986.

- [29] F.D. seaman, "Laser heat-treating," in *Industrial Laser Handbook*, pp. 155-165, Laser Institute of America, 1987.
- [30] T. Bell, "Surface heat treatment of steel to combat wear," *Acta Metallurgia*, vol. 49, no. 3, pp. 103-111, 1982.
- [31] J. Mazumder, "Laser heat treatment: the state of the art," *Journal of Metals*, vol. 35, no. 5, pp.18-26, 1983.
- [32] V. G. Gregson, "Laser heat treatment," in *Laser Materials Processing* (M. Bass, Ed.), Ch. 4, North-Holland Publishing Company, 1984.
- [33] M. F. Ashby, and K. E. Easterling, "The transformation hardening of steel surfaces by laser beam," *Acta Metallurgia*, vol. 32, no. 11, pp.1935-1948, 1984.
- [34] M. Tayal and K. Mukherjee, "Thermal and microstructural analysis for laser surface hardening of steel," *Journal of Applied Physics*, vol. 75, no. 8, pp. 3855-3861, 1994.
- [35] D. N. H. Trafford, T. Bell, J. H. P. C. Megaw, and A. D. Bransden, "Laser treatment of gray iron," *Metal Technology*, vol. 10, no. 2, pp. 69-77, 1983.
- [36] I. C. Hawkes, A. M. Walker, W. M. Steen, and D. R. F. West, "Application of laser surface melting and alloying to alloys based on the Fe-C system," in *Laser Processing of Materials* (K. Mukherjee and J. Mazumder, Eds.), pp. 169-182 AIME, Warrendale, PA, 1985.
- [37] H. W. Bergmann, "Laser surface melting of iron-base alloys," in *Laser Surface Treatment of Metals* (C. W. Draper and P. Mazzoldi, Eds.). pp. 351-368, Martinus Nijhoff Publishers, 1986.
- [38] W. M. Steen, Z. D. Chen, and D. R. F. West, "Laser surface melting of cast irons and alloy cast irons," in *Industrial Laser Annual Hand book 1987* (D. Belforte and M. Levitt, Eds.), pp. 80-96.
- [39] W. J. Tomlinson and M. G. Talks, "Cavitation erosion of heat-treated low alloy cast irons," *Wear*, vol. 137, no. 1, pp.143-146, 1990.
- [40] M. Gremaud, M. Carrard, and W. Kurz, "Microstructure of rapidly solidified Al-Fe alloys subjected to laser surface treatment," *Acta Metallurgica et Materialia*, vol.38, no.12, pp. 2587-2599, 1990.
- [41] M. Pierantoni and E. Blank, "Effect of laser surface remelting and alloying on the wear behaviour of Al-Si alloys," *Key Engineering Materials*, vol. 46-47, pp. 354-367, 1990.

- [42] J. M. Pelletier, D. Pergue, F. Fouquet, and H. Mazille, "Laser surface melting of low and medium carbon steels. Influence on mechanical and electrochemical properties," *Journal of Materials Science*, vol. 24, no. 12, pp. 4343-4349, 1989.
- [43] D. R. K. Rao, B. Venkataraman, M. K. Asundi, and G. Sundararajan, "Effect of lasersurface melting on the erosion behaviour of a low alloy steel," *Surface & Coatings Technology*, vol. 58, no. 2, pp. 85-92, 1993.
- [44] S. Saendig and P. Wiesner, "Laser surface melting of cutting tool materials," in *Laser Materials Processing* (P. Denney, I. Miyamoto, and B. L. Mordike, Eds.), vol. 2306, pp. 835-846. Published by Laser Institute of America, 1994.
- [45] R. Vilar, R. Colaco, and A. Almeida, "Laser surface treatment of tool steels," *Optical and Quantum Electronics*, vol. 27, no. 12, pp. 1273-1289, 1995.
- [46] C. Marsden, D. R. F. West and W. M. Steen, "Laser Surface Alloying of Stainless Steel with Carbon," in *Laser Surface Treatment of Metals* (C.W. Draper and P. Mazzoldi, Eds.), pp. 461-474. Martinus Nijhoff Publishers, 1986.
- [47] T. Chande, A. Ghose, and J. Mazumder, "surface properties and microstructures of AISI 1016 steel laser surface alloyed with chromium and nickle," in *Laser Processing of Materials* (K. Mukherjee and J. Mazumder, Eds.), pp. 117-130. AIME, 1985.
- [48] N. B. Dahotre, and K. Mukherjee, "Development of microstructure in laser surface alloying of steel with chromium," *Journal of Materials Science*, vol. 25, no.1B, pp. 445-454, 1990.
- [49] T. R. Tucker, A. H. Clauer, S. L. Ream and C. T. Walkers, "Rapidly solidified microstructures in surface layers of laser alloyed molybdenum on Fe-C substrates" in *Proc. Conf. Rapidly Solididifted Amorphous and Crystalline Alloys* (B. H. Kear, B. C. Giessen, and M. Cohen, Eds.), pp 541-545. Elsevier Science Publishing Inc., New York, 1982.
- [50] C. W. Draper, "Laser surface alloying: the state of the art," in *Lasers in Metallurgy* (K. Mukherjee and J. Mazumder, Eds.), pp. 67-92. AIME, 1981.
- [51] J. Mazumder, "Wear Properties of Laser Alloyed and clad Fe-Cr-Mn-C Alloys," in *Proc. ICALEO '84* (J. Mazumder, Ed.), vol. 44, pp. 159-167. Published by Laser Institute of America, 1985.
- [52] E. MaCatterty and P. G. Moore, "Electrochemical behavior of laser-processed metal surface," in *Laser Surface Treatment of Metals* (C.W. Draper and P. Mazzoldi, Eds.), pp. 263-295. Martinus Nijhoff Publishers, 1986.

- [53] L. Renaud, F. Fouquet, J. P. Millet, and J. L. Crolet, "Corrosion resistance of Fe-Ni-Cr laser surface alloys," *Surface & Coatings Technology*, vol. 45, no. 1-3, pp. 449-456, 1991.
- [54] M. A. Anjos, R. Vilar, R. Li, M. G. Ferreira, W. M. Steen, and K. Watkins, "Fe-Cr-Ni-Mo-C alloys produced by laser surface alloying," *Surface & Coatings Technology*, vol. 70, no. 2-3, pp. 235-242, 1995.
- [55] E. Gaffet, J. M. Pelletier, and S. Bonnet-Jobez, "Laser surface alloying of Ni film on Al-based alloy," *Acta Metallurgica*, vol. 37, no. 12, pp. 3205-3215, 1989.
- [56] A. Almeida, R. Vilar, and R. Colaco, "Laser alloying of Al and 7175 Al alloy for enhanced corrosion resistance," in *Laser Materials Processing* (P. Denney, I. Miyamoto, and B. L. Mordike, Eds.), vol. 2306, pp. 903-912. Published by Laser Institute of America, 1994.
- [57] S. Yerramareddy and S. Bahadur, "Effect of laser surface treatments on the tribological behavior of Ti-6Al-4V," *Wear*, vol. 157, no. 2, pp. 245-262, 1992.
- [58] O. V. Akgun and O. T. Inal, "Laser surface modification of Ti-6Al-4V alloy," *Journal of Materials Science*, vol. 29, no. 5, pp. 1159-1168, 1994.
- [59] J. D. Ayers, "Particulate composite surfaces by laser processing," in *Lasers in Metallurgy* (K. Mukherjee and J. Mazumder, Eds.), pp. 115-125. AIME, 1981.
- [60] J. D. Ayers and T. R. Tucker, "Particulate TiC hardened surface by laser melt injection," *Thin Solid Films*, vol. 73, pp. 201-207, 1980.
- [61] S. Ariely, J. Shen, M. Bamberger, F. Dausiger, and H. Hugel, "Laser surface alloying of steel with TiC," *Surface & Coatings Technology*, vol. 45, no.1-3, pp. 403-408, 1991.
- [62] B. Gruenenwald, E. Bischoff, J. Shen, and F. Dausinger, "Laser surface alloying of case hardening steel with tungsten carbide and carbon" *Materials Science and Technology*, vol. 8, no. 7, pp. 637-643, 1992.
- [63] D. Pantelis, H. Michaud, and M. de Freitas, "Wear behaviour of laser surface hardfaced steels with tungsten carbide powder injection," *Surface & Coatings Technology*, vol. 57, no. 2-3, pp. 123-131, 1993.
- [64] B. S. Yilbas, R. Davies, and Z. Yilbas, "Laser alloying of metal surfaces by injecting titanium carbide powders," *International Journal of Machine Tool & Manufacture*, vol. 29, no. 4, pp. 499-503, 1989.

- [65] X. B. Zhou and J.Th. M. De Hosson, "Metal-ceramic interfaces in laser coated aluminum alloys," *Acta Metallurgica et Materialia*, vol. 42, no. 4, pp.1155-1162, 1994.
- [66] J. H. Abboud and D. F. R. West, "Ceramic-metal composites produced by laser surface treatment," *Materials Science and Technology*, vol. 5, pp. 725-728, 1989.
- [67] J. A. Folkes and K. Shibata, "Laser cladding of Ti-6Al-4V with various carbide powders," *Journal of Laser Applications*, vol. 6, no. 2, pp. 88-94, 1994.
- [68] A. Weisheit and B. L. Mordike, "Laser surface alloying of titanium with VC and MoSi₂ to improve wear resistance," in *Laser Materials Processing* (P. Denney, I. Miyamoto, and B. L. Mordike, Eds.), vol. 2306, pp. 923-933. Published by Laser Institute of America, 1994.
- [69] K. Komvopoulos, "Effect of process parameters on the microstructure, geometry and microhardness of laser-clad coating materials," *Materials Science Forum*, vol. 163, no. 6, pt. 1, pp. 417-422, 1994.
- [70] K. P. Cooper and P. Slebodnick, "Recent development in laser melt/particles injection processing," in *Laser Materials Processing* (G. Bruck, Ed.), pp. 3-16. Springer-Verlag: IFS (Publications) Ltd., UK, 1989.
- [71] J. Choi and J. Mazumder, "Non-equilibrium synthesis of Fe-Cr-C-W alloy by laser cladding," *Journal of Materials Science*, vol. 29, no. 17, pp. 4460-4476, 1994.
- [72] A. Frenk and W. Kurz, "High speed laser cladding: solidification conditions and microstructure of a cobalt-based alloy," *Materials Science and engineering*, vol. A173, pp. 339-342, 1993.
- [73] W. Aihua, T. Zengyi, and Z. Beidi, "Laser beam cladding of slating surfaces on exhaust valves," *Welding Research Supplement*, vol. 70, no. 4, pp. 106s-109s, 1991.
- [74] S. J. Matthews, "Laser fusing of hardfacing alloy powders," in *Laser in Materials Processing* (E. A. Metzbower, Ed.), pp. 138-148. ASM International, 1983.
- [75] B. C. Oberlander and E. Lugscheider, "Composition of properties of coatings produced by laser cladding and conventional methods," *Materials Science and Technology*, vol. 8, pp. 657-665, 1992.
- [76] T. Takeda, W. M. Steen, and D. R. F. West, "Laser Cladding with Mixed Powder Feed", in *Proc. conf. ICALEO '84* (J. Mazumder, Ed.), vol. 44, pp. 151-158, Published by Laser Institute of America, 1985.

- [77] P. Sallamand and J. M. Pelletier, "Laser cladding on aluminium-base alloys: Microstructural features," *Materials Science and Engineering*, vol. A171, no. 1-2, pp. 263-270, 1993.
- [78] Y. Liu, J. Koch, J. Mazumder, and K. Shibata, "Processing, microstructure, and properties of laser-clad Ni alloy FP-5 on Al alloy AA333," *Metallurgical Transactions*, vol. 25B, pp. 425-434, 1994.
- [79] C. Ribaud, S. Sircar, and J. Mazumder, "Laser-clad Ni₇₀Al₂₀Cr₇Hf₃ alloys with extended solid solution of Hf. Part II: Oxidation behavior," *Metallurgical Transactions*, vol. 20A, no. 11, pp. 2267-2277, 1989.
- [80] J. De Damborenea and A. J. Vazquez, "Laser cladding of high-temperature coatings," *Journal of Materials Science*, vol. 28, pp. 4775-4780, 1993.
- [81] G. Abbas and D. R. F. West, "Laser surface cladding of stellite and stellite-SiC composite deposits for enhanced hardness and wear," *Wear*, vol. 143, no. 2, pp. 353-363, 1991.
- [82] Y. P. Pei, J. H. Ouyang, T. C. Lei, and Y. Zhou, "Microstructure of laser-clad SiC-(Ni alloy) composite coating," *Materials Science & Engineering*, vol. A194, no. 2, pp. 219-224, 1995.
- [83] H. W. Gu, "Laser cladding of Ni based WC alloy," *Jiguang Jishu/Laser Technology*, vol. 17, no. 4, pp.220-223, 1993.
- [84] E. Ramous, L. Giordano, A. Tiziani, B. Badan, and M. T. Cantello, "Laser cladding of ceramic and metallic coatings on steel," *Key Engineering Materials*, vol. 46-47, pp. 425-433, 1990.
- [85] W. Cerri, R. Maryinella, and G. P. Mor, "Laser deposition of carbide-reinforced coatings," *Surface and Coatings Technology*, vol.49, pp. 40-45, 1991.
- [86] A. Techel, A. Luft, A. Mueller, and S. Nowotny, "Production of hard metal-like protection coatings by CO₂ laser cladding," *Optical and Quantum electronics*, vol. 27, no. 12, pp. 1313-1318, 1995.
- [87] Y. P. Hu, C. W. Chen, and K. Mukherjee, "Synthesis of laminated metal-matrix composites by laser cladding technique," submitted to *Surface and Coatings Technology*, 1999.
- [88] J.E. Smugersky and D.M. Keichner, "Laser engineered direct fabrication/manufacturing of metals," in *Lasers in Surface Engineering* (N.B. Dahotre Ed.), pp. 1-34, ASM International, 1998.

- [89] D. S. Gnanamuthu, "Laser surface treatment," in *Source Book on Applications of the Laser in Metalworking*, pp. 324-358, ASM International, 1981.
- [90] J. I. Nurminen and J. E. Smith, "Parametric evaluation of laser/clad interaction for hardfacing applications," in *Lasers in Materials Processing* (E. A. Metzbower, Ed.), pp. 94-106, ASM International, 1984.
- [91] E. M. Breinan, D. B. Snow, C. O. Brown, and B. H. Kear, "New developments in laser melting using continuous prealloyed powder feed," in *Source Book on Applications of the Laser in Metalworking*, pp. 279-291, ASM International, 1981.
- [92] V. M. Weerasinghe and W. M. Steen, "Laser Cladding with Pneumatic Powder Delivery," In *Lasers in Materials Processing* (E. A. Metzbower, Ed.), pp. 166-175, ASM International, 1984.
- [93] R. P. Harrison, "Laser powder welding," *Turbomachinery International*, vol. 35, no. 6, pp. 52-53, 1994.
- [94] P. A. Vetter, Th. Engel, and J. Fontaine, "Laser cladding: the relevant parameters for process control," in *Laser Materials Processing: Industrial and Microelectronics Applications* (E. Beyer, M. Cantello, A. V. La Rocca, L. D. Laude, F. O. Olsen and G. Sepold, Eds.), SPIE vol. 2207, pp. 452-462, SPIE-The International Society for Optical Engineering, 1994.
- [95] Y. P. Hu, C. W. Chen, and K. Mukherjee, "Innovative laser-aided manufacturing of patterned stamping and cutting dies: processing parameters," *Materials and Manufacturing Processes*, vol. 13, no. 3, pp. 369-387, 1998.
- [96] R. Mah, "Directed light fabrication," *Advanced Materials & Processes*, vol.151, no. 3, pp. 31-33, 1997.
- [97] J. Mazumder, J. Choi, K. Nagarathnam, K. Koch, and D. Hetzner, "The direct metal deposition of H13 tool steel for 3-D components," *JOM*, vol.49, no. 5, pp. 55-60, 1997.
- [98] R. M. Macintyre, "The use of lasers in Rolls-Royce," in *Laser Surface Treatment of Metals* (C.W. Draper and P. Mazzoldi, Eds.), pp. 545-549, Martinus Nijhoff Publishers, 1986.
- [99] Minoru Kawasaki, Koyu Takase, Sinji Kato, Masahiro Nakagawa, and Kazuhiko Mori, "Development of engine valve seats directly deposited onto aluminum

- cylinder head by laser cladding process," In *SAE Technical Paper Series*, pp.1-15, Published by SAE, 1992. SAE Paper No. 920571.
- [100] K. E. Pinnow and W. Stasko, "P/M tool steels," in *Metals Handbook*, vol. 1, 10th Ed. pp. 780-792, ASM International, 1990.
- [101] Y. P. Hu, C. W. Chen, and K. Mukherjee, "An analysis of the powder feeding systems on the quality of laser cladding," in *Advances in Powder Metallurgy & Particulate Materials-1997* (R.A. McKotch and R. Webb, Eds.), vol. 3, pp.17-31, published by Metal Powder Industries Federation, 1997.
- [102] Y. P. Hu, C. W. Chen, and K. Mukherjee, "Measurement of temperature distributions during laser cladding process," accepted to be published by *Journal of Laser Applications*, 1999.
- [103] Y.-N. Liu and E. Kannatey-Asibu, Jr., "Experimental study of dual-beam laser welding of AISI 4140 steel," *Welding Journal*, vol. 8, pp. 342-s-348-s, 1997.
- [104] P.-A. Vetter, J. Fontaine, T. Engel, L. Lagrange, and T. Marchione, "Characterization of laser-material interaction during laser cladding process," in *Computer Methods and Experimental Measurements for Surface Treatment Effects* (M. H. Aliabadi, and C. A. Brebbia, Eds.), pp. 185-194, Computational Mechanics Publications, 1994.
- [105] J. Lin and W. M. Steen, "Design characteristic and development of a nozzle for coaxial laser cladding," *Journal of Laser Applications*, vol. 10, pp. 55-63, 1998.
- [106] A .F. A. Hoadley and M. Rappaz, "A thermal model of laser cladding by powder injection," *Metallurgical Transactions B*, vol. 23B, 1992, pp. 631-640.
- [107] M. Picasso, C. F. Marsden, J.-D. Wagniere, A. Frenk, and M. Rappaz, "A simple but realistic model for laser cladding," *Metallurgical Transactions B*, vol. 23B, 1994, pp. 281-291.
- [108] C. Hu and T. N. Baker, "Investigation of the temperature field developed by a spinning beam in laser processing," *Metallurgical Transactions A*, vol. 27A, 1996, pp. 4039-4047.
- [109] G. Robets and R. Cary, *Tool Steels*, 4th edition, ASM International, 1992.
- [110] R. Colaco and R. Vilar, "Laser surface melting of bearing steels," in *Laser Applications for Mechanical Industry* (S. Martellucci, and A. Scheggi, Eds.), pp. 305-314, Kluwer Academic Publishers, 1992.

- [111] Q. F. Peng, Z. Shi, and I. M. Hancock, and A. Bloyce, "Energy beam surface treatment of tool steels and their wear," *Key Engineering Materials*, vol. 46-47, pp. 229-244, 1990.
- [112] O.V. Akgun and O.T. Inal, "Laser surface melting and alloying of type 304L stainless steel Part I: Microstructural characterization," *Journal of Materials Science*, vol. 30, no. 23, pp. 6097-6104, 1995.
- [113] W. Bloehs, B. Grünenwald, F. Dausinger and H. Hügel, "Recent progress in laser surface treatment: I. Implications of laser wavelength," *Journal of Laser Applications*, vol. 8, pp. 15-23, 1996.
- [114] M. Ignatiev, I. Smurov, V. Martino, and G. Flamant, "High speed high spatial resolution pyrometry in laser machining," in *ICALEO '93 Laser Materials processing* (Paul Denny, Isamu Miyamoto, and B.L. Mordike Eds.), pp. 117-126, 1993.
- [115] F. Meriaudeau, and F. Truchetet, "Control and optimization of the laser cladding process using matrix cameras and image processing," *Journal of Laser Applications*, vol. 8, pp. 317-326, 1996.

MICHIGAN STATE UNIVERSITY LIBRARIES



3 1293 02092 9075